Ph.D. Thesis

Roles of Fluctuations in Pulsed Neural Networks

Supervisor Professor Yoichi Okabe

Takashi Kanamaru

Department of Advanced Interdisciplinary Studies,
Faculty of Engineering,
The University of Tokyo

December 15, 2000

Abstract

Concerning the fluctuation which is observed in biological sensory systems and cortical neuronal networks, the roles of fluctuations in pulsed neural networks are investigated. As a model of a single neuron, the FitzHugh-Nagumo model is used, and two kinds of couplings of neurons are considered, namely, the electrical coupling which is often observed in sensory systems, and the chemical coupling which is widely seen in cortical neuronal networks.

The network with electrical couplings with the periodic input shows typical properties of stochastic resonance, which is the phenomenon where a weak input signal is enhanced by its background fluctuations. It is found that the optimal fluctuation intensity which maximizes the correlation coefficient between the input and the output increases with the increase of the coupling strength of the network. Using these properties, the network in which the fluctuations in the system play significant roles in the information processing is proposed. The dependence of the correlation coefficient on the coupling strength of the network is also investigated, and it is found that the correlation coefficient takes a maximum also as a function of the coupling strength. This phenomenon called array-enhanced stochastic resonance is analyzed theoretically.

In the network with chemical couplings, the associative memory in the network is considered, and it is found that the memory retrieval is induced by the fluctuations in the system. Besides, for the network storing sparse patterns with hierarchical correlations, it is observed that the retrieved pattern is selected by controlling the fluctuation intensity.

Based on the results for both couplings, it is claimed that the fluctuations in the pulsed neural network might have beneficial effects on the information processing in the neural system.

Contents

Part I

Introduction

Chapter 1

Sources of Fluctuations in Neural Systems

1.1 Introduction

In this paper, the roles of fluctuations in the pulsed neural network are investigated. There are several sources of fluctuations in neural systems and we review them in this chapter. The regulation of the intensity of the fluctuations is an important concept in our research, thus we take notice of it in this chapter.

In Sec. 1.2, the fluctuations in the receptor cells in sensory systems are introduced. The receptor cells receive signals from the outer world, thus they are exposed to the fluctuations of the environment. In Sec. 1.3, the stochasticity of the ion channels is introduced. The ion channels are ubiquitous in the membranes of neurons, thus this fluctuation is thought to be universal in neural systems. In Sec. 1.4, the synaptic unreliability is introduced. In the central nervous system such as the hippocampus and the cortex, the synaptic transmission is less reliable than that of the peripheral nervous system such as the neuromuscler junction. In Sec. 1.5, the fluctuation of the sum of the presynaptic inputs is introduced. This fluctuation causes the cortical neurons to fire randomly. In Sec. 1.6, the chaotic behavior in the neural system is briefly reviewed. The summary of this chapter is presented in the final section.

1.2 Fluctuations in the Outer World

As shown in Fig. 1.1, the living organism receives the information from the outer world with the receptor cells in sensory systems, such as the photoreceptor cells in the retina and the hair cells in the ear [1]. Thus it is considered that the responses of the receptor cells reflect the fluctuations in the outer world, for example, fluctuations of the number of photons injected to the retina for photoreceptor cells, and the acoustic fluctuations for hair cells. The hair cells also work as the detectors of the hydrodynamic or aerial displacements in the outer world for some living organisms, for example, the fish [1], the crayfish [2, 3], the cricket [4], and the cockroach [5], and it is known that they play an important role in the predator avoidance behavior. Thus it is thought that the signals

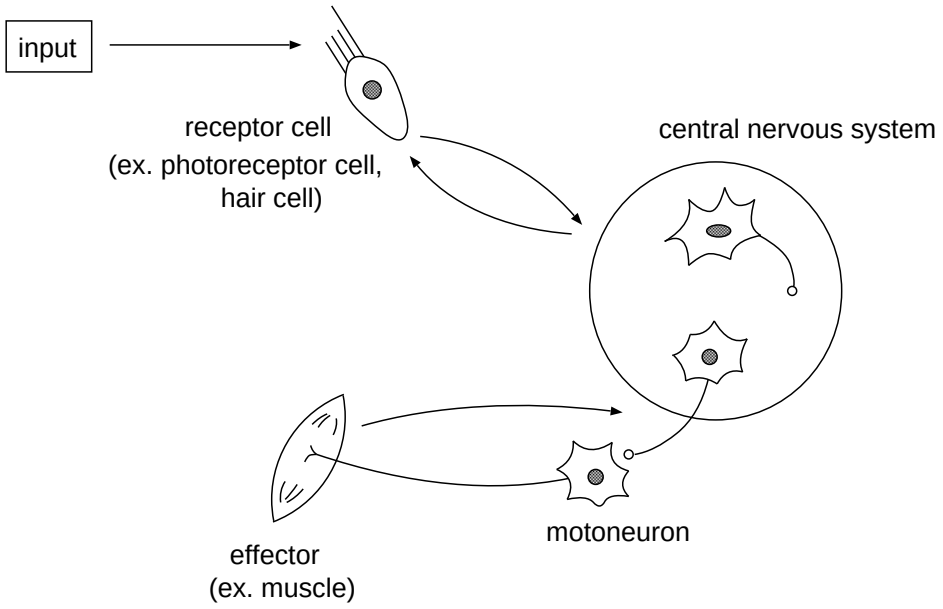

Figure 1.1 The flows of the information in living organisms.

which inform the approach of the predator are always exposed to the hydrodynamic or aerial fluctuations. The signal detection in such a noisy environment is of importance and has attracted considerable attention in recent years. We treat this problem in Part II.

1.3 Stochasticity of Ion Channels

The excitable membranes of the neurons can evoke the action potentials in response to the depolarizing input. The generation of the action potential is realized by the ionic and capacitive currents across the membrane. The main components of the ionic currents are sodium, potassium, and calcium, and those ions flow across the ion-selective and voltage-dependent channels in the membrane. Hodgkin and Huxley investigated the properties of the squid giant axon and showed that the transmembrane potential V obeys the equation

$$C\frac{dV}{dt} = -[g_{Na}(V - E_{Na}) + g_K(V - E_K) + g_L(V - E_L)], \tag{1.1}$$

where $C = 1$ [μF/cm^2] is the transmembrane capacitance, $E_{Na} = 55$ [mV], $E_K = -72$ [mV], and $E_L = -50$ [mV] are the reversal potentials for the sodium, the potassium, and the leak respectively, $g_{Na} = \bar{g_{Na}} m^3 h$ and $g_K = \bar{g_K} n^4$ are the voltage-dependent conductances with

$$\frac{dm}{dt} = \alpha_m(1 - m) - \beta_m m, \tag{1.2}$$

$$\frac{dh}{dt} = \alpha_h(1 - h) - \beta_h h, \tag{1.3}$$

$$\frac{dn}{dt} = \alpha_n(1-n) - \beta_n n, \tag{1.4}$$

where all α's and β's are functions of V, and $g_{\bar{Na}}$, $g_{\bar{K}}$ and g_L are constants [6]. Note that m, h, and n are continuous variables in the range from 0 to 1 and they determine the state of the sodium and potassium channels. Equations (1.1), (1.2), (1.3), and (1.4) compose a system of the deterministic differential equations, thus the behavior of the membrane potential V is also deterministic. However, the physiological experiments with the patch-clamp technique [7] revealed that each ion channel randomly fluctuates between the discrete states [7, 8, 9], namely, the "open" and "close" states, because of the thermal fluctuations, thus the modeling as stochastic processes might be more suitable.

In Ref. [10], the kinetics of the sodium and potassium channels are modeled by Markov processes with eight and six discrete states respectively, and the behavior of the membrane potential V written by eq. (1.1) with the conductances governed by the above Markov processes is investigated. Some stochastic behaviors of the membrane potential, for example, the fluctuation around the resting potential, and the occasional failures of the firing, are observed.

This stochasticity caused by the randomness of ion channels is thought to be universal in the neural system.

1.4 Synaptic Unreliability

In this section, we introduce the unreliability of the synapses which transfer the information from the pre-synaptic neurons to the post-synaptic neurons or other organs such as muscle fibers. With the terminology defined in Chap. 2, only the chemical synapses are treated in this section. As shown in Fig. 1.2, the arrival of the action potential at the pre-synaptic terminal causes the release of the chemical transmitters, for example, acetylcholine (ACh) or glutamate at excitatory synapses and γ-aminobutyric acid (GABA) at inhibitory synapses. It is known that the transmitters are released in multimolecular packets called as quanta [12] which contain thousands of molecules. The chemical transmitters diffuse across the synaptic cleft, and combine with the receptor molecules in the post-synaptic membrane. Then the channels open, the ionic current flows across the post-synaptic membrane, and the post-synaptic potential (PSP) is produced [11].

In the above process, it is known that the release of the chemical transmitters can be modeled by a stochastic process [13, 14, 15]. Let us denote the number of the release sites of the chemical transmitters as N. The probability of the release of transmitters depends on its environment such as the density of the calcium ion and the pre-synaptic potential. Let us consider the release of the transmitter induced by an action potential which arrives at the synaptic terminal, and assume the release probability p_r for each release site is uniform. If each site releases the quantum of transmitters independently, the number m of the release sites which release quanta follows the binomial distribution

$$P(m) = {}_N C_m \, {p_r}^m (1-p_r)^{N-m}. \tag{1.5}$$

The mean $\langle m \rangle$ and the standard deviation SD(m) of m are directly calculated as

$$\langle m \rangle = N p_r, \tag{1.6}$$

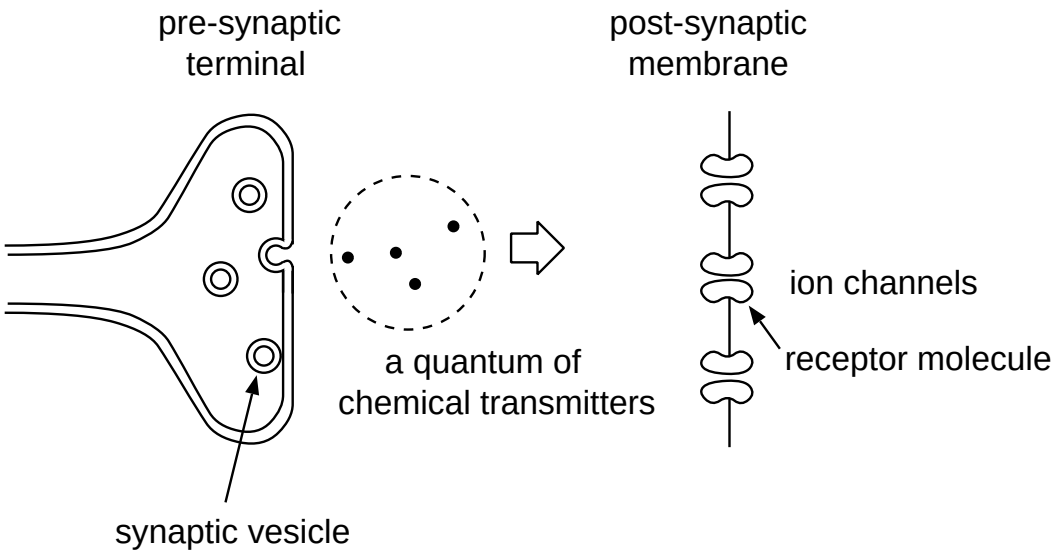

Figure 1.2 A schematic diagram of the synapse and the release of the chemical transmitters.

$$\mathrm{SD}(m) = \sqrt{Np_r(1-p_r)}. \tag{1.7}$$

If a single quantum of the transmitter produces a PSP with amplitude V_q at the post-synaptic organ, the amplitude V_{PSP} of the PSP evoked by a pre-synaptic action potential has the mean $\langle V_{PSP}\rangle$ and the standard deviation $\mathrm{SD}(V_{PSP})$ written as

$$\langle V_{PSP}\rangle = V_p\langle m\rangle = V_p N p_r, \tag{1.8}$$

$$\mathrm{SD}(V_{PSP}) = V_p\mathrm{SD}(m) = V_p\sqrt{Np_r(1-p_r)}. \tag{1.9}$$

Note that eq. (1.9) determines the degree of the unreliability of the single synapse.

Historically, the stochasticity of the synapses at the neuromuscular junctions has been often investigated because they are relatively reliable, and it is known that they have large $\langle m\rangle$ in the range from 100 to 300 and large p_r under the normal condition [11]. On the other hand, the synapses in the central nervous system such as the cortex and the hippocampus are less reliable and have small $\langle m\rangle$ in the range of 1 to 20 [11, 16, 17], and the recent careful physiological experiments suggest that the release probability in the cultured hippocampal neurons ranges from 0.09 to 0.54 [16]. As a result, the amplitude of EPSP largely fluctuates from trial to trial [18, 19, 20], for example, $\langle V_{PSP}\rangle = 1.67$ [mV] and $\mathrm{SD}(V_{PSP})$=0.271 [mV] for the synapses between the pairs of pyramidal neurons in slices of rat sensorimotor cortex [18], and $\langle V_{PSP}\rangle = 0.607$ [mV] and $\mathrm{SD}(V_{PSP})$=0.37 [mV] for the synapses between the pyramidal and non-pyramidal neurons in slices of rat sensorimotor cortex [19].

In Ref. [21], the capacity of the information transfer by neurons with unreliable synapses is investigated theoretically.

Note that the degree of the unreliability eq.(1.9) can be regulated by controlling the release probability p_r, and such a regulation might be realized by the synaptic potentiation and depression [16, 17, 22].

1.5 Sum of Synaptic Inputs

1.5.1 Definition of the Coefficient of Variance C_v

In this section, we introduce the fluctuations of the sum of the synaptic inputs observed in the cortical neurons [27] and the motoneurons [23]. First, let us define the coefficient of variance C_v, which is often used to measure the degree of randomness of a spike train of cortex neurons. Spike trains of cortex neurons are thought to be highly variable, like

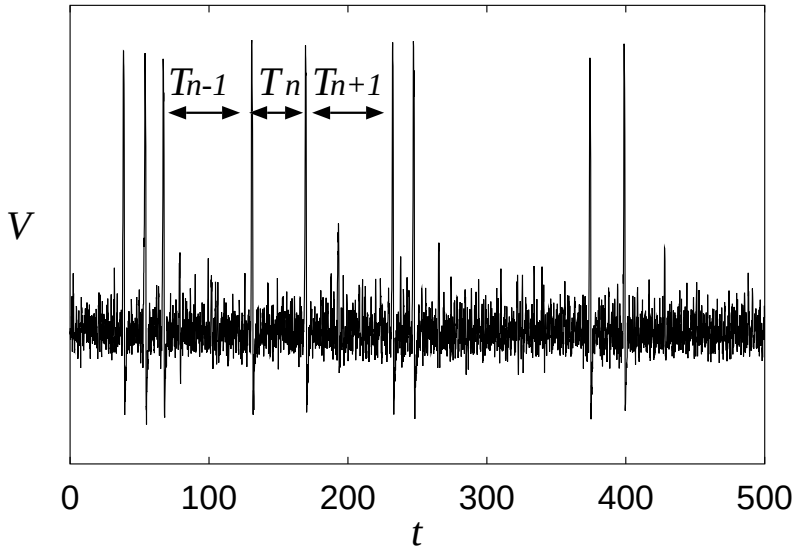

Figure 1.3 A spike train of a FitzHugh-Nagumo model neuron and its ISI sequence $\{T_i\}$.

a time series in Fig. 1.3, which is generated by a FitzHugh-Nagumo (FN) neuron model with additive Gaussian white noise. The definition of the FN model is given in Sec. 1.5.5.

Let us denote the time of the i-th firing as t_i. Then the interspike interval (ISI) T_i is defined as

$$T_i = t_i - t_{i-1}. \tag{1.10}$$

As shown in Fig. 1.3, T_i shall be a random variable. The histogram of the interspike interval sequence $\{T_i\}$ derived from the spike train in Fig. 1.3 is shown in Fig. 1.4. The

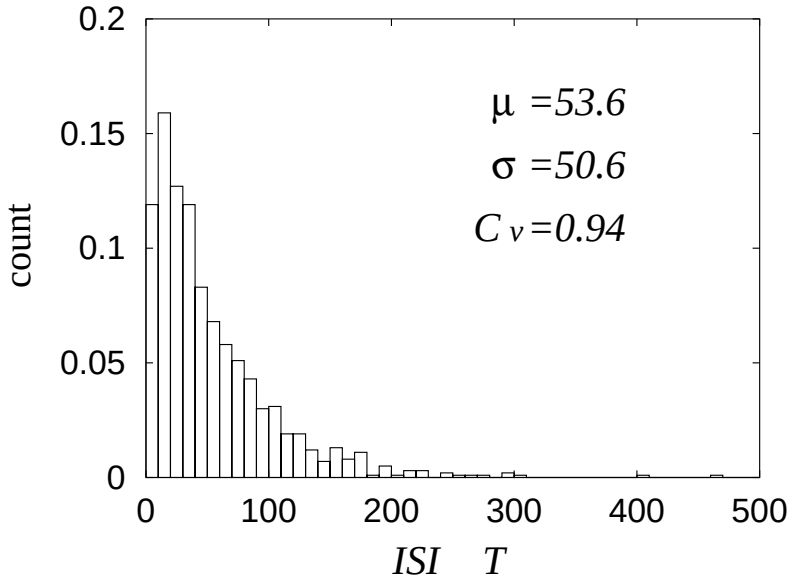

Figure 1.4 The histogram of the interspike interval sequence $\{T_i\}$ derived from the time series in Fig. 1.3. The value in vertical axis is normalized by the number $n = 1000$ of samples.

mean value μ and the variance σ^2 are defined as

$$\mu = \frac{1}{n}\sum_{i=1}^{n} T_i, \tag{1.11}$$

$$\sigma^2 = \frac{1}{n}\sum_{i=1}^{n} (T_i - \mu)^2, \tag{1.12}$$

where n is the number of samples. With μ and σ, the coefficient of variance C_v is defined as

$$C_v = \sigma/\mu. \tag{1.13}$$

To see the typical value of C_v, let us consider the case in which firings of a neuron take place according to the Poisson distribution. In such a case, the ISI T of the neuron follows the exponential distribution

$$P(T) = \lambda \exp(-\lambda T), \tag{1.14}$$

where λ is the firing rate of the neuron. From eq. (1.14), the mean value μ and the variance σ^2 of T are easily calculated as $\mu = 1/\lambda$ and $\sigma^2 = 1/\lambda^2$, so the coefficient of variance C_v takes the value 1 in this case.

Generally, C_v takes a large value around 1 for random spike trains, and it takes a small value around 0 for ordered spike trains, for example, periodic one. For the spike train treated in Fig. 1.4, $\mu \simeq 53.6$, $\sigma \simeq 50.6$, and $C_v \simeq 0.94$ are derived, so it can be concluded that it is a highly random spike train.

1.5.2 Large C_v Values in Cortex Neurons

It is known that the coefficient of variance C_v of ISIs of cortex neurons takes large values for behaving animals. For example, in Ref. [26], the spiking variability of neurons in the association cortex of the cat is investigated and it is reported that C_v takes a value about 1.2 when the cat is quietly awaking, and it takes a value about 1.5 during REM sleep. And in Ref. [27], the large C_v value over 1 is observed in the primary visual cortex of the awake, behaving macaque monkey.

It is thought that this variability of spikings of cortex neurons is due to the sum of enormous inputs from presynaptic neurons [31]. It is known that about 10^4 synapses connect to a postsynaptic neuron in the cortex. When all the presynaptic neurons are firing with the frequency 1$\sim$10 [Hz], their sum can behave like noise in the postsynaptic neuron.

This subjects have a lot to do with the dispute between Softky and Shadlen & Newsome [27, 28, 29, 30], so we treat it in the next subsection in detail.

1.5.3 Dispute Between Softky and Shadlen & Newsome

From 1993 to 1995, Softky and Shadlen & Newsome have disputed about the models which describe the large C_v values in cortex neurons on their papers [27, 28, 29, 30]. Before explaining their issues, let us introduce one of the simplest neuron models, the leaky integrate-and-fire (LIF) model written as

$$\tau \frac{dV}{dt} = -(V - V_0) + V_{in}(t), \tag{1.15}$$

$$\text{if } V > \theta, \quad V = V_0 \quad (\text{reset}), \tag{1.16}$$

where V is the membrane potential of the neuron, τ is the time constant of the membrane, V_0 is the resting potential, $V_{in}(t)$ is the external input, and $\theta > V_0$ is the threshold. Note that this model emits a spike when V exceeds the threshold θ, and resets to the resting potential V_0 immediately. The model without the first term of the righthand side of eq. (1.15) is called as the integrate-and-fire neuron model. In the cortex, it is observed that $\tau = 1 \sim 10$ [ms], $V_0 \simeq -60$ [mV], and $\theta \simeq -55$ [mV] [28]. In Fig. 1.5, the behavior of a single LIF neuron for $V_0 = -60$ [mV], $\tau = 5$ [ms], and $\theta = -55$ [mV] is shown. The input $V_{in}(t)$ is a step function with height 6.5 [mV] for $t > 1$ [ms].

Let us consider the case in which the input $V_{in}(t)$ to the neuron is the sum of the synaptic inputs from the presynaptic neurons. The positive influence of a presynaptic input to the potential of the postsynaptic neuron is called as the excitatory postsynaptic potential (EPSP), and the negative one is called as the inhibitory postsynaptic potential (IPSP). As a waveform $K(t)$ of EPSP and IPSP, the following functions are often used: the alpha function

$$\alpha(t) = \begin{cases} \dfrac{t}{\tau_0} \exp\left(1 - \dfrac{t}{\tau_0}\right) & \text{if } t > 0 \\ 0 & \text{otherwise} \end{cases}, \tag{1.17}$$

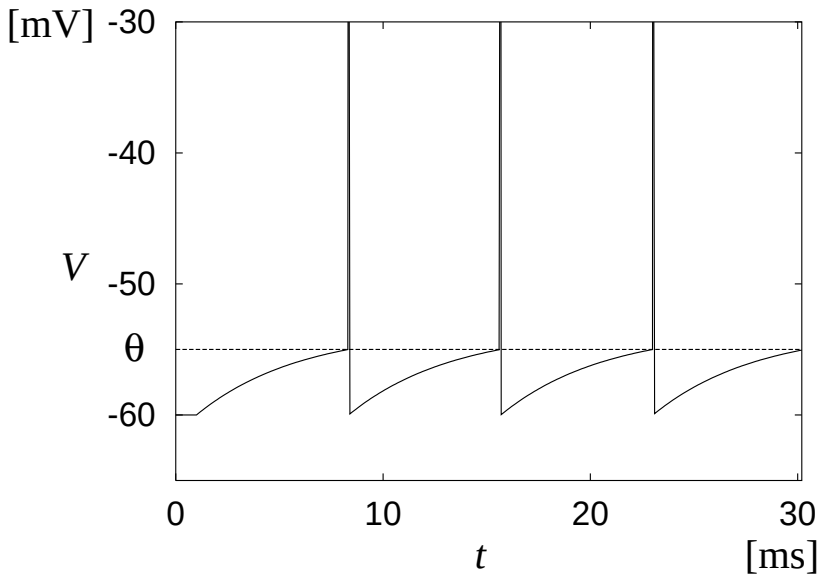

Figure 1.5 The behavior of a single LIF neuron for $V_0 = -60$ [mV], $\tau = 5$ [ms], and $\theta = -55$ [mV]. The input $V_{in}(t)$ is a step function with height 6.5 [mV] for $t > 1$ [ms]. When the membrane potential V exceeds the threshold θ, a spike is emitted and V resets to the resting potential V_0.

shown in Fig. 1.6; and the exponential function

$$e(t) = \begin{cases} \exp\left(-\dfrac{t}{\tau_0}\right) & \text{if } t > 0 \\ 0 & \text{otherwise} \end{cases} . \tag{1.18}$$

Note that τ_0 is the time constant of the synapse and it can differ for different synapses, but we consider only the case in which τ_0 is uniform for all the synapses for simplicity in the following. With $K(t)$, the input $V_{in}(t)$ is written as

$$V_{in}(t) = \sum_{i=1}^{m} \sum_{k=1}^{\infty} w_i K(t - t_k^i), \tag{1.19}$$

where m is the number of synapses, t_k^i is the time of k-th firing of the i-th synapse, and w_i is the synaptic weight which takes positive values for excitatory synapses and takes negative values for inhibitory synapses.

When the i-th presynaptic neuron is firing according to the Poisson distribution with frequency λ_i [Hz], eq. (1.19) can be regarded as shot noise [33] and its mean μ_{in}, variance σ_{in}^2 and correlation function $C_{in}(t)$ are written as

$$\mu_{in} = \sum_{i=1}^{m} \lambda_i w_i \int_0^{\infty} K(t) dt, \tag{1.20}$$

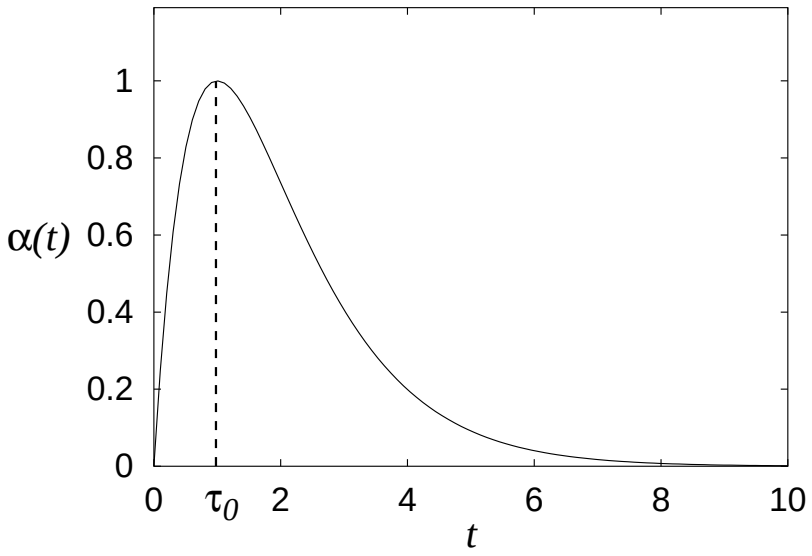

Figure 1.6 The α function $\alpha(t)$ for $\tau_0 = 1$.

$$\sigma_{in}^2 = \sum_{i=1}^{m} \lambda_i w_i^2 \int_0^\infty K(t)^2 dt, \tag{1.21}$$

$$C_{in}(t) \equiv \langle (V_{in}(0) - \langle V_{in} \rangle)(V_{in}(t) - \langle V_{in} \rangle) \rangle, \tag{1.22}$$

$$= \sum_{i=1}^{m} \lambda_i w_i^2 \int_0^\infty K(t')K(t'+t)dt'. \tag{1.23}$$

Note that the input $V_{in}(t)$ to the cortex neuron is regarded as noise with mean μ_{in}, variance σ_{in}^2 and correlation function $C_{in}(t)$ given by eqs. (1.20), (1.21) and (1.23).

Equations (1.20), (1.21) and (1.23) give

$$\mu_{in} = \tau_0 e \sum_{i=1}^{m} \lambda_i w_i, \tag{1.24}$$

$$\sigma_{in}^2 = \frac{\tau_0 e^2}{4} \sum_{i=1}^{m} \lambda_i w_i^2, \tag{1.25}$$

$$C_{in}(t) = \sigma_{in}^2 \left(1 + \frac{t}{\tau_0}\right) \exp\left(-\frac{t}{\tau_0}\right), \tag{1.26}$$

for the alpha function $\alpha(t)$, and

$$\mu_{in} = \tau_0 \sum_{i=1}^{m} \lambda_i w_i, \tag{1.27}$$

$$\sigma_{in}^2 = \frac{\tau_0}{2} \sum_{i=1}^{m} \lambda_i w_i^2, \tag{1.28}$$

$$C_{in}(t) = \sigma_{in}^2 \exp\left(-\frac{t}{\tau_0}\right), \tag{1.29}$$

for the exponential function $e(t)$. Note that $V_{in}(t)$ characterized by eqs. (1.27), (1.28), and (1.29) can be modeled by the Ornstein-Uhlenbeck process written as

$$\frac{d}{dt}V_{in}(t) = -\frac{1}{\tau_0}(V_{in}(t) - \mu_{in}) + \sqrt{\frac{2\sigma_{in}^2}{\tau_0}}\eta(t), \tag{1.30}$$

$$\langle \eta(t)\eta(t') \rangle = \delta(t - t'), \tag{1.31}$$

where $\eta(t)$ is Gaussian white noise [34].

With the above preliminaries, let us introduce the dispute between Softky and Shadlen & Newsome.

In Ref. [27], to reproduce the large C_v values in cortex neurons, Softky & Koch considered the statistics of the spikings of a LIF neuron to which enormous EPSPs are injected, namely, eqs. (1.15), (1.16), and (1.19) for $w_i > 0$. This model shows various C_v values dependent on the time constant τ, but in the physiologically plausible range, only the small C_v value are observed. So they concluded that cortex neurons do not work as integrators unlike the usual LIF model, and claimed that they work as coincidence detectors [31, 32] which detect the coincident firings of some presynaptic neurons. To realize the coincidence detector by the LIF model, a very short time constant τ is required, but such a short time constant has not been found in physiological experiments. As candidates to realize the coincidence detector, they proposed some mechanisms, such as, the effective reduction of the time constant by the sum of enormous presynaptic inputs [35], and the active dendrite [36, 37, 38] in which pulses can generate and propagate.

On the other hand, in Ref. [28], Shadlen & Newsome claimed that the small C_v value of Softky's model is due to the fact that they treat only EPSPs. They constructed a neuron model to which almost the same amount of EPSPs and IPSPs are injected, and demonstrated that such balanced EPSPs and IPSPs, or the balanced-inhibition, can yield large C_v values even in a simple LIF neuron.

In Fig. 1.7, the typical behaviors of their models are shown. The data are generated by eq. (1.15) for $\tau = 5$ [ms], $V_0 = -60$ [mV], and $\theta = -55$ [mV], and the input $V_{in}(t)$ is described by the Ornstein-Uhlenbeck process (1.30). The behavior of the model by Softky & Koch, to which the sum of only EPSPs is injected, is shown in Fig. 1.7(a). The parameters are $m = 5000$, $\lambda_i = 0.5$ [Hz], $\tau_0 = 1$ [ms], and $w_i = 0.5$. As described above, the coefficient of variance C_v of this model takes a small value 0.52. In Fig. 1.7(b), the behavior of the model by Shadlen & Newsome, to which the sum of balanced EPSPs and IPSPs is injected, is shown. The parameters are $\lambda_i = 10$ [Hz], $\tau_0 = 1$ [ms], $w_i = 0.5$ for 5000 excitatory synapses, and $w_i = -0.5$ for 5000 inhibitory synapses. The large C_v value over 1 is observed under the balanced-inhibition.

Softky approved the idea of the balanced-inhibition and argued that the time constant of the membrane effectively decreases under the balanced-inhibition, and cortex neurons work as coincidence detectors [29]. Based on this argument, he proposed that the information in the cortex is carried by the timings of the firing of each neuron, in other words, the cortex neurons transmit the information using the temporal coding scheme.

Against Softky's proposition, Shadlen & Newsome claimed that the LIF neuron works as a integrator which integrates the noise-like presynaptic inputs and its dynamics is governed by the Brownian motion, so its output cannot reflect the timing of the input

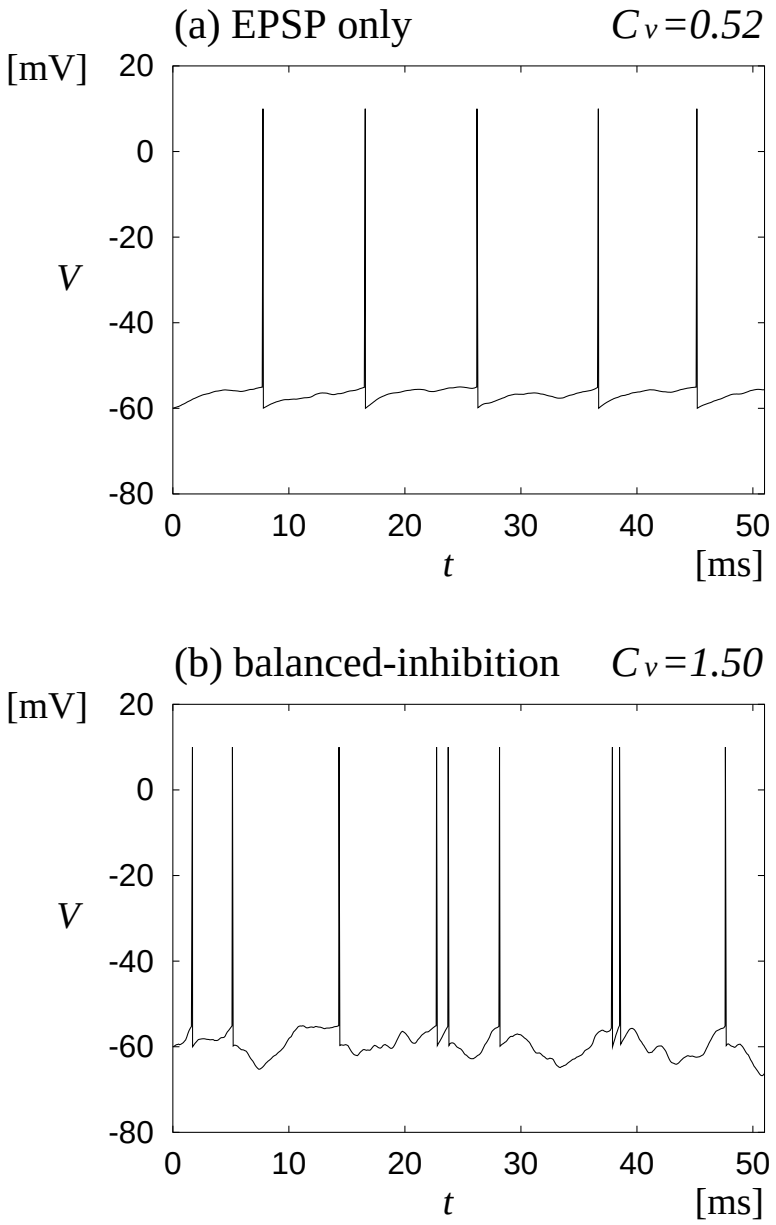

Figure 1.7 The typical behaviors of model neurons to reproduce the large C_v values in the cortex. The input is (a) the sum of only EPSPs and (b) the sum of balanced EPSPs and IPSPs.

pulses [30]. He proposed that the information in the cortex is carried by the firing rate of each neuron.

As mentioned above, the dispute between Softky and Shadlen & Newsome is relevant to the problem of the functional mode of the neuron, namely, the coincidence detector or the integrator, and the problem of the information coding, that is, the temporal

coding or the firing rate coding. Their claims are based on theoretical studies, but the experimental evidences are required to determine which standpoint is valid in the cortex neurons.

As for the functional mode of the neuron, the idea of the coincidence detector is of theoretical interest, but it is uncertain whether it is realizable under the physiological conditions. Similarly, though it is accepted that the large C_v values are realized by the balanced-inhibition, there is no physiological evidence that EPSPs and IPSPs are precisely balanced. Thus this question is still an open problem.

The problem of the carrier of the information in cortex neurons is also still controversial. However, there is a view that the temporal coding is realizable without the coincidence detector. This idea is introduced in Sec. 1.5.5.

1.5.4 Development After the Dispute

In this subsection, we introduce the related issues to the dispute between Softky and Shadlen & Newsome.

In Ref. [39], Shinomoto et al. showed that the Ornstein-Uhlenbeck process, namely, the LIF model with Gaussian white noise, cannot reproduce the physiological data, and in the next paper [40], they found that the LIF model with colored noise, namely, eqs. (1.15) and (1.30), can reproduce the data. In Ref. [41], it is observed that the burst firings can generate large C_v values than that of neurons under the balanced-inhibition.

In Refs. [42, 43], the dynamics of the network of neuron models under the balanced-inhibition is investigated.

In Ref. [44], it is reported that the C_v values derived from spike trains of the neuron in the visual cortex of the monkey remarkably decrease if the data are carefully chosen when the eyes of the monkey are at a standstill. This experimental result disapproves the "common sense" that the C_v values in cortex neurons are very large for behaving animals.

Thus further researches are required both experimentally and theoretically to understand the role of cortex neurons.

1.5.5 Reliability of Spike Timings

In the dispute with Softky, Shadlen & Newsome claimed that cortex neurons integrate the noise-like presynaptic input and their spikes seem to be random. If one follows their arguments, it is concluded that the timing of firings of neurons cannot carry the information, so the idea of the temporal coding is rejected. But recent theoretical and experimental studies show that the timing of firings of neurons might be essential even in the conventional neuron models. It is known as the problem of the reliability of spike timings. In this subsection, we introduce this problem.

As a neuron model, let us consider the FitzHugh-Nagumo (FN) equation written as

$$\tau \frac{du}{dt} = -v + u - \frac{u^3}{3} + V_{in}(t) + \eta(t), \tag{1.32}$$

$$\frac{dv}{dt} = u - \beta v + \gamma, \tag{1.33}$$

$$\langle \eta(t)\eta(t') \rangle = D\delta(t - t'), \tag{1.34}$$

where β, γ, and τ are parameters, u is the fast variable which denotes the internal state of the neuron, v is the slow variable which represents the refractory period, $V_{in}(t)$ is the input to the neuron, and $\eta(t)$ is Gaussian white noise with intensity D which models thermal noise. Note that all the variables and constants are dimensionless in the above equations. The parameters are set at $\beta = 0.8$, $\gamma = 0.7$, and $\tau = 0.1$ in the following. As the input $V_{in}(t)$, a static input

$$V_{in}(t) = U(t - t_0), \tag{1.35}$$

$$\equiv \begin{cases} U_0 & \text{if } t \geq t_0 \\ 0 & \text{otherwise} \end{cases}, \tag{1.36}$$

or a fluctuating input governed by eq. (1.30) is used.

In Fig. 1.8(a), the firing times of an FN model with a static input are plotted for $U_0 = 0.35$ and $D = 0.0001$. The firing times fluctuate from trial to trial because of thermal noise $\eta(t)$.

In Fig. 1.8(b), the firing times of an FN model with a fluctuating input, and the waveform of the input are plotted for $D = 0.0001$, $\tau_0 = 5$, and $\sigma^2 = 0.2$. Note that the particular input waveform is injected repeatedly, but $\eta(t)$ is injected independently for each trial. Despite thermal noise $\eta(t)$, the spike timings of the FN neuron are reliable for each trial.

Regarding the fluctuating input $V_{in}(t)$ as the sum of presynaptic inputs, the above result shows that this neuron model can respond to the input from presynaptic neurons reliably despite thermal noise.

The similar results are observed both theoretically [48, **?**] and experimentally, for example, in motion detecting neurons *in vivo* of the fly [45], and in retinal ganglion neurons *in vivo* of the tiger salamander and the rabbit [46], in neocortical slices of the rat [47, **?**], and in slices of the visual cortex of the ferret [49].

This high reliability of neurons might be an important mechanism to realize the temporal coding.

1.6 Chaos

In this section, chaos, namely, the deterministic but complex behaviors in nonlinear systems, is introduced as an example of the random behaviors in neural systems.

Experimentally, chaos in neural systems is firstly observed in the periodically stimulated neurons, for example, the Onchidium giant neuron [51] and the squid giant axon [52]. The similar phenomena can be numerically reproduced in the periodically stimulated Hodgkin-Huxley equation [53]. A chaotic behavior of the periodically stimulated Hodgkin-Huxley equation is shown in Fig. 1.9. It is observed that the response of the model to a periodic pulse current with period 5.5 [ms], width 0.5 [ms], and height 19 [μA/cm^2] is chaotic.

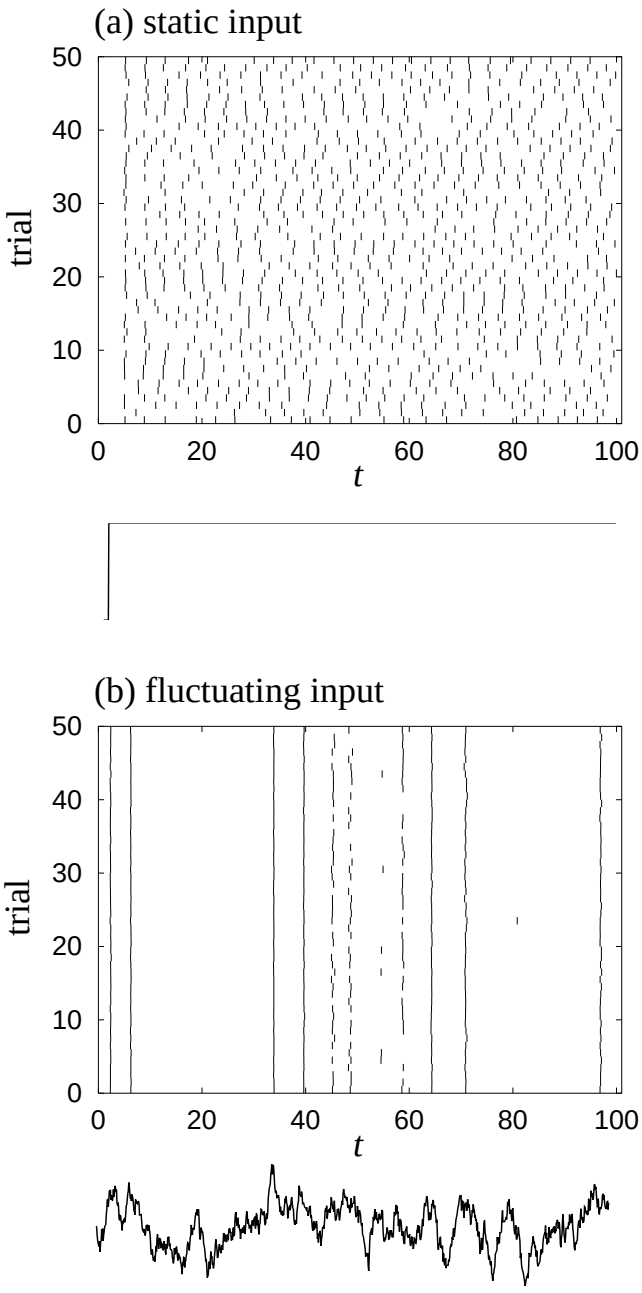

Figure 1.8 The firing times of an FN model with (a) a static input and (b) a fluctuating input. The waveform of the input $V_{in}(t)$ is also shown below each graph.

After these observations, it is found that the self-sustained firings of the Onchidium pacemaker neuron without periodic inputs also show chaotic behaviors [54], and it is suggested that the intracellular slow oscillation of the membrane is concerned with the

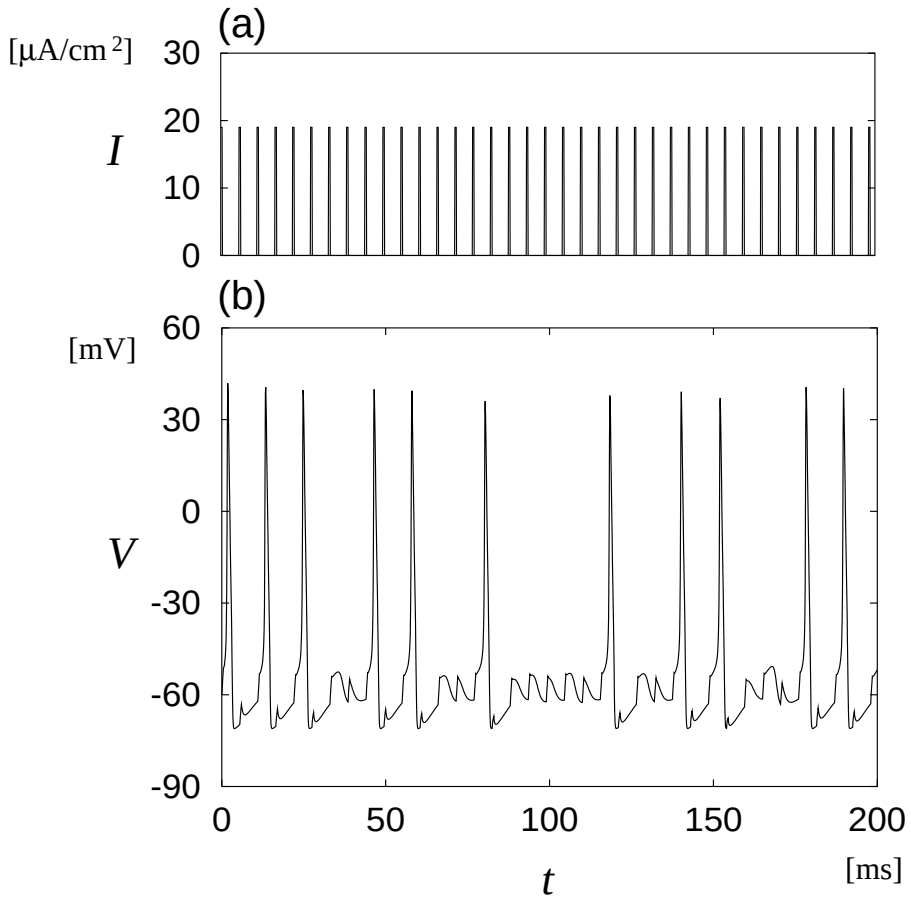

Figure 1.9 A chaotic behavior of the periodically stimulated Hodgkin-Huxley equation. (a) A periodic pulse current with period 5.5 [ms], width 0.5 [ms], and height 19 [μA/cm^2] injected to the model. (b) The behavior of the membrane potential V of the Hodgkin-Huxley model.

self-sustained chaos. In Ref. [55], the neuron model incorporating the membrane conductances and the intracellular calcium dynamics is numerically analyzed and the chaotic behaviors are also observed.

As for the high-dimensional chaos, the electroencephalographic (EEG) waves in the olfactory bulb of the rabbit show the chaotic behaviors [56], and the relationship between this phenomenon and the memory in the brain is discussed [57, 58]. Theoretically, the associative memory in chaotic neural networks is investigated by several authors [59, 60, 61].

In this paper, we consider the roles of the sub-threshold fluctuations in the membrane potential of the neuron. On the other hand, as previously shown, chaos in the single neuron is observed only in its pulse train, particularly in its interspike interval, and the

sub-threshold chaos has not been found experimentally at least in our knowledge. Thus it is not clear whether chaos can be a candidate for the fluctuations treated in this paper.

1.7 Summary

The several sources of fluctuations introduced in this chapter are summarized in Table 1.1. Note that it is impossible to control the fluctuation intensity for the fluctuations in

	sensory system	central nervous system	regulation of intensity
outer world	◯	×	×
ion channel	◯	◯	×
synapse	△	◯	◯
synaptic input	×	◯	◯
chaos	?	◯	?

Table 1.1 The sources of fluctuations in neural systems and their possibilities for the regulation of the fluctuation intensity.

the outer world and the stochasticity of ion channels, and it is possible for the synaptic unreliability and the sum of synaptic input by the synaptic potentiation and depression.

The regulation of the fluctuation intensity is an important concept in our research, and, in Chap. 5, we will find that the array-enhanced stochastic resonance gives a mechanism for an effective regulation of the fluctuation intensity even for the "uncontrollable" fluctuations.

Chapter 2

Modeling the Network of Spiking Neurons

2.1 Model of Spiking Neurons

In this chapter, we introduce the general model of the network of spiking neurons. Depending on its mathematical expression, the couplings of the network are classified into two groups, namely, the electrical coupling and the chemical coupling.

Let us consider a single spiking neuron model governed by a d-dimensional differential equation written as

$$\frac{d\boldsymbol{x}}{dt} = \boldsymbol{F}(\boldsymbol{x}) + \boldsymbol{S}(t) + \boldsymbol{\eta}(t), \tag{2.1}$$

$$\boldsymbol{x} \in \mathbf{R}^d, \tag{2.2}$$

where $\boldsymbol{x} = (V, x_2, \cdots, x_d)^t$ is a d-dimensional vector which denotes the internal state of the neuron, V is the membrane potential of this neuron, $\boldsymbol{F}(\boldsymbol{x})$ is the function which describes the dynamics of the neuron, $\boldsymbol{S}(t) = (S_1(t), S_2(t), \cdots, S_d(t))^t$ is the external input, and $\boldsymbol{\eta}(t) = (\eta_1(t), \eta_2(t), \cdots, \eta_d(t))^t$ denotes background fluctuations in the network. The FitzHugh-Nagumo model is a model for $d = 2$ and written as

$$\tau\frac{du}{dt} = -v + u - \frac{u^3}{3} + S(t) + \eta(t), \tag{2.3}$$

$$\frac{dv}{dt} = u - \beta v + \gamma, \tag{2.4}$$

where β, γ, and τ are parameters, $S(t)$ is the external input, $\eta(t)$ is the background fluctuation, u is the variable which models the membrane potential of the neuron, and v is the variable which represents the refractoriness after the firing of the neuron. Note that eqs. (2.3) and (2.4) are rewritten as eq. (2.1) with $\boldsymbol{x} = (u, v)^t$, $\boldsymbol{S}(t) = (S(t)/\tau, 0)^t$, and $\boldsymbol{\eta}(t) = (\eta(t)/\tau, 0)^t$. A single FN model shows a characteristic of an excitable system, namely, it has a stable rest state, and with an appropriate amount of disturbance it generates a pulse with a characteristic magnitude of height and width. The time series of $u(t)$ for $\beta = 0.8$, $\gamma = 0.7$, $\tau = 0.1$, and $S(t) = 0$ with Gaussian white noise characterized by eq. (1.34) for $D = 0.002$ is shown in Fig. 2.1.

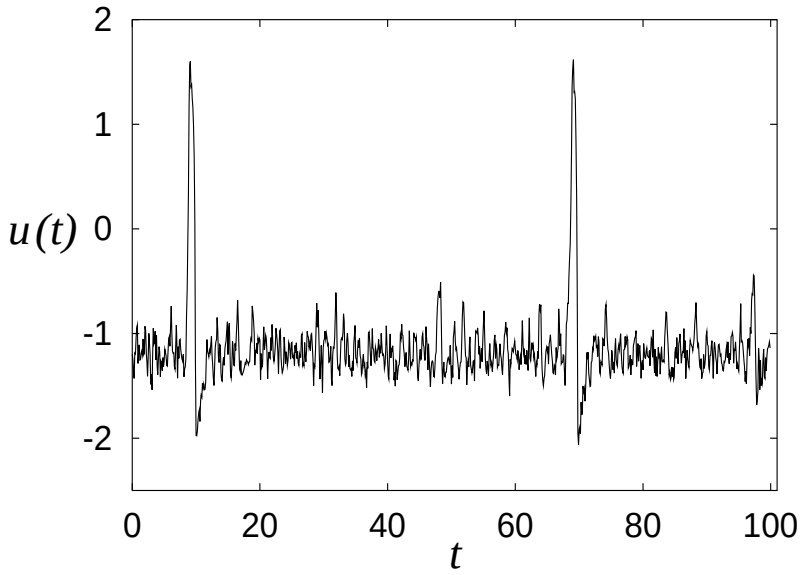

Figure 2.1 A time series of a FN model for $\beta = 0.8$, $\gamma = 0.7$, $\tau = 0.1$, and $S(t) = 0$ with Gaussian white noise characterized by eq. (1.34) for $D = 0.002$.

Besides the FN model, the leaky integrate-and-fire neuron model ($d = 1$) written as eq. (1.15), and the Hodgkin-Huxley neuron model [6] ($d = 4$) are often used by several authors. In the following, we mainly use the FN neuron model.

2.2 Modeling the Network of Spiking Neurons

Let us consider a network of spiking neurons written as

$$\begin{aligned} \frac{d\boldsymbol{x}^{(i)}}{dt} &= \boldsymbol{F}^{(i)}(\boldsymbol{x}^{(i)}) + \boldsymbol{G}^{(i)}(\boldsymbol{x}^{(1)}, \boldsymbol{x}^{(2)}, \cdots, \boldsymbol{x}^{(N)}), \\ i &= 1, 2, \ldots, N, \end{aligned} \tag{2.5}$$

where $\boldsymbol{x}^{(i)} \in \mathbf{R}^d$ is a vector which denotes the internal state of the i-th neuron, and $\boldsymbol{G}^{(i)}$ is the coupling term. The external input and the background fluctuation are omitted for simplicity.

Generally, the connection of neurons is thought to be the sum of the interactions of two neurons. Thus eq. (2.5) can be rewritten as

$$\begin{aligned} \frac{d\boldsymbol{x}^{(i)}}{dt} &= \boldsymbol{F}^{(i)}(\boldsymbol{x}^{(i)}) + \sum_{j=1}^{N} \boldsymbol{G}^{(ij)}(\boldsymbol{x}^{(i)}, \boldsymbol{x}^{(j)}), \\ i &= 1, 2, \ldots, N, \end{aligned} \tag{2.6}$$

where $\boldsymbol{G}^{(ij)}$ is the coupling term between the i-th neuron and the j-th neuron.

Depending on the mathematical expression of $\boldsymbol{G}^{(ij)}$, the couplings of the network are classified into two groups, namely, the electrical coupling and the chemical coupling.

2.3 Electrical Coupling

The coupling term of the electrical coupling is written as

$$\boldsymbol{G}^{(ij)}(\boldsymbol{x}^{(i)}, \boldsymbol{x}^{(j)}) = W^{(ij)}(\boldsymbol{x}^{(j)} - \boldsymbol{x}^{(i)}), \tag{2.7}$$

where $W^{(ij)}$ is a diagonal matrix with diagonal components $W_1^{(ij)}, W_2^{(ij)}, \cdots, W_d^{(ij)}$. This type of coupling is also called as the diffusive coupling and often used to model the high-dimensional dynamical system.

Physiologically, the electrical coupling is realized by the so-called electrical synapse, at which the electrical current is transfered directly to the postsynaptic neuron through the gap junction [11].

The electrical synapse is analogous to the electric circuit. Let us consider a circuit composed of resistances and capacitances shown in Fig. 2.2. From Kirchhoff's current

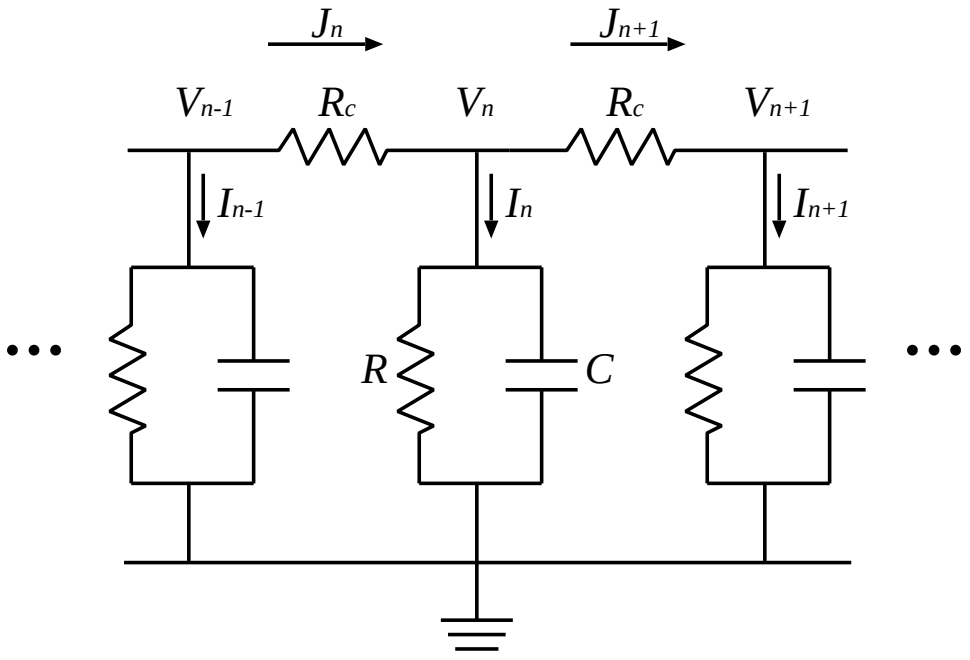

Figure 2.2 An electric circuit model.

law and voltage law, the following relationships hold.

$$I_n = \frac{V_n}{R} + C\frac{dV_n}{dt}, \tag{2.8}$$

$$I_n = J_n - J_{n+1}, \tag{2.9}$$

$$J_n = \frac{1}{R_c}(V_{n-1} - V_n), \tag{2.10}$$

$$J_{n+1} = \frac{1}{R_c}(V_n - V_{n+1}). \tag{2.11}$$

Substituting eqs. (2.9), (2.10), and (2.11) for (2.8), a differential equation

$$\frac{dV_n}{dt} = -\frac{1}{RC}V_n + \frac{1}{R_cC}\sum_{j=n-1,n+1}(V_j - V_n), \tag{2.12}$$

is derived. This equation denotes the dynamics of a chain of the electrically coupled leaky integrate-and-fire neurons without the spiking mechanism (1.16). Thus the electrical coupling can be understood as the coupling mediated by the resistance (or conductance).

The network with electrical couplings has the following properties [11]:

- Most electrical synapses do not exhibit rectification, but conduct in both directions;
- Even subthreshold fluctuations are transfered to the postsynaptic neuron;
- There is no characteristic delay unlike the chemical synapse;
- The velocity of the information transfer is very fast. Thus it is often observed in the system related to the escape from danger, for example, nerve fibers in the nerve cord of the crayfish, and motoneurons in the spinal cord of the frog;
- The electrical coupling can synchronize the elements in the network. The electrical fish utilizes this property to generate electricity.

2.4 Chemical Coupling

The coupling term of the chemical coupling is written as

$$\boldsymbol{G}^{(ij)}(\boldsymbol{x}^{(i)}, \boldsymbol{x}^{(j)}) = W^{(ij)} \sum_{k:t_j^k<t} \boldsymbol{K}^{(ij)}(t - t_j^k - \delta^{(ij)}), \tag{2.13}$$

where t_j^k is the k-th firing time of the j-th neuron, $\delta^{(ij)}$ is the sum of the delay from the j-th neuron to the i-th neuron, and $\boldsymbol{K}^{(ij)}(t)$ is the waveform of the post synaptic potential (PSP) from the j-th neuron to the i-th neuron.

Note that the information from the presynaptic neuron is transfered to the postsynaptic neuron only when the presynaptic neuron emit a spike, and its transfer is accompanied with a particular delay $\delta^{(ij)}$.

In Fig. 2.3, a schematic diagram of the delay in the network with the chemical coupling is shown. At the time $t = t_j^k$, a pulse is emitted from the j-th neuron, and it arrives at a synapse after the transmission delay, which is the time for a pulse to propagate on the axon. The conduction velocity of a pulse is known to be about $1 \sim 10$ [m/s] [62, 63], thus, if the length of the axon is 100 [μm], the transmission delay is about

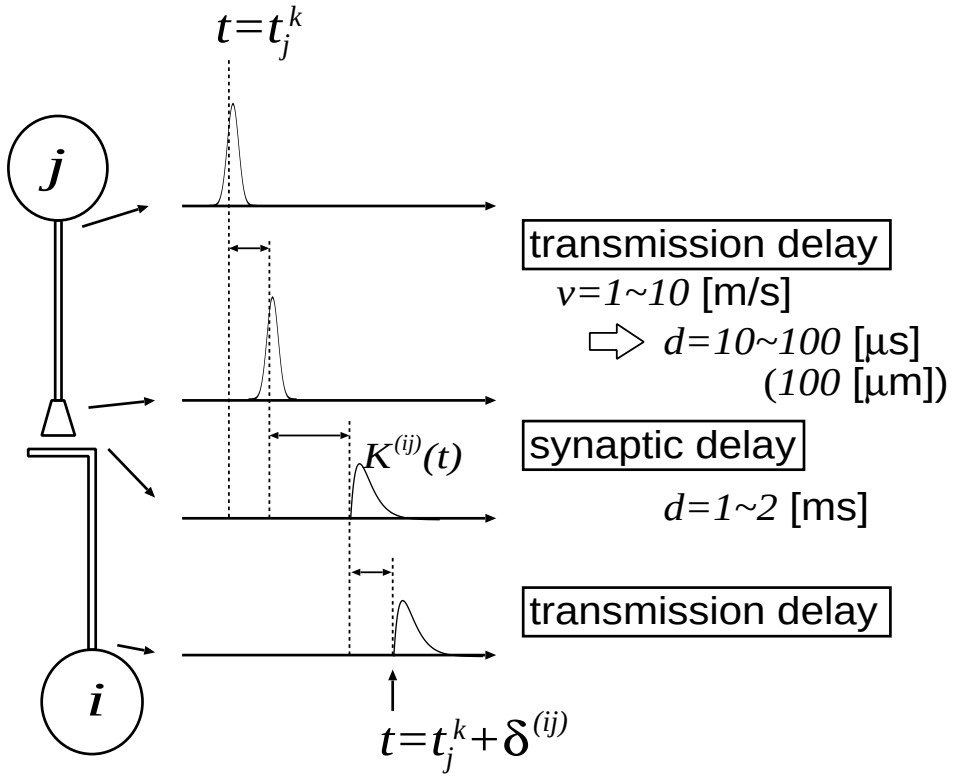

Figure 2.3 A schematic diagram of the delay in the network with chemical coupling.

$10 \sim 100$ [μs]. Then the chemical transmitters are released from the synapse to the dendrite of the postsynaptic neuron, and, as a result, an EPSP (or IPSP) is generated at the dendrite. This process takes about $1 \sim 2$ [ms] and this delay is called as the synaptic delay [11]. The EPSP arrives at the soma of the postsynaptic neuron after the sub-millisecond transmission delay. Thus the delay $\delta^{(ij)}$ is the sum of the transmission delays and the synaptic delay, and, as seen above, the synaptic delay is dominant in $\delta^{(ij)}$.

The properties of the chemical coupling are as follows:

- There is a particular synaptic delay;
- The information is not transfered without the presynaptic pulse;
- It is observed in the wide area of the brain.

Chapter 3

Organization of This Thesis

3.1 Purpose

This thesis is devoted to the understanding of the roles of fluctuations in pulsed neural networks. As shown in Chap. 1, the environment where the biological neurons operate has several sources of fluctuations, thus their effects cannot be neglected in analyzing the behavior of the biological neuronal networks.

Recently, it is reported that the fluctuations in some nonlinear systems bring the beneficial effects to the system, for example, the noise-induced order [65] and the noise-induced entrainment of oscillators [66]. Particularly, stochastic resonance (SR) is a phenomenon where the input to the system is enhanced by its background fluctuations [67, 68, 69, 70]. It is proposed that the biological sensory neuron utilizes SR to detect the weak signals for escaping from enemies, and some physiological experiments reinforce this hypothesis. If the fluctuations are beneficial to a single sensory neuron, they might work effectively also in coupled sensory systems and in cortical neural networks.

We investigate the dynamics of the networks of spiking neurons where the fluctuations work effectively, and discuss its possibility in the neural system. The two groups of the networks are considered, namely, the network with electrical couplings and the network with chemical couplings. The former is the model of sensory systems, and the latter is the model of cortical neural networks. The roles of fluctuations in the system are discussed in each case.

3.2 Organization of This Thesis

In Part II, the network with electrical couplings is treated.

In Chap. 4, the network composed of the electrically coupled FitzHugh-Nagumo neurons without delays is analyzed. The periodic input pulse train and Gaussian white noise which models the fluctuations in the system are added to the system. The system shows the typical property of stochastic resonance, namely, the existence of the optimal fluctuation intensity which maximizes the correlation between the input and the output, and it is observed that the optimal fluctuation intensity increases with the increase of

the coupling strength. Using this property, we construct a network which processes the input signal by controlling the fluctuation intensity.

In Chap. 5, the system treated in Chap. 4 is analyzed again. It is observed that the correlation coefficient takes a maximum as a function of not only the fluctuation intensity but also the coupling strength. This phenomenon called array-enhanced stochastic resonance is theoretically analyzed in this chapter.

In Chap. 6, the network composed of the electrically coupled FitzHugh-Nagumo neurons with a delay is treated, and the results similar to the previous chapters are observed.

In Part III, the network with chemical couplings is treated.

In Chap. 7, the associative memory in the network of chemically coupled FitzHugh-Nagumo neurons is treated, and it is found that the memory retrieval is realized by adding the fluctuations to the system. This fluctuation-induced memory retrieval is analyzed with a one-dimensional map. Moreover, it is also found that the alternate retrieval of two patterns is realized in our network.

In Chap. 8, the associative memory in the network storing sparse patterns with hierarchical correlations is treated. It is observed that the target pattern and the OR pattern are retrieved individually by controlling the fluctuation intensity.

Conclusions and discussions are given in the final chapter in Part IV.

Part II

Dynamics of the Network with Electrical Couplings

Chapter 4

Stochastic Resonance in the Network without Delays

4.1 Introduction

In noisy nonlinear systems, stochastic resonance (SR) is a well-known phenomenon where a weak periodic signal is enhanced by its background fluctuations and observed in many nonlinear systems, such as bistable ring lasers, semiconductor devices, chemical reactions, and neural systems (for reviews, see Refs. [67, 68, 69, 70]). When a periodic signal and fluctuations are injected to such systems simultaneously, the signal to noise ratio (SNR) of the output signal is maximized at an optimal fluctuation intensity.

As shown in Chap. 1, the neural system has several sources of fluctuations, thus SR may play a significant role. The theoretical works on SR in a single neuron are performed on the integrate-and-fire model [71], the leaky integrate-and-fire model [72, 73], the FitzHugh-Nagumo model [74, 75, 76], and the Hodgkin-Huxley model [77, 92]. In those works, it is observed that the output SNR [75, 77, 92] or the peak height of the interspike interval distribution [71, 72, 73, 74] takes a maximum as a function of the fluctuation intensity. Some physiological experiments reinforce the hypothesis that the neural system utilizes SR to detect weak signals [78, 79, 80, 81, 82]. In Ref. [78], sinusoidally stimulated mechanoreceptor cells of a crayfish with additive fluctuations show the property of SR, namely, the existence of the optimal fluctuation intensity which maximizes the output SNR. In Ref. [79], SR is observed in caudal photoreceptor interneurons of a crayfish by intrinsic and not external fluctuations.

SR in spatially extended systems is also investigated and some new features are demonstrated [88, 89, 90, 91, 92]. In Ref. [89], the dependence of the normalized power norm, which measures the correlation between the aperiodic input and the output of the system, on the fluctuation intensity by increasing the number of neuron models composing the system is investigated. In Ref. [92], the dependence of SR on the input frequency in a coupled system is suggested to be important for the neural information processing.

In this chapter, based on Ref. [93], we shall consider SR in the single FitzHugh-Nagumo model and in an electrically coupled FitzHugh-Nagumo model. The background

fluctuations are modeled by Gaussian white noise and added to the system. For a single neuron, the dependence of SR on the input frequency is considered, and the eigenfrequency of the neuron is defined. For a coupled system, we shall consider a network with a superimposed periodic pulse train, namely, a sum of three periodic pulse trains with mutually irrational frequencies and show the system can separate three periodic pulse trains by controlling the fluctuation intensity.

4.2 SR in the single FN Model

As a model of a neuron, we use the FitzHugh-Nagumo model written as

$$\tau \frac{du}{dt} = -v + u - \frac{u^3}{3} + S(f;t) + \eta(t), \tag{4.1}$$

$$\frac{dv}{dt} = u - \beta v + \gamma, \tag{4.2}$$

$$S(f;t) = \begin{cases} S_0 & \text{if } n/f \le t \le n/f + h \ \ (n = 0, 1, 2, \cdots) \\ 0 & \text{otherwise} \end{cases}, \tag{4.3}$$

$$\langle \eta(t)\eta(t') \rangle = D\delta(t - t'), \tag{4.4}$$

where $S(f;t)$ is a periodic pulse train with height S_0, width h, and frequency f, and $\eta(t)$

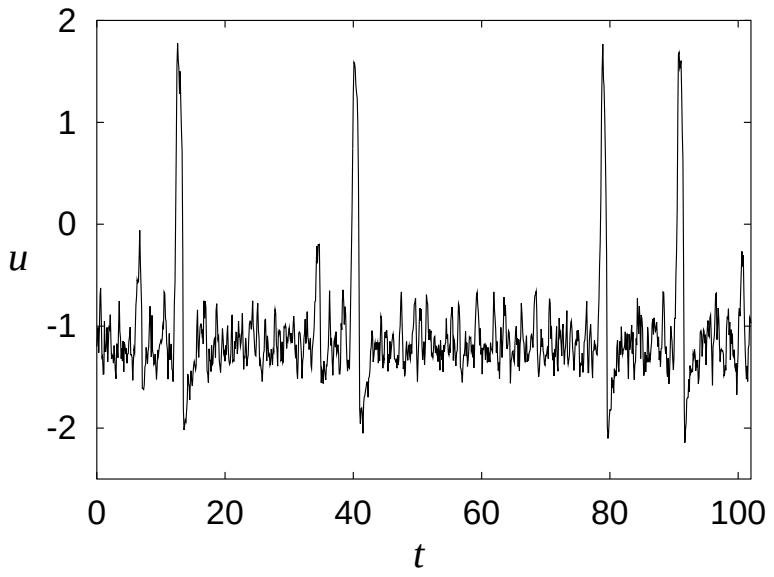

Figure 4.1 A time series of u for $S_0 = 0.1$, $f = 0.5$ and $D = 0.003$.

is Gaussian white noise with intensity D which models the fluctuations in the system. In the following, parameter values $\beta = 0.8$, $\gamma = 0.7$, $\tau = 0.1$, and $h = 0.3$ are mainly

used, and the pulse height S_0 is set small so that the system does not generate a pulse without a certain amount of fluctuations, namely, the input pulse is sub-threshold.

To numerically integrate the stochastic differential equations (4.1) and (4.2), we use the following procedure. Applying the fourth-order Runge-Kutta algorithm [103] to the deterministic part of the equation, namely, eqs. (4.1) and (4.2) with $\eta(t) = 0$, the data $u(t)$ and $v(t)$ at the time t are evolved into $u_{rk}(t + \Delta t)$ and $v_{rk}(t + \Delta t)$, respectively, where Δt is the time step of the numerical integration and the value $\Delta t = 0.01$ is mainly used in the following. To incorporate the effect of $\eta(t)$, $\sqrt{D\Delta t}\, G(0, 1)$ is added to $u_{rk}(t + \Delta t)$, where $G(0, 1)$ is a random number following Gaussian distribution with the mean 0 and the variance 1. The value $D\Delta t$ of the variance is determined from the following calculation.

$$\left\langle \left(\int_0^{\Delta t} \eta(t)\, dt \right)^2 \right\rangle = \int_0^{\Delta t} \int_0^{\Delta t} dt dt' \langle \eta(t)\eta(t') \rangle, \tag{4.5}$$

$$= \int_0^{\Delta t} \int_0^{\Delta t} dt dt' D\delta(t - t'), \tag{4.6}$$

$$= D\Delta t. \tag{4.7}$$

Thus the time-evolved data $u(t + \Delta t)$ and $v(t + \Delta t)$ are determined as $u_{rk}(t + \Delta t) + \sqrt{D\Delta t}\, G(0, 1)$ and $v_{rk}(t + \Delta t)$, respectively.

Under the above conditions, a typical time series of u for $S_0 = 0.1$, $f = 0.5$ and $D = 0.003$ is shown in Fig. 4.1. When u takes a larger value than 1, we call that the system *fires*. The system cannot fire without fluctuations because of the smallness of S_0,

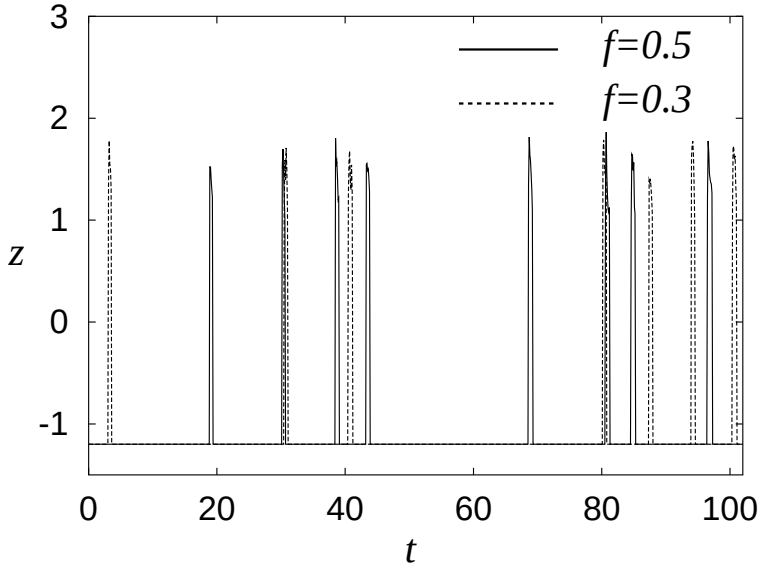

Figure 4.2 Time series of z for $f = 0.5$ and 0.3 with $S_0 = 0.1$ and $D = 0.003$.

but Fig. 4.1 indicates that it can fire with the help of fluctuations. Let us assume that only the firing of the system can be observed, and regard

$$z(t) = \Theta(u(t)) \equiv \begin{cases} u(t) & \text{if } u(t) > 1.0 \\ u_{eq} = -1.2 & \text{otherwise} \end{cases} \tag{4.8}$$

as the output of the system, where u_{eq} is the equilibrium value of $u(t)$ for $S(f;t) = \eta(t) = 0$. Note that u_{eq} is a solution of a cubic equation

$$u^3 + 3pu + q = 0, \tag{4.9}$$

$$p = \frac{1-\beta}{\beta}, \tag{4.10}$$

$$q = \frac{3\gamma}{\beta}, \tag{4.11}$$

derived from eqs. (4.1) and (4.2) with $du/dt = dv/dt = 0$, $S(f;t) = 0$, and $\eta(t) = 0$, and it is analytically solved as

$$u_{eq} = \left(\frac{-q + \sqrt{q^2 + 4p^3}}{2}\right)^{\frac{1}{3}} + \left(\frac{-q - \sqrt{q^2 + 4p^3}}{2}\right)^{\frac{1}{3}}. \tag{4.12}$$

In Fig. 4.2, time series of $z(t)$ are shown for $f = 0.5$ and 0.3 with $S_0 = 0.1$ and $D = 0.003$. Because all the peak heights of $z(t)$ are almost identical for each frequency, only the timing of the firing is essential in $z(t)$.

To measure the correlation between the input $S(f;t)$ and the output $z(t)$, we define three measures, namely, the signal-to-noise ratio (SNR), the correlation coefficient C, and the mutual information I.

First, let us define SNR. The power spectrum $P(f)$ of the output $z(t)$ is defined as

$$P(f) = \lim_{T\to\infty} \frac{1}{T} \left| \int_0^T z(t) e^{i2\pi f t}\, dt \right|^2, \tag{4.13}$$

$$= \lim_{N\to\infty} \frac{\Delta_p}{N} \left| \sum_{n=0}^{N-1} z(n\Delta_p) e^{i2n\pi f \Delta_p} \right|^2, \tag{4.14}$$

where Δ_p is the time step to derive $P(f)$. Using the fast Fourier transform (FFT) algorithm [103], $P(f)$ is numerically derived for $S_0 = 0.1$, $f = 0.5$, $D = 0.003$, $N = 2^{13}$, and $\Delta_p = 0.1$, and shown in Fig. 4.3, which shows a sharp peak at the frequency f of the input pulse train. The signal to noise ratio (SNR) is defined as the ratio of the peak value S at the input frequency f and the power N of background noise, namely

$$\text{SNR} = S/N, \tag{4.15}$$

which is often used to measure the correlation between the periodic input and the output in the literature of SR [67, 68, 69, 70].

Next, let us define the correlation coefficient C between the input and output pulse trains [100]. To incorporate the effect of the firing delay d_f of the FN model, which is

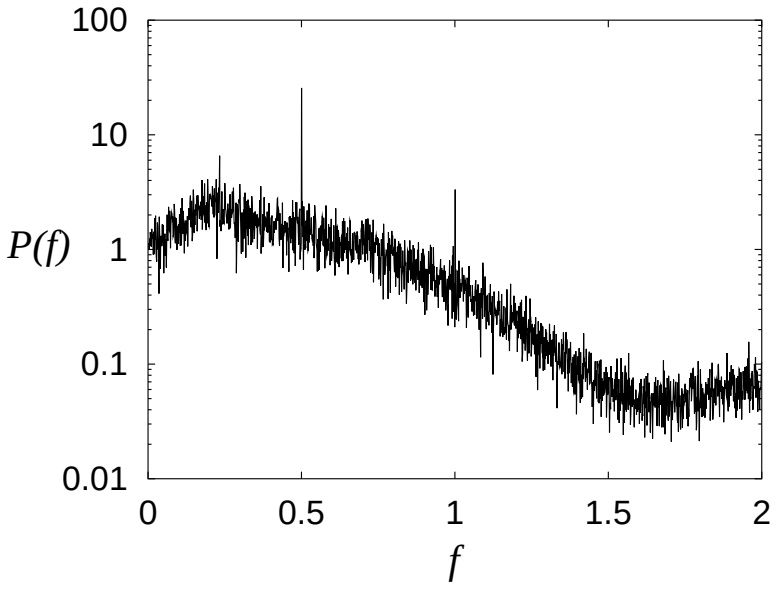

Figure 4.3 The power spectrum $P(f)$ of the output $z(t)$ for $S_0 = 0.1$, $f = 0.5$, $D = 0.003$, $N = 2^{13}$, and $\Delta_p = 0.1$.

the time lag of the firing since an input pulse is injected, the shift $t \to t - d_f$ is applied to the time series of the output pulse train. Then the time series are divided into n bins of the width Δ_b, and the number of pulses in the i-th bin is denoted as X_i and Y_i for the input and output pulses, respectively. Note that the width Δ_b is sufficiently small so that X_i and Y_i take the value 0 or 1. Then $X = \sum X_i$ and $Y = \sum Y_i$ are the numbers of input and output pulses respectively, and $Z = \sum X_i Y_i$ is the number of coincident firings. A schematic diagram for the derivation of X, Y, and Z is shown in Fig. 4.4. The correlation coefficient C between the input and output pulse trains is defined as

$$C = \frac{Z - (XY)/n}{\sqrt{X(1 - X/n)Y(1 - Y/n)}} \in [-1, 1]. \tag{4.16}$$

Consider the periodic input with frequency f such that

$$X_i = \begin{cases} 1 & \text{if } \ i\Delta_b \bmod f^{-1} < \Delta_b \\ 0 & \text{otherwise} \end{cases} . \tag{4.17}$$

If the output series Y_i is identical with X_i, namely, if the relation $X_i = Y_i$ is satisfied for all i, the correlation coefficient C takes the value 1. If the output series Y_i has no correlation with X_i, the correlation coefficient C takes the value 0 in the large n limit. We set $\Delta_b = 0.5$ in the following.

With the variables X_i, Y_i, and Z_i, we can also define the mutual information I [101, 102]. The empirical distributions $P(Y_i)$ and $P(Y_i|X_i)$ are defined as

$$P(Y_i = 1) \ = \ \frac{Y}{n}, \tag{4.18}$$

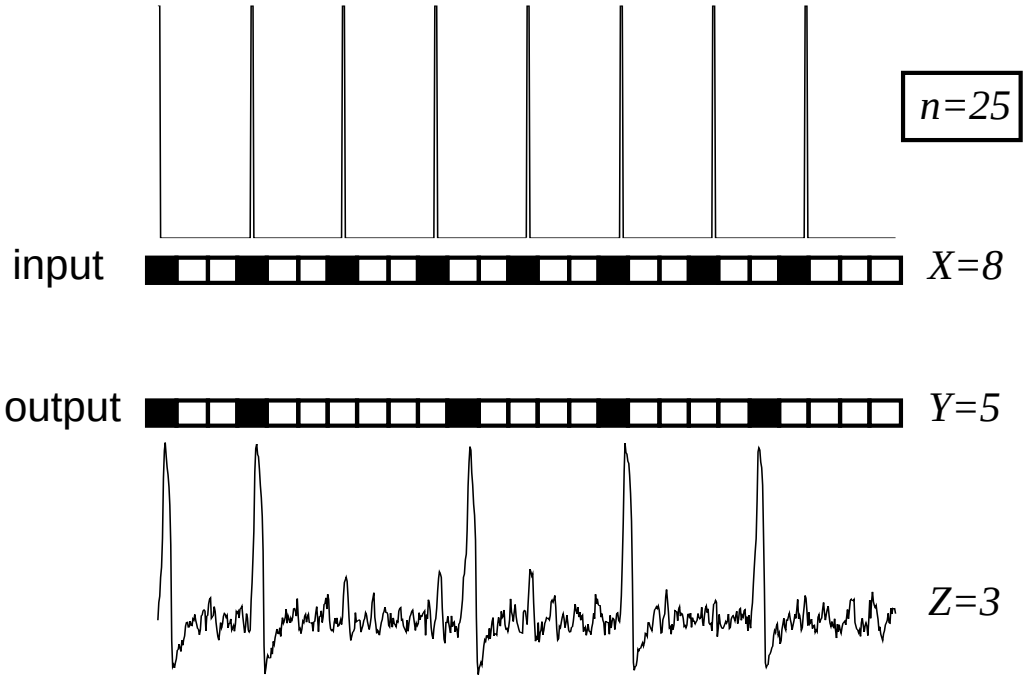

Figure 4.4 A schematic diagram for the derivation of X, Y, and Z.

$$P(Y_i = 0) = 1 - \frac{Y}{n}, \tag{4.19}$$

$$P(Y_i = 1|X_i = 1) = \frac{Z}{X}, \tag{4.20}$$

$$P(Y_i = 0|X_i = 1) = 1 - \frac{Z}{X}, \tag{4.21}$$

$$P(Y_i = 1|X_i = 0) = \frac{Y - Z}{n - X}, \tag{4.22}$$

$$P(Y_i = 0|X_i = 0) = 1 - \frac{Y - Z}{n - X}. \tag{4.23}$$

Then the mutual information is defined as

$$I(X_i; Y_i) = H(Y_i) - H(Y_i|X_i), \tag{4.24}$$

$$H(Y_i) = -\sum_{Y_i \in \{0,1\}} P(Y_i) \log_2 P(Y_i), \tag{4.25}$$

$$H(Y_i|X_i) = -\sum_{X_i, Y_i \in \{0,1\}} P(Y_i, X_i) \log_2 P(Y_i|X_i). \tag{4.26}$$

Using SNR, the correlation coefficient C, and the mutual information I, we measure the correlation between the input and output in the system, and investigate their dependences on the fluctuation intensity D. In Fig. 4.5, SNR, C, and I are plotted against the

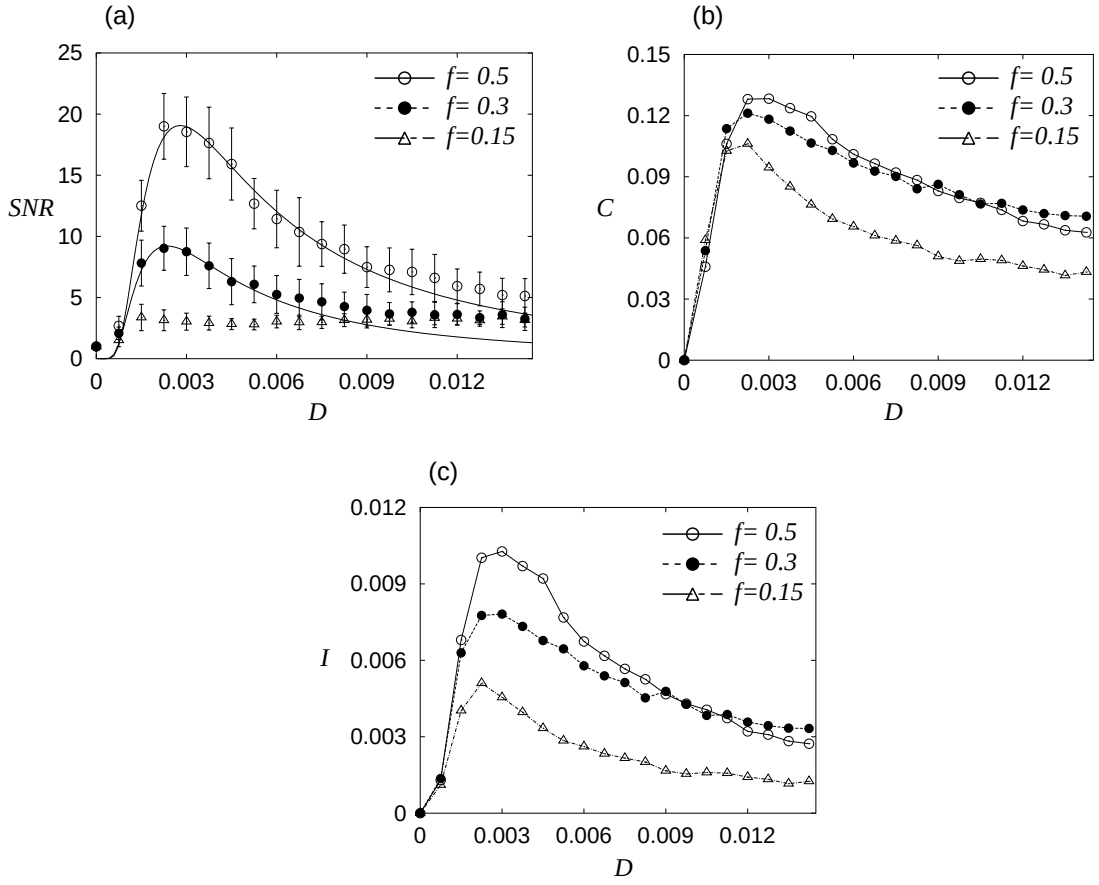

Figure 4.5 The dependences of (a) SNR, (b) the correlation coefficient C, and (c) the mutual information I on the fluctuation intensity D for $S_0 = 0.1$ with $f = 0.15$, 0.3, and 0.5. Each measure has a maximum at the optimal fluctuation intensity about $D \simeq 0.003$. The lines in (a) are the fitting curves given by eq. (4.27) and the error bars denote the standard deviation for 50 samples.

fluctuation intensity D for $f = 0.15$, 0.3, and 0.5 with $S_0 = 0.1$. All the measures show the typical behavior of SR, namely, the existence of the optimal fluctuation intensity which maximizes the measures.

In many systems, it is reported that the dependence of SNR on the fluctuation intensity D obeys the relation

$$\mathrm{SNR} = \frac{A}{D^2} \exp\left(-\frac{B}{D}\right), \tag{4.27}$$

where A and B are constants which depend on system parameters [67, 68, 69, 70]. SNR

takes its maximum at $D = D_0$ given by

$$D_0 = \frac{B}{2}. \tag{4.28}$$

The fitting curves in Fig. 4.5(a) for $f = 0.3$ and 0.5 indicate that the eq. (4.27) is also valid for small D in the FN model [75].

Figure 4.5 also shows that the peak height of each measure depends on the input frequency f. This dependence is investigated in the next section. The optimal fluctuation intensity also depends on f, and this dependence is investigated by several authors [73, 76, 77]. But this dependence is very weak and depends also on the measure, as shown in Fig. 4.5. Thus we do not treat this subject in this paper.

4.3 The Dependence of SR on the Input Frequency

In this section, we examine the dependence of SR on the input frequency f for fixed parameter values $S_0 = 0.1$ and $D = 0.003$. As shown in Fig. 4.6, each measure takes a maximum value at a frequency in the range from 0.5 to 0.6. This frequency preference may be due to the classical resonance phenomenon between the input frequency and the sub-threshold time scale of the FN model. An analytical derivation of this optimal frequency is difficult and it depends also on the measure as shown in Fig. 4.6. In the following, we call the frequency which maximizes the correlation coefficient C as the eigenfrequency f_e of this model only for convenience, and we treat only the correlation coefficient C to measure the correlation between the input and output, but the similar results are obtained also for other measures.

In Fig. 4.6(b), it is observed that the eigenfrequency of this model is $f_e \simeq 0.5$. The eigenfrequency f_e depends on the system parameters, β, γ, and τ, and the waveform of the input. For a fixed input waveform, by changing the values of β, γ, and τ the eigenfrequency f_e can be adjusted by a series of numerical experiments and the system is denoted by the value of its eigenfrequency as neuron f_e. We prepare the three kinds of neurons f_1, f_2 and f_3, which satisfy the relationships $f_1 \simeq 0.5$, $f_2 = f_1/\sqrt{2} \simeq 0.35$, and $f_3 = f_1/\sqrt{5} \simeq 0.22$ for convenience in the following sections. The dependence of C on the input frequency of each neuron f_1, f_2 and f_3 for $D = 0.003$ is shown in Fig. 4.7(a). It is observed that the peak of each C is located at each eigenfrequency.

The dependence of C on the fluctuation intensity D for each neuron f_i with the input frequency f_i equal to its eigenfrequency, is plotted in Fig. 4.7(b). It is observed that each neuron has almost the same optimal fluctuation intensity $D_0 \simeq 0.003$.

4.4 SR in an Electrically Coupled System

In this section, we treat an electrically, *i.e.*, diffusively coupled FitzHugh-Nagumo model, written as

$$\tau_i \frac{du_i}{dt} = -v_i + u_i - \frac{u_i^3}{3} + S(f;t) + \eta_i(t) + \frac{1}{N}\sum_{j=1}^{N} w_{ij}(u_j - u_i), \tag{4.29}$$

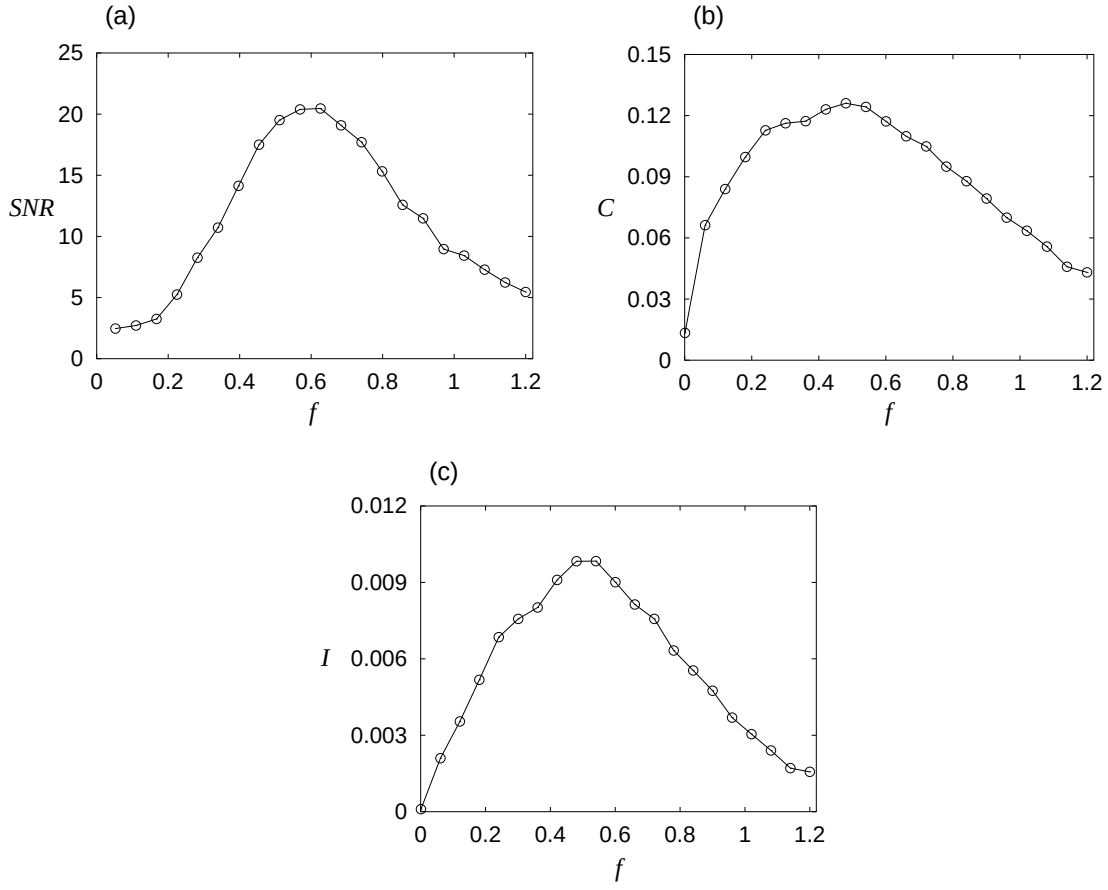

Figure 4.6 The dependence of (a) SNR, (b) the correlation coefficient C, and (c) the mutual information I on the input frequency f for $S_0 = 0.1$ and $D = 0.003$.

$$\frac{dv_i}{dt} = u_i - \beta_i v_i + \gamma_i, \tag{4.30}$$

$$\langle \eta_i(t)\eta_j(t')\rangle = D\delta_{ij}\delta(t-t'), \tag{4.31}$$

for $i = 1, 2, \cdots, N$, where β_i, γ_i, and τ_i are system parameters of the i-th neuron and δ_{ij} denotes Kronecker's delta. Note that the connection of each neuron is electrical, the periodic pulse train $S(f;t)$ is applied to all the neurons, and fluctuations for different neurons are statistically independent.

Firstly, let us examine the effect of the coupling strength w_{ij}. For $N = 2$, $\beta_1 = \beta_2 = 0.8$, $\gamma_1 = \gamma_2 = 0.7$, $\tau_1 = \tau_2 = 0.1$ and $w_{12} = w_{21} = w$, since the behaviors of the two neurons may be statistically identical by the symmetry of the system, only $z_1 \equiv \Theta(u_1)$ is observed as the output.

In Fig. 4.8, The correlation coefficient C is plotted against D for $w = 0$, 0.2, and 1.0, with $S_0 = 0.1$ and $f = 0.5$. Similarly to the one neuron case, each C has a maximum,

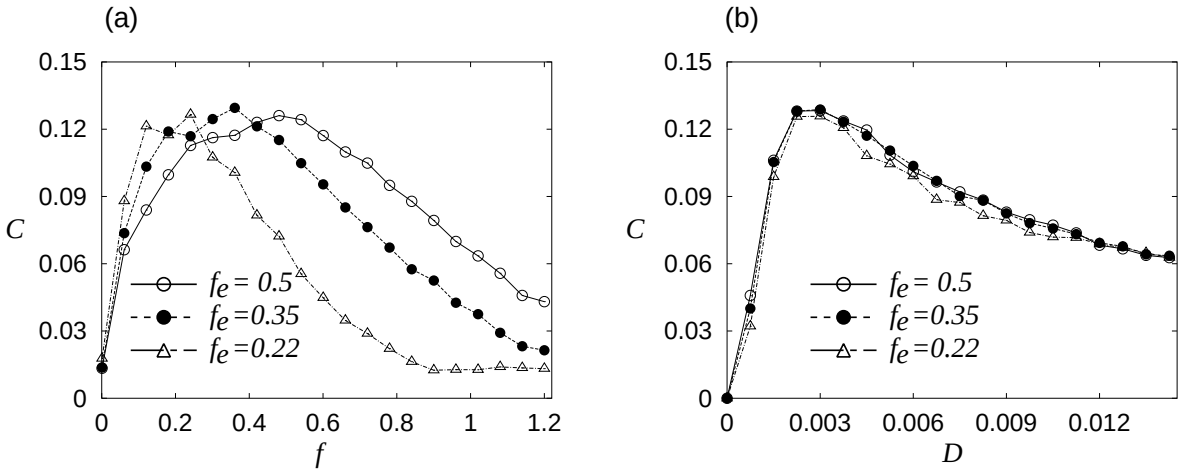

Figure 4.7 (a) The dependence of C on the input frequency f for the three kinds of neurons with the eigenfrequencies f_e=0.22, 0.35, and 0.5, where $S_0 = 0.1$ and $D = 0.003$. (b) The dependence of C on the fluctuation intensity D for the three kinds of neurons with the eigenfrequencies f_e=0.22, 0.35, and 0.5 with $S_0 = 0.1$. Each input frequency to the neurons is set for each eigenfrequency.

but the optimal fluctuation intensities D_0's take different values depending on w. In Fig. 4.9, the optimal fluctuation intensity $D_0(w)$ for the coupling strength w is plotted against w. It is observed that $D_0(w)$ is an increasing function of w and converges to $D_0(\infty) \simeq 0.0055$.

To analyze the dependence of $D_0(\infty)$ on N generally, let us consider a coupled system composed of N oscillating neurons. For $i = 1, 2, \cdots, N$, by introducing $\boldsymbol{x}^{(i)} = (x_1^{(i)}, x_2^{(i)}, \cdots, x_d^{(i)})^t$, $\boldsymbol{\eta}^{(i)} = (\eta_1^{(i)}, \eta_2^{(i)}, \cdots, \eta_d^{(i)})^t$, and a d-dimensional diagonal matrix A with positive diagonal components $A_1, \cdots, A_d$, a coupled system is written as

$$\frac{d\boldsymbol{x}^{(i)}}{dt} = \boldsymbol{F}(\boldsymbol{x}^{(i)}) + wA\left(\frac{1}{N}\sum_{j=1}^{N}\boldsymbol{x}^{(j)} - \boldsymbol{x}^{(i)}\right) + \boldsymbol{\eta}^{(i)}, \tag{4.32}$$

$$\langle \eta_k^{(i)}(t)\eta_l^{(j)}(t')\rangle = D_k\delta_{ij}\delta_{kl}\delta(t-t'), \tag{4.33}$$

$$i, j = 1, 2, \cdots, N, \text{ and } k, l = 1, 2, \cdots, d,$$

where $\boldsymbol{F}(\boldsymbol{x}^{(i)})$ generates the internal motion of the i-th neuron and w denotes the coupling strength. Let us define the mean value $\boldsymbol{X}$ and the deviation $\delta\boldsymbol{x}^{(i)}$ from $\boldsymbol{X}$ as

$$\boldsymbol{X} = \frac{1}{N}\sum_i \boldsymbol{x}^{(i)}, \tag{4.34}$$

$$\delta\boldsymbol{x}^{(i)} = \boldsymbol{x}^{(i)} - \boldsymbol{X}, \tag{4.35}$$

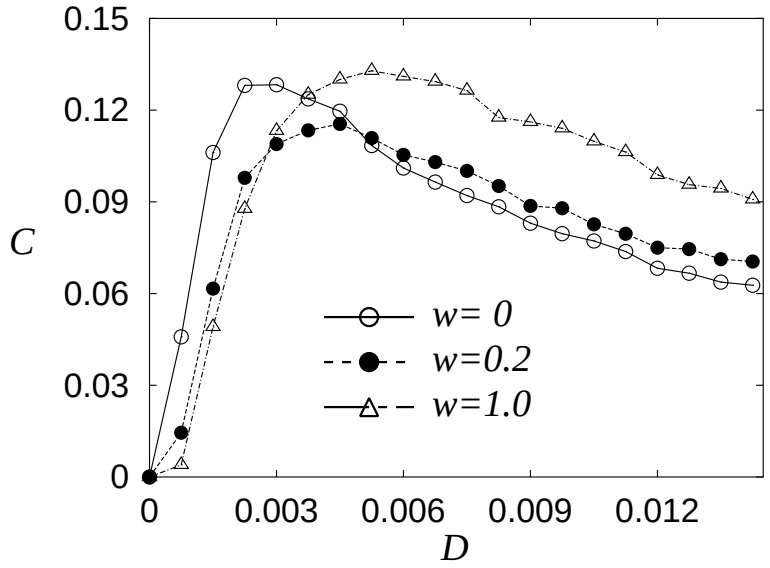

Figure 4.8 The correlation coefficient C against D for $w = 0$, 0.2, and 1.0, with $S_0 = 0.1$ and $f = 0.5$.

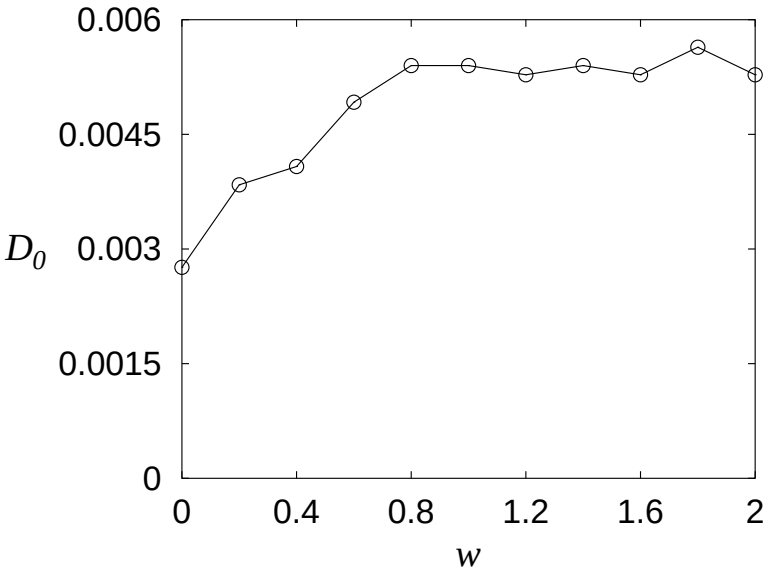

Figure 4.9 The optimal fluctuation intensity D_0 against w for $S_0 = 0.1$ and $f = 0.5$.

then $\boldsymbol{X}$ and $\delta\boldsymbol{x}^{(i)}$ obey

$$\frac{d\boldsymbol{X}}{dt} = \boldsymbol{F}(\boldsymbol{X}) + \sum_{i=1}^{N} \frac{\boldsymbol{\eta}^{(i)}}{N} + O(|\delta\boldsymbol{x}^{(i)}|^2), \tag{4.36}$$

$$\frac{d}{dt}\delta\boldsymbol{x}^{(i)} = (D\boldsymbol{F}(\boldsymbol{X}) - wA)\,\delta\boldsymbol{x}^{(i)} + \boldsymbol{\eta}^{(i)} - \sum_{j=1}^{N}\frac{\boldsymbol{\eta}^{(j)}}{N} + O(|\delta\boldsymbol{x}^{(i)}|^2), \tag{4.37}$$

where $D\boldsymbol{F}(\boldsymbol{x})$ is the Jacobian matrix of $\boldsymbol{F}(\boldsymbol{x})$. In the large w limit, eq. (4.37) becomes

$$\frac{d}{dt}\delta\boldsymbol{x}^{(i)} = -wA\delta\boldsymbol{x}^{(i)} + \boldsymbol{\eta}^{(i)} - \sum_{j=1}^{N}\frac{\boldsymbol{\eta}^{(j)}}{N}, \tag{4.38}$$

thus the variance of $\delta\boldsymbol{x}^{(i)}$ is estimated to be

$$\langle(\delta x_k^{(i)})^2\rangle \simeq \frac{(1-N^{-1})D_k}{2wA_k}. \tag{4.39}$$

Equations (4.35), (4.36), and (4.39) indicate that the dynamics of each neuron for large w approaches to the dynamics of the single neuron with the scaled fluctuation intensity D_k/N $(k = 1, 2, \cdots, d)$.

For the coupled FitzHugh-Nagumo model with uniform coupling, $d = 2$, $A_1 = 1/\tau$, $A_2 = 0$, $D_1 = D/\tau^2$, $D_2 = 0$, and eq. (4.38) is modified to

$$\frac{d}{dt}\delta x_1^{(i)} = -\frac{w}{\tau}\delta x_1^{(i)} + \eta_1^{(i)} - \sum_{j=1}^{N}\frac{\eta_1^{(j)}}{N}, \tag{4.40}$$

$$\frac{d}{dt}\delta x_2^{(i)} = \delta x_1^{(i)} - \beta\delta x_2^{(i)}. \tag{4.41}$$

Thus the variance of $\delta x_2^{(i)}$ can be estimated to be

$$\langle(\delta x_2^{(i)})^2\rangle \simeq \frac{\langle(\delta x_1^{(i)})^2\rangle}{\beta(\beta + \tau^{-1}w)}, \tag{4.42}$$

$$\sim \frac{1}{w^2}, \tag{4.43}$$

and it can be concluded that the dynamics of each neuron for large w is governed by eq. (4.36). Thus, between the optimal fluctuation intensity $D_0^{(N)}(\infty)$ for N neurons and $D_0^{(1)}(\infty)$ for a single neuron, the relation

$$D_0^{(N)}(\infty) = ND_0^{(1)}(\infty) \tag{4.44}$$

holds. As shown in Fig. 4.10, numerically observed $D_0^{(N)}(\infty)$ shows a good agreement with eq. (4.44). The asymptotic value $D_0^{(N)}(\infty)$ is estimated by $D_0^{(N)}(w)$ with $w = 2.0$, which is large enough for the saturation of $D_0(w)$ (see Fig. 4.9).

As shown in eq. (4.36), for finite w, the intensity of the effective fluctuation on the mean motion $\boldsymbol{X}$ depends on $\delta\boldsymbol{x}^{(i)}$. Since the magnitude of $\delta\boldsymbol{x}^{(i)}$ is thought to be a decreasing function of w, the effective fluctuation intensity is also a decreasing function of w leading to a conclusion that the optimal fluctuation intensity $D_0(w)$ is an increasing function of w as shown in Fig. 4.9. Further analysis on $D_0(w)$ is a future work.

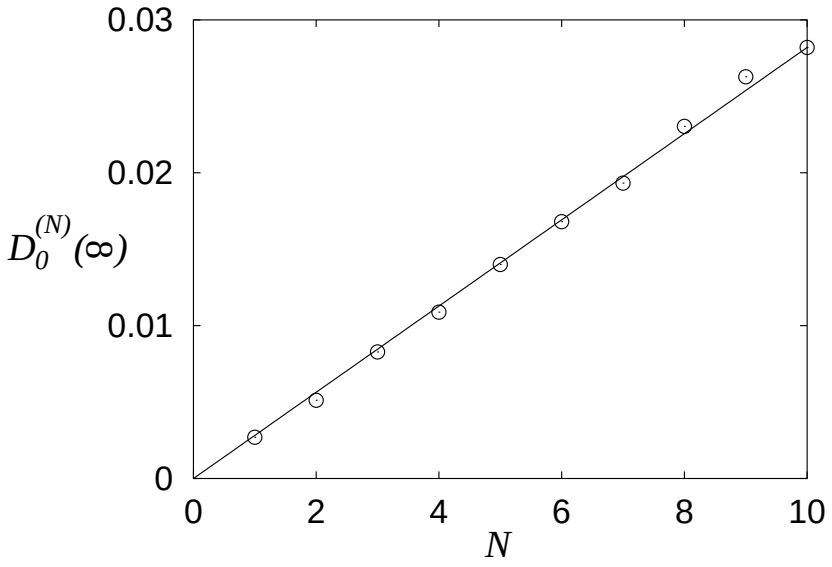

Figure 4.10 The dependence of the asymptotic value $D_0^{(N)}(\infty)$ of the optimal fluctuation intensity on the number N of neurons.

4.5 Separation of a Superimposed Periodic Pulse Train

Using the preceding properties of SR, we construct a network which can separate a superimposed periodic pulse train (SPPT) by tuning the fluctuation intensity.

Let us define SPPT as

$$T(t) = \max_{1 \le k \le m} S(f_k; t), \tag{4.45}$$

where m is the number of periodic components and f_k is the frequency of each component. In the following, we set $m = 3$, $f_1 = 0.5$, $f_2 = f_1/\sqrt{2}$, and $f_3 = f_1/\sqrt{5}$. As shown in Fig. 4.11, the SPPT $T(t)$ is applied to the network composed of three subnetworks, where each subnetwork contains ten neurons with the eigenfrequency f_k and the coupling strength w_k $(k = 1, 2, 3)$, that is, each subnetwork is governed by eqs. (4.29) and (4.30) with $N = 10$, $w_{ij} = w_k$, and $T(t)$ instead of $S(f; t)$. Note that $T(t)$ and the statistically independent fluctuations with the same intensity D are applied to all the thirty neurons, and the output $Z(t)$ of the network is defined as

$$Z(t) = \sum_{k=1}^{3} z_1^{(k)}(t) = \sum_{k=1}^{3} \Theta(u_1^{(k)}(t)), \tag{4.46}$$

where $z_1^{(k)}$ is the output of the k-th subnetwork.

The correlation coefficients C_k's $(k = 1, 2, 3)$ which measure the correlations between $Z(t)$ and the periodic pulse trains with frequency f_k are plotted against the fluctuation

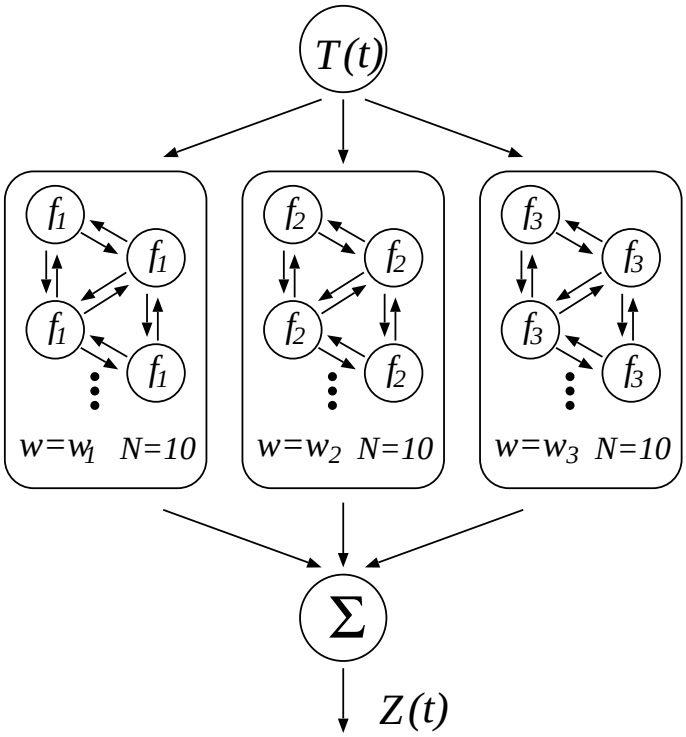

Figure 4.11 A network composed of thirty neurons.

intensity D for $w_1 = w_2 = w_3 = 0$ in Fig. 4.12, and we observe that the optimal fluctuation intensities are almost identical for the three frequencies. It is because the optimal fluctuation intensities of all the neurons are almost identical for $w_1 = w_2 = w_3 = 0$.

On the other hand, as shown in Fig. 4.13, each C_k has the different optimal fluctuation intensity for $w_1 = 2.0$, $w_2 = 0.8$, and $w_3 = 0.6$. If the fluctuation intensity D is set around 0.008, 0.015, or 0.04, then the output signal $Z(t)$ is dominated by a periodic motion with the frequency f_3, f_2, or f_1, respectively, since, at each fluctuation intensity, the correlation coefficient at the corresponding frequency is superior compared with those at the other frequencies. Thus a separation of SPPT by controlling the fluctuation intensity is realized.

This result implies that the fluctuations cannot only enhance weak signals, but also control the response of the system.

4.6 Results and Discussions

Using the properties of SR in a coupled system, a new feature in a noisy neural network is reported. In the case of a single neuron, the existence of the optimal fluctuation intensity and the optimal input frequency is observed in the single FitzHugh-Nagumo model. The former is a common characteristic of the conventional SR phenomena, and the latter is caused by the classical resonance between the input frequency and the

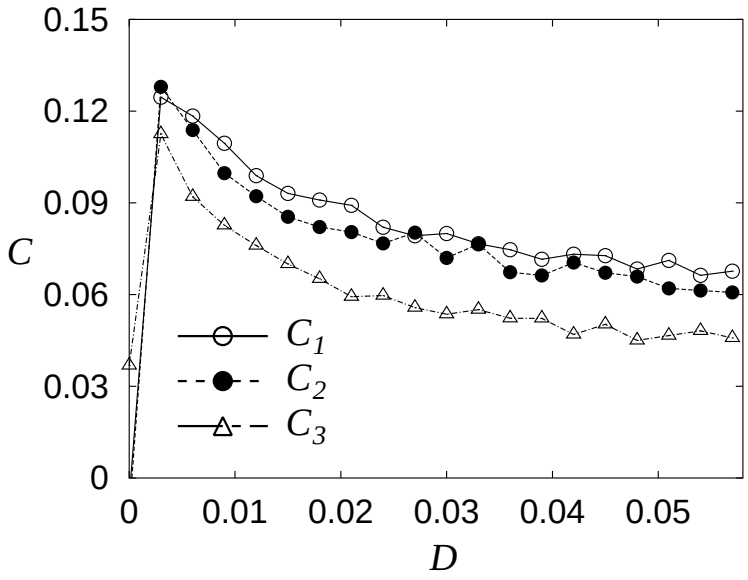

Figure 4.12 The correlation coefficients of each frequency for $S_0 = 0.1$ and $w_1 = w_2 = w_3 = 0$.

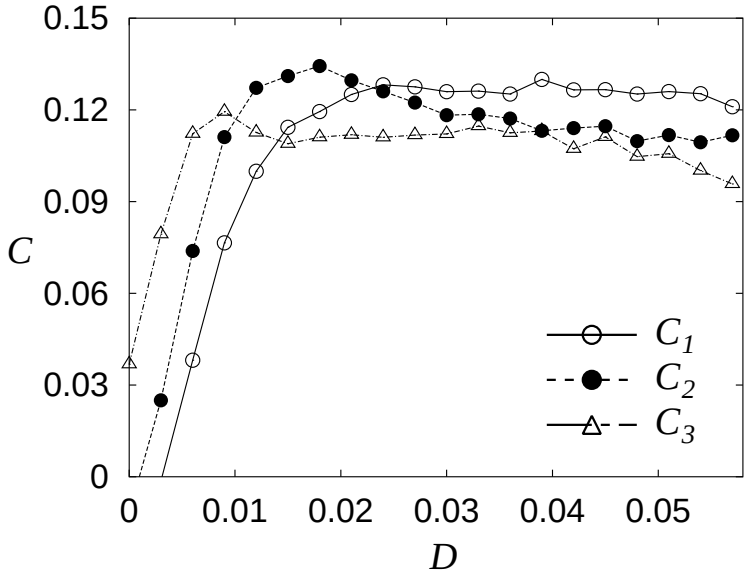

Figure 4.13 The correlation coefficient of each frequency for $S_0 = 0.1$, $w_1 = 2.0, w_2 = 0.8$ and $w_3 = 0.6$.

sub-threshold time scale of the FitzHugh-Nagumo model. The optimal frequency can

be controlled by parameters of the system. In the case of the two neurons, the optimal fluctuation intensity is found to be an increasing function of the coupling strength and the relationship between its saturation value and the number of coupled neurons is derived analytically. Using this property, a network composed of thirty neurons, which can separate a superimposed periodic pulse train by controlling the fluctuation intensity, is constructed. In Ref. [89], Collins *et al.* considered an ensemble of the FitzHugh-Nagumo models, and examined the dependence of the normalized power norm, which measures the correlation between the aperiodic input and the output of the system, on the fluctuation intensity. They found the flattening of the normalized power norm for sufficiently large number of neurons in the ensemble, and suggested that the sensory systems could detect weak signals without tuning the fluctuation intensity. Similar results, that is, the increase of the optimal fluctuation intensity with the magnitude of coupling strength (Fig. 4.9) and with the number of neurons (Fig. 4.10), are observed in our numerical experiments, but the separation of SPPT suggests that the fluctuation intensity might control the response of the system and play a similar role to a parameter of dynamical systems.

In the problem of the information processing in the brain, the question of what carries the information in the brain is controversial. From physiological experiments, a single neuron is known to operate under a very noisy environment and its response seems to be stochastic, thus it might be natural to assume that the information is coded in the firing rate of a single neuron or an ensemble of neurons. On the other hand, there is a hypothesis called temporal coding, which claims that the information is coded spatio-temporally by the temporal formation of cell assemblies whose neurons are spiking correlatively [99]. Because the exact timing of spiking is important for the temporal coding, it seems to be difficult to construct a network composed of physiological stochastic neurons, which communicate using the temporal coding. But the fluctuation-induced enhancement of the correlation between the input and the output, which is one of the properties of SR, may make the temporal coding possible. Although we have treated periodic inputs and Gaussian white noise, SR is observed for aperiodic inputs [85, 86, 87, 89], for colored noise [74, 76, 87], and for the fluctuations in the sum of presynaptic inputs [83, 84, 85, 86]. Thus there is a possibility that SR plays an important role in the neural information processing.

Chapter 5

Array-Enhanced Stochastic Resonance

5.1 Introduction

As shown in Fig. 4.8, the peak value C_{peak} of the correlation coefficient C also depends on the coupling strength w, and it is known that C_{peak} takes a maximum against the coupling strength w for systems with the large number N of neurons. Such a phenomenon where the correlation between the input and the output takes a maximum as a function of not only the fluctuation intensity but also the coupling strength is called array-enhanced stochastic resonance (AESR) and observed in some nonlinear systems [95, 96, 97].

The term AESR is introduced by Linder et al. [96] to describe the enhancement of the output SNR of a chain of periodically driven damped oscillators, and they found that the degree of synchronization of the elements is also maximized when the output SNR is optimized. Similar phenomenon is also observed in a circuit of diode resonators [97].

Though the above researches treat only the system with periodic inputs, it it known that the coupling of the elements also enhances the "coherence" and the degree of synchronization of the elements of the system without the common periodic signal, and this phenomenon is called array-enhanced coherence resonance [98]. Thus the array-enhancement is thought to be the universal phenomenon independent of the input.

In this chapter, we consider the mechanism of AESR in the electrically coupled FitzHugh-Nagumo model. In Sec. 5.2, the properties of AESR are introduced, namely, the scaling of the optimal fluctuation intensity in the large coupling limit, and the enhancement of the correlation between the input and the output caused by the coupling. In Secs. 5.3 and 5.4, we transform the dynamics of the network of N neurons into that of the mean dynamics $\boldsymbol{X}$ and the deviation $\delta\boldsymbol{x}^{(i)}$, and construct the models which describe AESR. It is found that AESR is caused by the correlation between the mean dynamics $\boldsymbol{X}$ and the deviation $\delta\boldsymbol{x}^{(i)}$. In Sec. 5.5, we investigate the characteristics of the fluctuations of the deviation $\delta\boldsymbol{x}^{(i)}$ and consider why the model deviates from the dynamics of the network of N neurons. Results and discussions are given in the final section.

5.2 AESR in the Electrically Coupled FN model

In this chapter, we treat the electrically coupled FitzHugh-Nagumo model governed by eqs. (4.1), (4.2), (4.3), and (4.4) again. The parameters are fixed at $S_0 = 0.1$, $h = 0.3$, and $f = 0.5$.

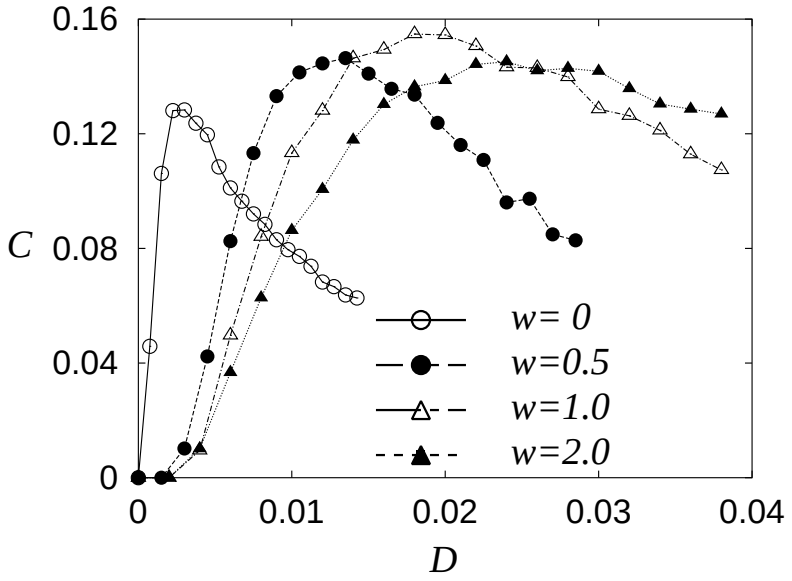

Figure 5.1 The dependence of the correlation coefficient C on the fluctuation intensity D for $w = 0$, 0.5, 1.0, and 2.0 with $N = 10$.

The dependence of the correlation coefficient C on the fluctuation intensity D for $w = 0$, 0.5, 1.0, and 2.0 with $N = 10$ is shown in Fig. 5.1. The data for each w shows the typical property of stochastic resonance, namely, the existence of the maximum of the correlation coefficient C as a function of the fluctuation intensity D. It is also observed that the optimal fluctuation intensity D_0 increases with the increase of the coupling strength w, and the maximum value C_{peak} of C depends on w.

The dependence of the optimal fluctuation intensity D_0 on the coupling strength w for $N = 10$, 50, and 100 is shown in Fig. 5.2. For large w, it is observed that D_0 converges to the value dependent on the number N of neurons. As shown in Chap. 4, the asymptotic value $D_0^{(N)}(\infty)$ of the optimal fluctuation intensity for the network of N neurons satisfies

$$D_0^{(N)}(\infty) = N D_0^{(1)}(\infty). \tag{5.1}$$

The dependence of C_{peak} on the coupling strength w for $N = 10$, 50, and 100 is shown in Fig. 5.3, and it is observed that C_{peak} takes a maximum as a function of w. This phenomenon where the correlation between the input and the output takes a maximum as a function of not only the fluctuation intensity but also the coupling strength is called

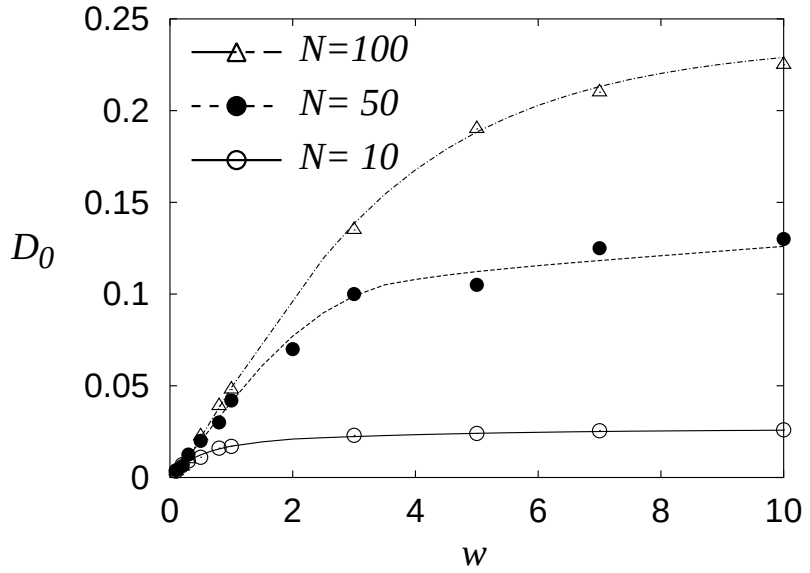

Figure 5.2 The dependence of the optimal the fluctuation intensity D_0 on the coupling strength w for $N = 10$, 50, and 100.

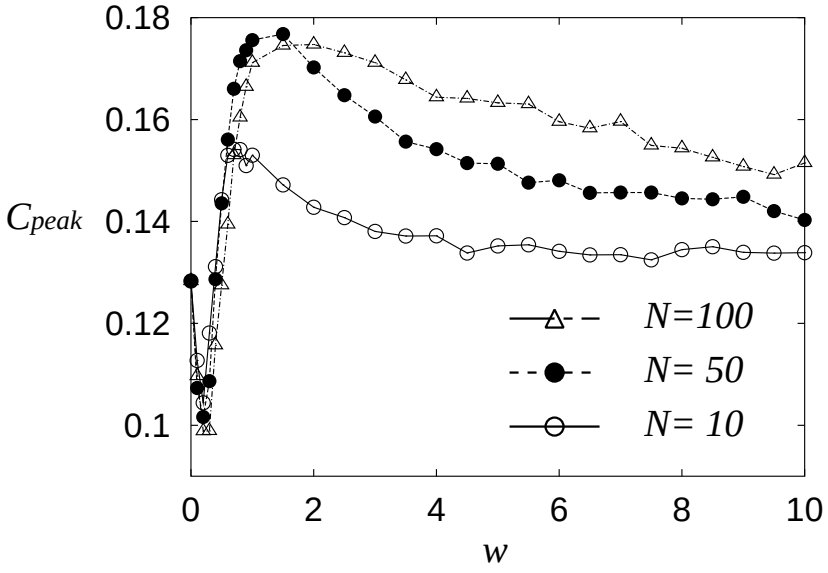

Figure 5.3 The dependence of the maximum value C_{peak} of the correlation coefficient C on the coupling strength w for $N = 10$, 50, and 100.

array-enhanced stochastic resonance (AESR) and observed in some nonlinear systems

[95, 96, 97].

In the following sections, we analyze the mechanism of AESR in the electrically coupled FitzHugh-Nagumo model.

5.3 Model of AESR: Approximation 1

To analyze the mechanism of AESR, the dynamics of the coupled FN model composed of N neurons is rewritten as

$$\begin{aligned}
\frac{d\boldsymbol{x}^{(i)}}{dt} &= \boldsymbol{F}(\boldsymbol{x}^{(i)}) + \frac{w}{\tau} A\left(\boldsymbol{X} - \boldsymbol{x}^{(i)}\right) + \frac{1}{\tau}\boldsymbol{\eta}^{(i)}, && (5.2)\\
\boldsymbol{X} &= \frac{1}{N}\sum_{i=1}^{N} \boldsymbol{x}^{(i)}, && (5.3)\\
\langle \eta_i(t)\eta_j(t')\rangle &= D\delta_{ij}\delta(t-t'), && (5.4)\\
i, j &= 1, 2, \cdots, N,
\end{aligned}$$

where $\boldsymbol{x}^{(i)} = (x_1^{(i)}, x_2^{(i)})^t = (u_i, v_i)^t$, $\boldsymbol{\eta}^{(i)} = (\eta_i, 0)^t$, and A is a two dimensional diagonal matrix with diagonal components $A_1 = 1$ and $A_2 = 0$. Note that $\boldsymbol{F}(\boldsymbol{x}^{(i)}) = (F_1(\boldsymbol{x}^{(i)}), F_2(\boldsymbol{x}^{(i)}))^t$ with

$$\begin{aligned}
F_1(\boldsymbol{x}^{(i)}) &= \frac{1}{\tau}\left(-v_i + u_i - \frac{u_i^3}{3} + S(f;t)\right), && (5.5)\\
F_2(\boldsymbol{x}^{(i)}) &= u_i - \beta v_i + \gamma, && (5.6)
\end{aligned}$$

denotes the internal motion of the i-th neuron. Let us define the deviation $\delta\boldsymbol{x}^{(i)}$ of the i-th neuron from the mean dynamics $\boldsymbol{X}$ as

$$\delta\boldsymbol{x}^{(i)} = \boldsymbol{x}^{(i)} - \boldsymbol{X}. \tag{5.7}$$

As shown in Sec. 4.4, the variables $\boldsymbol{X}$ and $\delta\boldsymbol{x}^{(i)}$ obey

$$\begin{aligned}
\frac{d\boldsymbol{X}}{dt} &= \boldsymbol{F}(\boldsymbol{X}) + \frac{1}{\tau N}\sum_{i=1}^{N}\boldsymbol{\eta}^{(i)} + O(|\delta\boldsymbol{x}^{(i)}|^2), && (5.8)\\
\frac{d}{dt}\delta\boldsymbol{x}^{(i)} &= \left(D\boldsymbol{F}(\boldsymbol{X}) - \frac{w}{\tau}A\right)\delta\boldsymbol{x}^{(i)} + \frac{1}{\tau}\left(\boldsymbol{\eta}^{(i)} - \frac{1}{N}\sum_{j=1}^{N}\boldsymbol{\eta}^{(j)}\right) + O(|\delta\boldsymbol{x}^{(i)}|^2), && (5.9)
\end{aligned}$$

where $D\boldsymbol{F}(\boldsymbol{x})$ is the Jacobian matrix of $\boldsymbol{F}(\boldsymbol{x})$. In the large w limit, eq. (5.9) becomes

$$\begin{aligned}
\frac{d}{dt}\delta x_1^{(i)} &= -\frac{w}{\tau}\delta x_1^{(i)} + \frac{1}{\tau}\left(\eta_i - \frac{1}{N}\sum_{j=1}^{N}\eta_j\right), && (5.10)\\
\frac{d}{dt}\delta x_2^{(i)} &= \delta x_1^{(i)} - \beta\delta x_2^{(i)}, && (5.11)
\end{aligned}$$

where β is the parameter in eq. (4.2). Thus the variances of $\delta x_1^{(i)}$ and $\delta x_2^{(i)}$ are estimated to be

$$\langle (\delta x_1^{(i)})^2 \rangle \simeq \frac{(1-N^{-1})D}{2\tau w}, \tag{5.12}$$

$$\langle (\delta x_2^{(i)})^2 \rangle \simeq \frac{\langle (\delta x_1^{(i)})^2 \rangle}{\beta(\beta + \tau^{-1} w)}, \tag{5.13}$$

$$\sim \frac{1}{w^2}. \tag{5.14}$$

As shown in eqs. (5.12) and (5.14), $\langle (\delta x_1^{(i)})^2 \rangle$ and $\langle (\delta x_2^{(i)})^2 \rangle$ converge to zero in the large w limit, thus the mean dynamics $\boldsymbol{X}$ approaches to the dynamics of the single neuron governed by eq. (5.8).

To analyze AESR, let us take the quadratic term in eq. (5.8) into consideration. From the definition (5.3), the dynamics of $\boldsymbol{X}$ is written as

$$\frac{d\boldsymbol{X}}{dt} = \frac{1}{N}\sum_{i=1}^{N} \boldsymbol{F}(\boldsymbol{x}^{(i)}) + \frac{1}{\tau N}\sum_{i=1}^{N} \boldsymbol{\eta}^{(i)}, \tag{5.15}$$

$$= \boldsymbol{F}(\boldsymbol{X}) + \frac{1}{\tau N}\sum_{i=1}^{N} \boldsymbol{\eta}^{(i)} + \boldsymbol{\epsilon}, \tag{5.16}$$

where

$$\boldsymbol{\epsilon} \equiv \frac{1}{N}\sum_{i=1}^{N} \boldsymbol{F}(\boldsymbol{x}^{(i)}) - \boldsymbol{F}(\boldsymbol{X}). \tag{5.17}$$

Obviously the second component of the deviation $\boldsymbol{\epsilon}$ is zero, thus we consider only the first component

$$\epsilon = \frac{1}{N}\sum_{i=1}^{N} F_1(\boldsymbol{x}^{(i)}) - F_1(\boldsymbol{X}), \tag{5.18}$$

of $\boldsymbol{\epsilon}$ in the following. From eq. (5.5), the deviation ϵ is calculated to be

$$\epsilon = -\frac{1}{\tau N}\sum_{i=1}^{N} \left(X_1 (\delta x_1^{(i)})^2 + \frac{(\delta x_1^{(i)})^3}{3} \right), \tag{5.19}$$

$$\simeq -\frac{X_1}{\tau N}\sum_{i=1}^{N} (\delta x_1^{(i)})^2, \tag{5.20}$$

$$= -\frac{1}{\tau} X_1 (\delta x_1)^2, \tag{5.21}$$

where

$$(\delta x_1)^2 \equiv \frac{1}{N}\sum_{i=1}^{N} (\delta x_1^{(i)})^2. \tag{5.22}$$

The time series of $(\delta x_1)^2$ and X_1 for $N = 50$, $w = 10$, and $D = 0.125$ are shown in Fig. 5.4. It is observed that $(\delta x_1)^2$ largely fluctuates around its mean value. From eq.

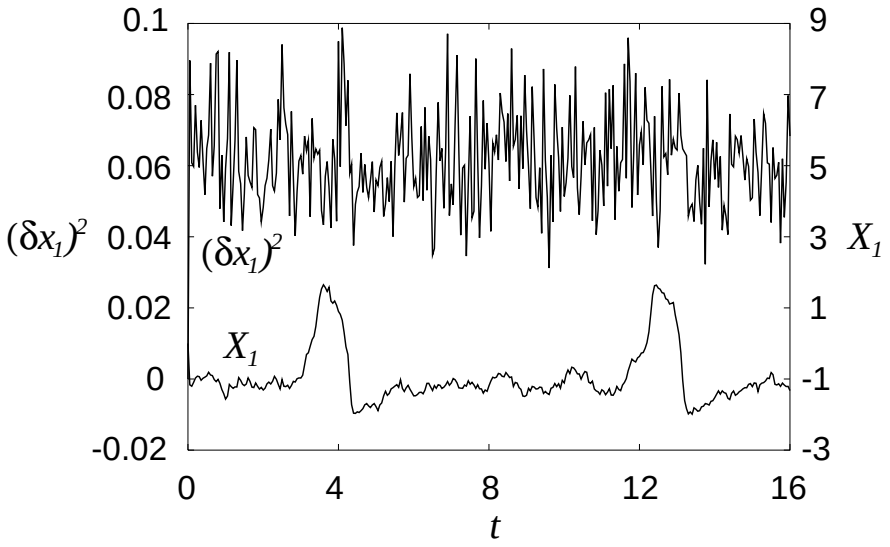

Figure 5.4 The time series of $(\delta x_1)^2$ and X_1 for $N = 50$, $w = 10$, and $D = 0.125$.

(5.12), the expectation $\langle(\delta x_1)^2\rangle$ of $(\delta x_1)^2$ is estimated to be

$$\begin{aligned} \langle(\delta x_1)^2\rangle &= \frac{1}{N}\sum_{i=1}^{N}\langle(\delta x_1^{(i)})^2\rangle, && (5.23)\\ &\simeq \frac{(1-N^{-1})D}{2\tau w}, && (5.24)\\ &\equiv \langle(\delta x_1)^2\rangle_{app1}. && (5.25) \end{aligned}$$

Meanwhile, let us define the numerically obtained mean value $\langle(\delta x_1)^2\rangle_{sim}$ of $(\delta x_1)^2$ as

$$\langle(\delta x_1)^2\rangle_{sim} \equiv \lim_{T\to\infty}\frac{1}{T}\int_0^T(\delta x_1)^2 dt. \tag{5.26}$$

In Fig. 5.5, $\langle(\delta x_1)^2\rangle_{app1}$ and $\langle(\delta x_1)^2\rangle_{sim}$ for $N = 10$ and 50 along the curves in $w - D$ plane in Fig. 5.3 are plotted against w. It is observed that $\langle(\delta x_1)^2\rangle_{app1}$ well describes the behavior of $\langle(\delta x_1)^2\rangle_{sim}$ for large w.

Based on the above discussions, let us describe the mean dynamics $\boldsymbol{X}$ by

$$\begin{aligned} \frac{d\boldsymbol{X}}{dt} &= \boldsymbol{F}(\boldsymbol{X}) + \frac{1}{\tau}\hat{\boldsymbol{\eta}} + \boldsymbol{\epsilon}, && (5.27)\\ \hat{\boldsymbol{\eta}} &\equiv (\hat{\eta}, 0)^t, && (5.28)\\ \boldsymbol{\epsilon} &\equiv \left(-\frac{1}{\tau}X_1\langle(\delta x_1)^2\rangle_{sim}, 0\right)^t, && (5.29)\\ \langle\hat{\eta}(t)\hat{\eta}(t')\rangle &= D/N\delta(t-t'). && (5.30) \end{aligned}$$

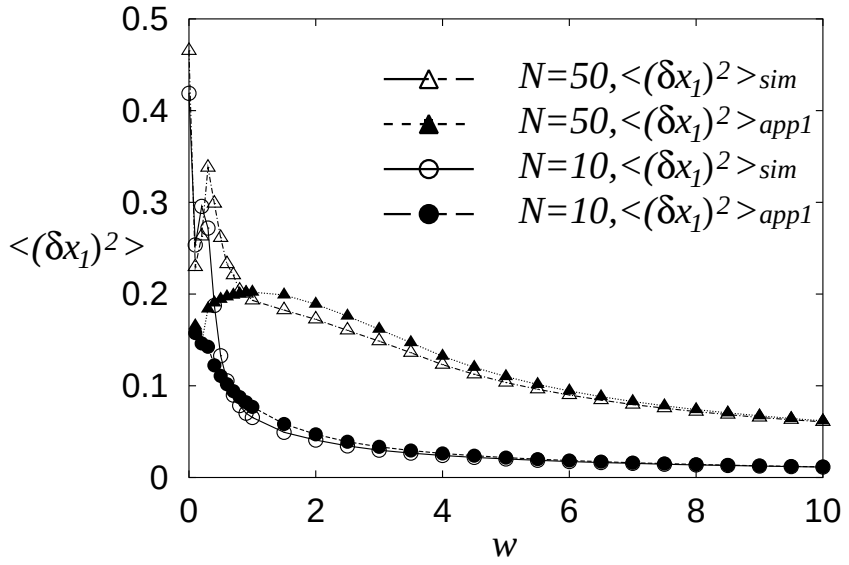

Figure 5.5 The values of $\langle(\delta x_1)^2\rangle_{app1}$ and $\langle(\delta x_1)^2\rangle_{sim}$ for $N = 10$ and 50 along the curves in $w - D$ plane in Fig. 5.3 are plotted against w.

Note that this model is derived by substituting the constant value $\langle(\delta x_1)^2\rangle_{sim}$ for $(\delta x_1)^2$ in eq. (5.21). In the following, the system governed by eqs. (5.27) and (5.29) is called as the approximation 1. The numerical simulations of the approximation 1 are performed as follows:

- Fix a set of values of w and D on the curve in the $w - D$ plane in Fig. 5.2;
- Numerically obtain the value of $\langle(\delta x_1)^2\rangle_{sim}$ for the network of N neurons with the above fixed w and D;
- Obtain the correlation coefficient C for the approximation 1 with the above D and $\langle(\delta x_1)^2\rangle_{sim}$.

The dependences of the peak values C_{peak}'s of the correlation coefficient C on the coupling strength w of the approximation 1 and the network of N neurons are compared in Fig. 5.6. It is observed that the approximation 1 does not show the enhancement of C_{peak}. In other words, the quadratic term $(\delta x_1)^2$ modeled by the constant $\langle(\delta x_1)^2\rangle_{sim}$ cannot reproduce the properties of AESR.

In the next section, we take the correlation between $\langle(\delta x_1)^2\rangle$ and the mean dynamics $\boldsymbol{X}$ into consideration.

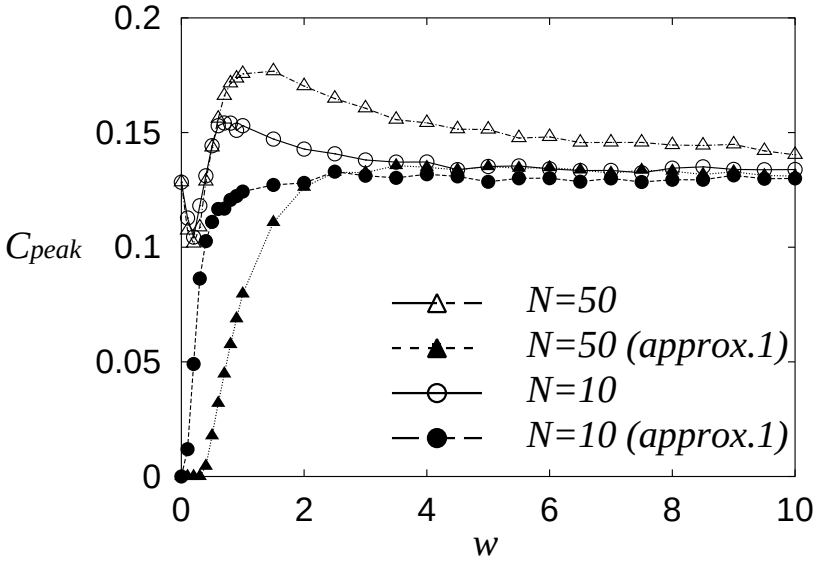

Figure 5.6 The dependences of the peak values C_{peak}'s of the correlation coefficient C on the coupling strength w of the approximation 1 and the network of N neurons.

5.4 Model of AESR: Approximation 2

With the term $D\boldsymbol{F}(\boldsymbol{X})$, eq. (5.9) is modified to

$$\frac{d}{dt}\delta x_1^{(i)} = -\frac{1}{\tau}(w + X_1^2 - 1)\delta x_1^{(i)} - \frac{1}{\tau}\delta x_2^{(i)} + \frac{1}{\tau}\tilde{\eta}_i, \tag{5.31}$$

$$\langle \tilde{\eta}_i(t)\tilde{\eta}_j(t')\rangle = (1 - N^{-1})D\delta_{ij}\delta(t - t'). \tag{5.32}$$

Equation (5.31) indicates that the statistics of $\delta x_1^{(i)}$ depends on the mean dynamics X_1 of the N neurons.

As shown in the Appendix A, for large $(w-1)/\tau > 0$, $\langle(\delta x_1)^2\rangle$ is estimated to be

$$\langle(\delta x_1)^2\rangle_{app2} = \frac{(1 - N^{-1})D}{2\tau(w - 1 + X_1^2)}. \tag{5.33}$$

Note that $\langle(\delta x_1)^2\rangle_{app2}$ is interpreted as the variance of the Ornstein-Uhlenbeck process governed by eq. (5.31) with $\delta x_2^{(i)} = 0$ and the constant X_1.

Let us consider the approximation 2 governed by eq. (5.27) with

$$\boldsymbol{\epsilon} \equiv \left(-\frac{1}{\tau}X_1\langle(\delta x_1)^2\rangle_{app2}, 0\right)^t. \tag{5.34}$$

The dependences of C_{peak}'s of the approximation 2 and network of N neurons on w are shown in Fig. 5.7. It is observed that the enhancement of C_{peak} for $w > 0$ is qualitatively

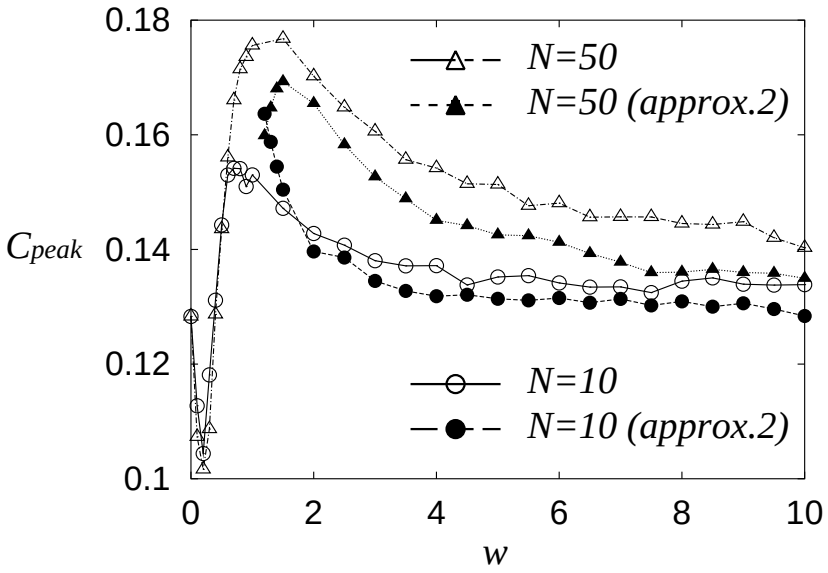

Figure 5.7 The dependences of C_{peak}'s of the approximation 2 and network of N neurons on w.

described by the approximation 2.

From the above discussions, it can be concluded that AESR is caused by the correlation between the term $(\delta x_1)^2$ and the mean dynamics X_1 of N neurons. Let us understand this mechanism by observing the time series of $\langle(\delta x_1)^2\rangle_{app2}$ and X_1 shown in Fig. 5.8. It is observed that $\langle(\delta x_1)^2\rangle_{app2}$ is positively perturbed when the mean dynamics X_1 generates a pulse and when it resets to the equilibrium. This positive perturbation acts as a positive input to the dynamics of X_1 for $X_1 < 0$ through eq. (5.21), thus the enhancement of C_{peak} takes place.

Meanwhile, as shown in Fig. 5.7, C_{peak} of the approximate 2 takes smaller values than that of the network of N neurons even for large w. It might be because the deviation of $(\delta x_1)^2$ from the expectation $\langle(\delta x_1)^2\rangle_{app2}$ is large and cannot be neglected. This effect is considered in the next section.

5.5 Characteristics of Fluctuations of $(\delta x_1)^2$

If the fluctuations of $(\delta x_1)^2$ cause the deviation of the approximation 2 from the network of N neurons, they must enhance C_{peak} of the approximation 2 as shown in Fig. 5.7. However, the fluctuations of $(\delta x_1)^2$ without the correlations with X_1 and $\langle(\delta x_1)^2\rangle$ might lower the values of C_{peak}. In this section, we investigate the characteristics of the fluctuations of $(\delta x_1)^2$, and consider how C_{peak} of the approximation 2 is enhanced.

The time series of the fluctuations of $(\delta x_1)^2$ is shown in Fig. 5.9, and it is observed that the fluctuations have large intensity and cannot be neglected in comparison with

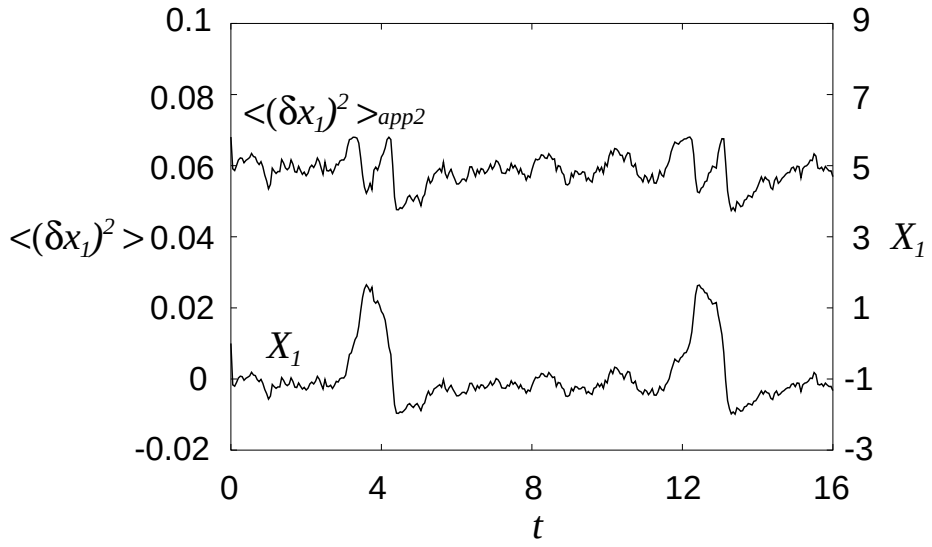

Figure 5.8 The time series of $\langle(\delta x_1)^2\rangle_{app2}$ and the mean dynamics X_1 of N neurons for $N = 50$, $w = 10$, and $D = 0.125$.

$\langle(\delta x_1)^2\rangle_{app2}$.

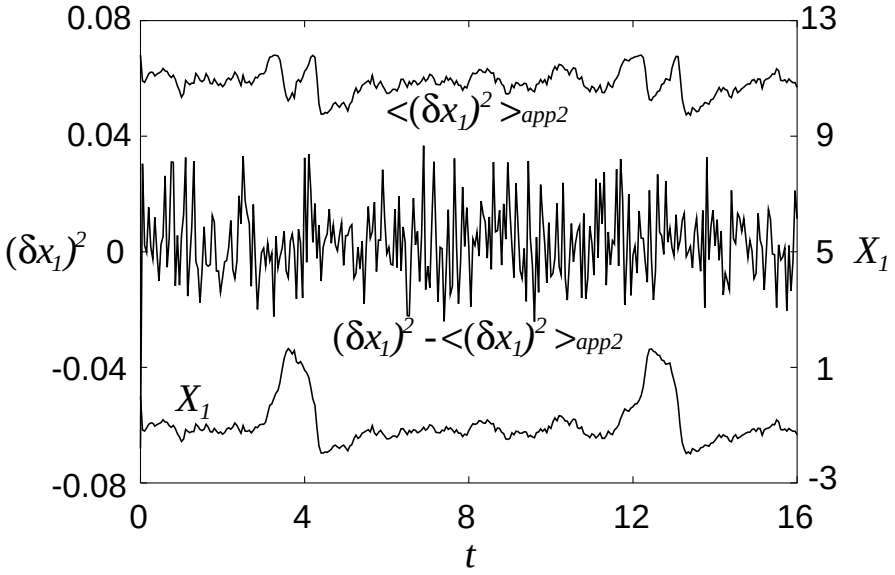

Figure 5.9 The time series of the fluctuations of $(\delta x_1)^2$. The time series of X_1 and $\langle(\delta x_1)^2\rangle_{app2}$ are also shown.

The probability density function of the fluctuations of $(\delta x_1)^2$ is shown in Fig. 5.10. It is observed that it is highly asymmetric, thus the fluctuations of $(\delta x_1)^2$ tend to take large positive values. Note that the large positive fluctuations of $(\delta x_1)^2$ help the mean

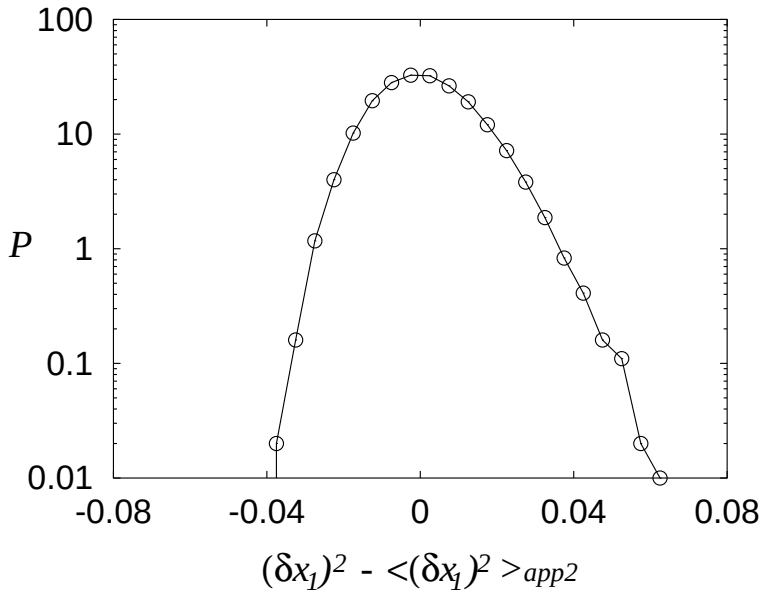

Figure 5.10 The distribution of the fluctuations of $(\delta x_1)^2$.

dynamics X_1 to fire because the term $\propto -X_1(\delta x_1)^2$ in eq. (5.21) gives the positive influences to $X_1(< 0)$ in the equilibrium.

Furthermore, the variance of $(\delta x_1)^2$ is written as

$$\begin{aligned} \mathrm{Var}[(\delta x_1)^2] &= \mathrm{Var}\left[\frac{1}{N}\sum_{i=1}^{N}(\delta x_1^{(i)})^2\right], && (5.35)\\ &\sim \frac{1}{N^2}\sum_{i=1}^{N}\mathrm{Var}\left[(\delta x_1^{(i)})^2\right], && (5.36)\\ &= \frac{1}{N^2}\sum_{i=1}^{N}\left[\langle(\delta x_1^{(i)})^4\rangle - \langle(\delta x_1^{(i)})^2\rangle^2\right]. && (5.37) \end{aligned}$$

With the assumption that the distribution of $(\delta x_1)^2$ is Gaussian, $\langle(\delta x_1^{(i)})^4\rangle$ is written as

$$\langle(\delta x_1^{(i)})^4\rangle = 3\langle(\delta x_1^{(i)})^2\rangle^2, \tag{5.38}$$

thus the variance of $(\delta x_1)^2$ is written as

$$\begin{aligned} \mathrm{Var}[(\delta x_1)^2] &= \frac{2}{N}\langle(\delta x_1^{(i)})^2\rangle^2, && (5.39)\\ &= \frac{2}{N}\left(\frac{(1-N^{-1})D}{2\tau(w-1+X_1^2)}\right)^2. && (5.40) \end{aligned}$$

Equations (5.39) and (5.40) indicate that the fluctuations of $(\delta x_1)^2$ correlate with X_1 and $\langle(\delta x_1)^2\rangle$. As shown in Fig. 5.11, the power-spectrum of the square of the fluctuations of $(\delta x_1)^2$ has peaks at the input frequency $f = 0.5$ and its higher harmonics. These peaks

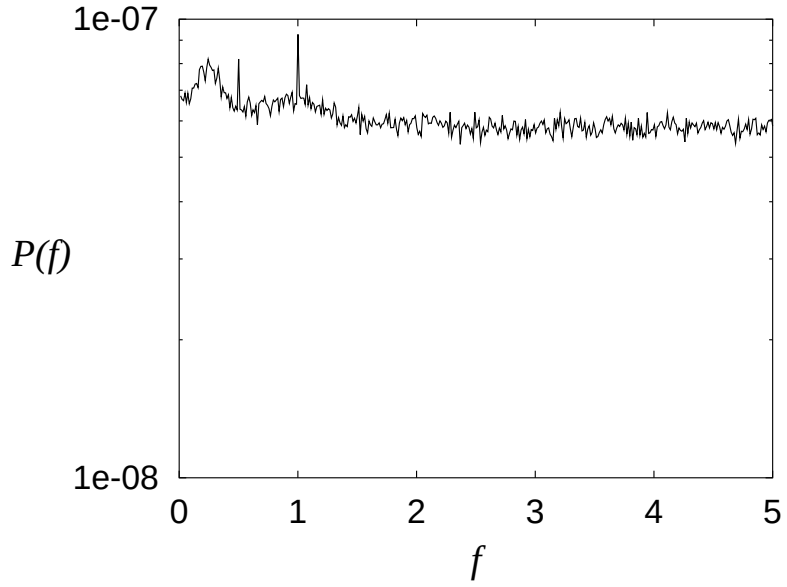

Figure 5.11 The power-spectrum of the square of the fluctuations of $(\delta x_1)^2$.

reflect eq. (5.40) and indicate that the fluctuations of $(\delta x_1)^2$ contain the time scale of X_1. As shown in eqs. (5.39) and (5.40), the fluctuations of $(\delta x_1)^2$ take large value when $\langle(\delta x_1)^2\rangle$ is large, thus it can be concluded that the fluctuations of $(\delta x_1)^2$ helps the mean dynamics X_1 to fire when X_1 positively deviates from the equilibrium $X_1 \simeq -1.2$.

The above characteristics, namely, the asymmetry of the distribution and the correlation between the fluctuations of $(\delta x_1)^2$ and X_1, cause the deviation of the approximation 2 from the network of N neurons.

On the other hand, the deviation of the approximation 2 from the network of N neurons becomes larger for the large N as shown in Fig. 5.7. This observation can be understood in the following way. With the nonlinear terms, the dynamics of the deviation $\delta x_1^{(i)}$ (eq. (5.31)) is strictly governed by

$$\begin{aligned}\frac{d}{dt}\delta x_1^{(i)} &= -\frac{1}{\tau}(w + X_1^2 - 1)\delta x_1^{(i)} - \frac{1}{\tau}\delta x_2^{(i)} + \frac{1}{\tau}\tilde{\eta}_i \\ &\quad -\frac{1}{\tau}\left(X_1(\delta x_1^{(i)})^2 + \frac{(\delta x_1^{(i)})^3}{3}\right) \\ &\quad +\frac{1}{\tau N}\sum_{j=1}^{N}\left(X_1(\delta x_1^{(j)})^2 + \frac{(\delta x_1^{(j)})^3}{3}\right). \end{aligned} \tag{5.41}$$

The term $X_1(\delta x_1^{(i)})^2$ in the second line and the term $(1/N)\sum_j X_1(\delta x_1^{(j)})^2$ in the third line in eq. (5.41) have the size $\sim N$ with a large but fixed w because of eq. (5.33) and the scaling $D \sim N$. Thus the approximation with eq. (5.31) cannot hold for the large N.

5.6 Results and Discussions

The array-enhanced stochastic resonance (AESR) in the coupled FitzHugh-Nagumo model is investigated. AESR is characterized by the following two properties, namely, the scaling of the optimal fluctuation intensity $D_0^{(N)}(\infty)$ for N neurons with the sufficiently large coupling strength obeying

$$D_0^{(N)}(\infty) = N D_0^{(1)}(\infty), \tag{5.42}$$

and the enhancement of the maximum value C_{peak} of the correlation coefficient C as a function of the coupling strength w.

By transforming the dynamics of N neurons into that of the mean dynamics $\boldsymbol{X}$ and the deviation $\delta\boldsymbol{x}^{(i)}$, it is found that AESR is caused by the term $\propto -X_1(\delta x_1)^2$, particularly by the correlation between $(\delta x_1)^2$ and X_1.

The characters of the fluctuations of $(\delta x_1)^2$ are also investigated, and it is found that the deviation of the peak value C_{peak} of the approximation from that of the network of N neurons is caused by the asymmetry of the distribution of the fluctuations of $(\delta x_1)^2$, and the correlation between the fluctuations of $(\delta x_1)^2$ and the mean dynamics X_1.

Note that our analyses are independent of the input, thus the above discussions are also applicable to the array-enhancement in the system without the input, namely, array-enhanced coherence resonance [98].

As for the information processing in the neural system, AESR gives a mechanism for an effective regulation of the fluctuation intensity even for the "uncontrollable" fluctuations. As shown in Fig. 5.12(a), the regulation of the fluctuation intensity in the $w - D$ plane is represented by a vertical arrow, and the dependence of the correlation coefficient C on the fluctuation intensity D along this arrow is shown in Fig. 5.1. Note that the correlation coefficient C takes a maximum when the arrow crosses the curve which shows the optimal fluctuation intensity. On the other hand, a horizontal arrow in Fig. 5.12(a) represents the regulation of the coupling strength, and the dependence of C on the coupling strength w along this arrow is shown in Fig. 5.12(b). It is shown that the correlation coefficient takes a maximum when w crosses the curve of optimal fluctuation intensity shown in Fig. 5.12(a). Thus the regulation of w might work as a mechanism for the effective regulation of the fluctuation intensity even for the "uncontrollable" fluctuations in the neural system.

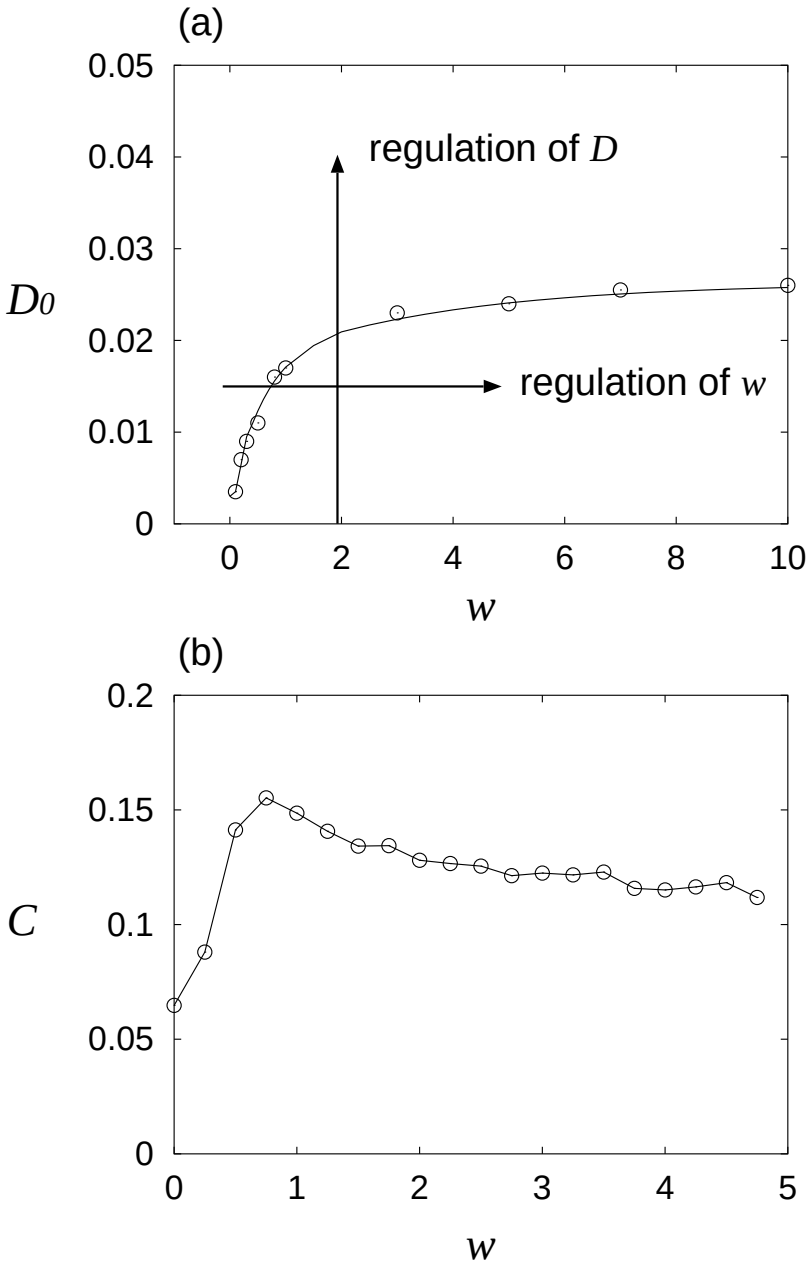

Figure 5.12 (a) The dependence of the optimal fluctuation intensity D_0 on the coupling strength w for $N = 10$. (b) The dependence of the correlation coefficient C on the coupling strength w for $D = 0.015$ and $N = 10$.

Chapter 6

Stochastic Resonance in the Network with Delays

6.1 Introduction

As stated in Secs. 2.3 and 2.4, the transmission delay depends on the distance between neurons. It is known that there are very long axons which regulate the transmission delays in the brain stem of the barn owl. The barn owl utilizes these delays to locate the sound sources by detecting the interaural time difference of the signal with the coincidence detector [64].

In this chapter, based on Ref. [94], we investigate an electrically coupled FitzHugh-Nagumo model with a time delay. In Sec. 6.2, an electrically coupled FitzHugh-Nagumo model with a time delay is defined. In Sec. 6.3, the dynamics of the coupled model is considered. With an appropriate set of system parameters, a deterministic firing induced by additive fluctuations is observed, and its dependence on the number of neurons is investigated. In Sec. 6.4, we construct a network composed of two assemblies and examine a competitive behavior in the network by controlling the fluctuation intensity. Results and discussions are given in the last section.

6.2 An Electrically Coupled FN Model with Delay

In this chapter, we treat an electrically coupled FitzHugh-Nagumo (FN) model with a time delay, written as

$$\tau \frac{du_i}{dt} = -v_i + u_i - \frac{u_i^3}{3} + w g_i(t) + S(f;t) + \eta_i(t) \tag{6.1}$$

$$\frac{dv_i}{dt} = u_i - \beta v_i + \gamma, \tag{6.2}$$

$$g_i(t) = \begin{cases} \displaystyle\sum_{j \neq i} \frac{1}{N-1} \left(u_j(t-d_p) - u_i(t) \right) & \text{if } N \geq 2 \\ 0 & \text{if } N = 1 \end{cases}, \tag{6.3}$$

$$S(f;t) = \begin{cases} S_0 & \text{if } t \leq h \bmod f^{-1} \\ 0 & \text{otherwise} \end{cases}, \tag{6.4}$$

$$\langle \eta_i(t)\eta_j(t')\rangle = D\delta_{ij}\delta(t-t'), \tag{6.5}$$

for $i, j = 1, 2, \cdots, N$, where $\beta = 0.8$, $\gamma = 0.7$, $\tau = 0.1$, $g_i(t)$ is the coupling term, and d_p is a time delay from the j-th neuron to the i-th neuron. Note that fluctuations for different neurons are statistically independent, the coupling strengths and the time delays are uniform in the network, and the coupling is electrical, *i.e.*, for a large enough w and $d_p = 0$ the neurons synchronize each other. The parameters of the periodic pulse train $S(f;t)$ are set as $f = 0.1$, $S_0 = 0.15$, and $h = 0.3$. Note that the height S_0 is so small that no neuron generates a pulse without fluctuations.

By the symmetry of the system, the behaviors of all the neurons are statistically identical, and we regard the internal state u_1 of the first neuron as the output of the network.

6.3 Fluctuation-induced Deterministic Firing

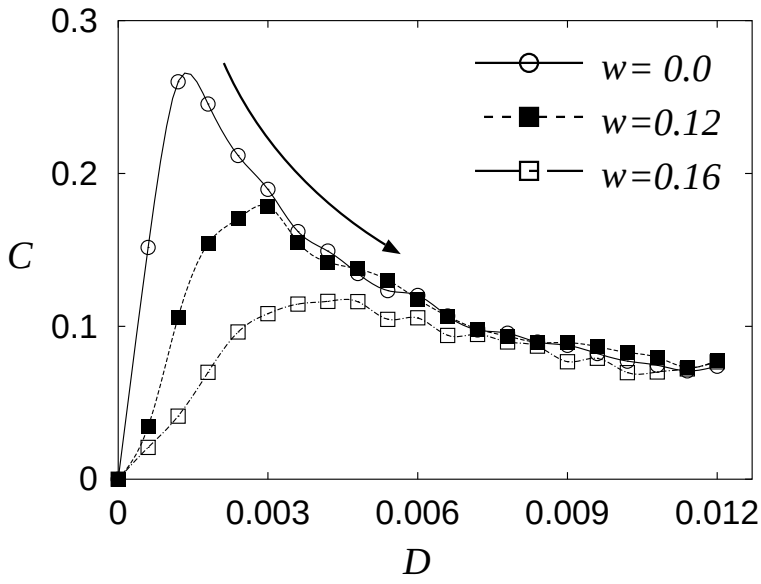

Figure 6.1 The dependence of the correlation coefficient C on the fluctuation intensity D for $d_p = 10$.

Firstly, the system with $N = 2$ is considered for simplicity. The frequency of the input pulse train is fixed at $f = 0.1$.

For $d_p = 10$, the firing at some moment may affect the firing in the next period of $S(f;t)$ since $1/f = 10$. The dependence of the correlation coefficient C on the fluctuation intensity D for $w = 0$, 0.12 and 0.16 with $d_p = 10$ is shown in Fig. 6.1. Similarly to the

case of $d_p = 0$ treated in Chap. 4, the correlation coefficient C has a peak at an optimal fluctuation intensity D_0 for $w = 0$, and D_0 increases with the increase of w. But it is also observed that the peak value of C decreases with the increase of w, unlike the case of $d_p = 0$. This difference of the behavior for $d_p = 0$ and 10 may come from the fact that the synchronized solution $u_1(t) = u_2(t - d_p)$ and $u_2(t) = u_1(t - d_p)$ cannot lock to the input pulse train $S(f;t)$ for $d_p = 10$.

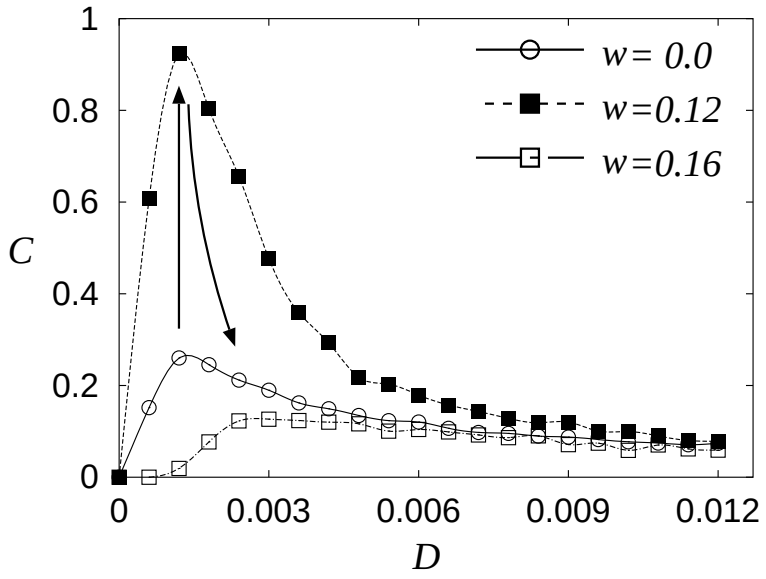

Figure 6.2 The dependence of the correlation coefficient C on the fluctuation intensity D for $d_p = 10 - d_f \simeq 9.7$.

Next, we treat the case with $d_p = 1/f - d_f \simeq 9.7$, where d_f is the time lag of firing since an input pulse is injected. Note that in this case an output pulse, which fires with the delay d_f after an input pulse is injected, can synchronize with the next input pulse. The correlation coefficient C for $w = 0$, 0.12, and 0.16 with $d_p = 9.7$ is plotted in Fig. 6.2, where each C shows the existence of the maximum. Note that the maximum of C for $w = 0.12$ reaches almost 1, which indicates that for $D \simeq 0.001$, fluctuation-induced deterministic firing (FIDF), namely, a 1:1 phase locking between the input and the output, takes place. For $w = 0.16$, this locking behavior is broken and the maximum decreases to about 0.1.

To investigate the range of w where FIDF takes place, the correlation coefficient C with the fixed fluctuation intensity $D = 0.001$ for $d_p = 0$, 9.7, and 10 is plotted against w in Fig. 6.3. It shows that the coupling strength w which enables FIDF is around $w = 0.12$ for $d_p = 9.7$. FIDF also takes place for $N > 2$ with $d_p = 9.7$ and $w \simeq 0.12$ (data not shown), but its optimal fluctuation intensity D_0 has a dependence on the number N of neurons. D_0 is shown as a function of N in Fig. 6.4. The monotonic increase of D_0 with N, and the convergence of D_0 to about 0.002 is observed.

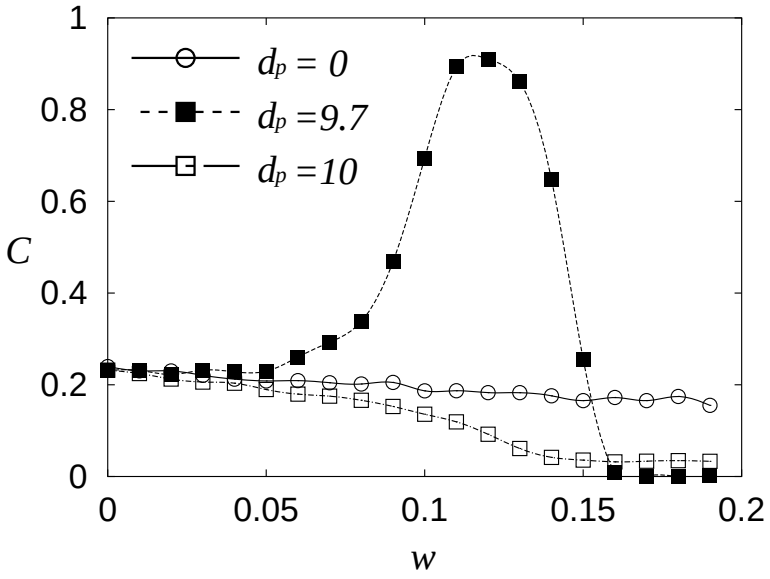

Figure 6.3 The dependence of the correlation coefficient C on the coupling strength w for $d_p = 0$, 9.7, and 10 with $D = 0.001$.

6.4 Competition of Two Assemblies under Fluctuations

Using the preceding properties of SR in an electrically coupled FN model with a time delay, we construct a network composed of two assemblies, in which a competitive behavior takes place by controlling the fluctuation intensity. Firstly, let us define the superimposed periodic pulse train (SPPT) as

$$T(t) = \max_{1 \le i \le m} S(f_i; t), \tag{6.6}$$

where m is the number of periodic components, and f_i is the frequency of each periodic component. In the following, we set $m = 2$, $f_1 = 0.1$, $f_2 = f_1/\sqrt{2}$, and $S_0 = 0.15$. Note that the height S_0 of $T(t)$ is so small that it cannot make each neuron generate a pulse without fluctuations. The SPPT $T(t)$ is injected to the network composed of two assemblies, shown in Fig. 6.5. The assembly 1 is composed of two neurons, namely, eqs. (6.1) and (6.2) with $N = N_1 = 2$, $d_p = d_1 \equiv 1/f_1 - d_f$ and $T(t)$ instead of $S(f;t)$, and assembly 2 is composed of eight neurons, namely, eqs. (6.1) and (6.2) with $N = N_2 = 8$, $d_p = d_2 \equiv 1/f_2 - d_f$ and $T(t)$ instead of $S(f;t)$. Note that there is a neuron which belongs to both assemblies simultaneously, and we regard its output as the output of the network. The coupling strength w is set at $w = 0.12$ so that FIDF takes place with a suitable fluctuation intensity. By the definition of the delay d_1 and d_2, it is expected that FIDFs with frequency f_1 and f_2 take place in the assembly 1 and 2, respectively. Then two correlation coefficients C_1 and C_2 are defined as the correlations

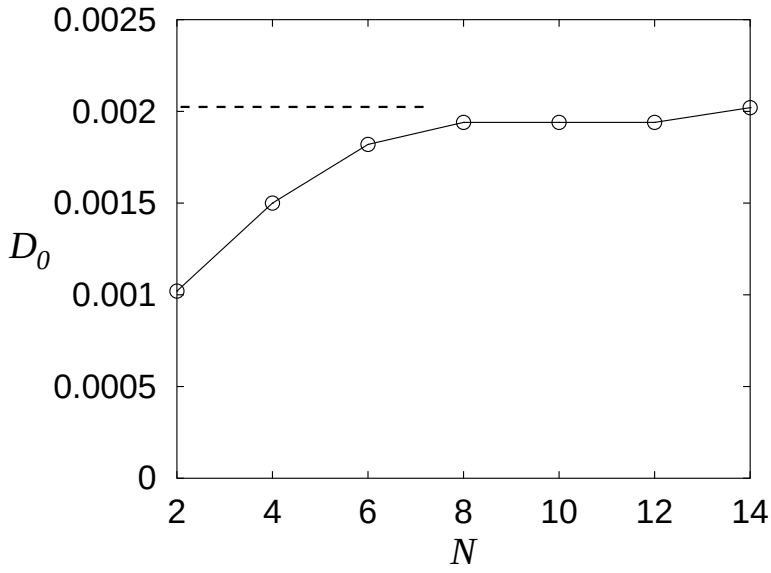

Figure 6.4 The dependence of the optimal fluctuation intensity D_0 on the number N of neurons for the fluctuation-induced deterministic firing.

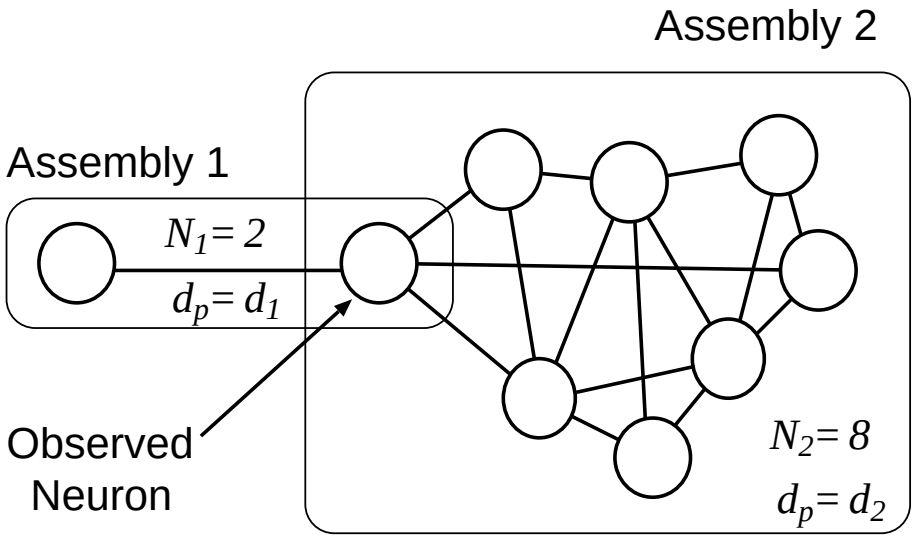

Figure 6.5 A network composed of two assemblies.

between the output pulse train of the network and the periodic pulse train $S(f_1; t)$ and $S(f_2; t)$, respectively. A large C_1 indicates that the observed neuron is dominated by the synchronized oscillation in the assembly 1, and a large C_2 indicates the domination of

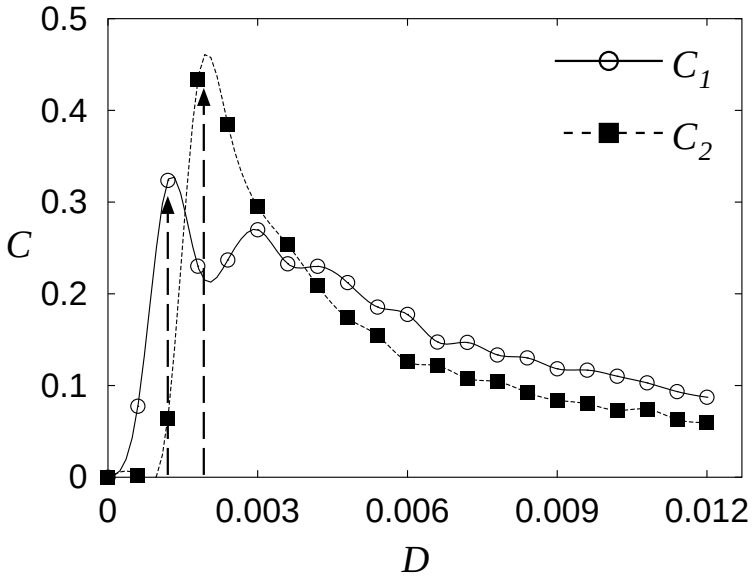

Figure 6.6 The dependences of the correlations C_1 and C_2 on the fluctuation intensity D.

the assembly 2.

The dependences of C_1 and C_2 on the fluctuation intensity D are shown in Fig. 6.6, which indicates that the optimal fluctuation intensity D_0 is $D_0 \simeq 0.001$ for C_1, and $D_0 \simeq 0.002$ for C_2. Note that C_1 is suppressed when C_2 is around the maximum value. The difference between the optimal fluctuation intensities for C_1 and C_2 is caused by the fact that the optimal fluctuation intensity D_0 depends on the number N of neurons (see Fig. 6.4).

The above phenomenon shows some new features of noisy pulse neural networks. The dominant frequency of the SPPT $T(t)$ in the network is controlled by the fluctuation intensity. In other words, the SPPT $T(t)$ is separated to each periodic component by controlling the fluctuation intensity. This implies that the fluctuation in a network might be used as a parameter of its dynamics. Secondly, the synchronously oscillating assembly is rearranged by controlling the fluctuation intensity. For example, for $D \simeq 0.001$, the observed neuron belongs mainly to the assembly 1 in which each neuron fires synchronously with frequency f_1, and for $D \simeq 0.002$, it belongs to the assembly 2 in which the periodic firing with frequency f_2 is dominant. These new features suggest that the fluctuations in the brain might have a functional role in the information processing.

6.5 Results and Discussions

Concerning SR, new features of the noisy pulse neural network with a time delay are reported. When the time delay d_p and the frequency f of the periodic input pulse train

satisfy the relationship $d_p = 1/f$, an optimal fluctuation intensity which maximizes the correlation coefficient increases with the increase of the coupling strength, and the peak value of the correlation coefficient decreases with the increase of the coupling strength. For the time delay $d_p = 1/f - d_f$ dependent on the firing delay d_f, a deterministic firing is induced at the optimal fluctuation intensity, which increases with the increase of the number of neurons.

Using these properties, a network composed of two assemblies is constructed. It separates a superimposed periodic pulse train, and its dynamics can be controlled by fluctuations. In this network, the rearrangement of the synchronously oscillating assembly by controlling the fluctuation intensity is observed.

Part III

Dynamics of the Network with Chemical Couplings

Chapter 7

Fluctuation-induced Memory Retrieval

7.1 Introduction

The associative memory in neural networks has been investigated for more than twenty years. In the autocorrelative associative memory model, the bit patterns are stored in the connection coefficients of the network and the stored patterns are retrieved using the neural dynamics.

Conventionally, the carrier of the information in associative memory models is thought to be the firing rate of a single neuron or an ensemble of neurons. Recently, there has been considerable interest in associative memory of neural networks composed of model neurons which change their dynamical states temporally, such as chaotic neurons [104, 105], oscillator neurons [106, 107, 108, 109, 110, 111, 112, 113], or spiking neurons [115, 116, 117, 118]. These networks are not only of theoretical interest, but also may have a lot to do with the problem of information coding in the brain [99].

Numerous authors have investigated coupled phase oscillators [106, 107, 108, 109, 110, 111, 112, 113], which are the general reduced model of the coupled limit-cycle oscillators. In this case, all the neurons oscillate with almost the same period, and the memory is represented in the relative phase differences of oscillators, so the neurons can store analog-valued patterns. This model has an advantage in that the usual techniques for theoretical analysis of associative memory [120, 121] are applicable.

On the other hand, neural networks composed of spiking neurons also show the properties of associative memory [115, 116, 117]. In those systems, the following models are often used as spiking neurons: the Hodgkin-Huxley model, which describes the dynamics of squid giant axons; the FitzHugh-Nagumo model, which is the reduced model of the Hodgkin-Huxley model; and the leaky integrate-and-fire model, which has an internal state described by a linear differential equation and a spiking mechanism with a threshold. The couplings among those neurons are accompanied with time delays which models the time lag from the presynaptic neuron to the postsynaptic neuron, and the memory is represented in the spatio-temporal firing pattern of the neurons.

Meanwhile, as shown in Chap. 1, the physiological environment where neurons op-

erate has several sources of fluctuations, thus their effects on the information processing may not be neglected. In this chapter, based on Ref. [118], the associative memory in the network of chemically coupled FitzHugh-Nagumo models with fluctuations is treated, and SR-like effects in this system are considered. In Sec. 7.2, a coupled FitzHugh-Nagumo model and some quantities are defined. The couplings are mediated by chemical synapses. In Sec. 7.3, the results of numerical simulations are presented. We consider memory retrieval after adding fluctuations into the system and examine its dependence on the fluctuation intensity. We observe an SR-like phenomenon. The basin of the attraction and the storage capacity of the system are also investigated numerically. In Sec. 7.4, theoretical analyses for the fluctuation-induced memory retrieval are presented. In Sec. 7.5, the simultaneous retrieval of two patterns is observed as the alternate firings of the particular neurons. Results and discussions are given in the final section.

7.2 Associative Memory Composed of Spiking Neurons

In the following, as a model of associative memory, we treat a chemically coupled FitzHugh-Nagumo (FN) model written as

$$\tau \frac{du_i}{dt} = -v_i + u_i - \frac{u_i^3}{3} + S_i(t) + \eta_i(t) + \sum_{j=1}^{N} J_{ij} \sum_{k \in \kappa(i,j)} \alpha(t - t_j^k - d_p), \quad (7.1)$$

$$\frac{dv_i}{dt} = u_i - \beta v_i + \gamma, \quad (7.2)$$

$$\alpha(t) = g_{peak} \frac{t}{t_0} \exp\left(1 - \frac{t}{t_0}\right), \quad (7.3)$$

$$\langle \eta_i(t) \eta_j(t') \rangle = D \delta_{ij} \delta(t - t'), \quad (7.4)$$

$$\kappa(i,j) \equiv \{k | t_i^f(t) - d_p < t_j^k < t - d_p\}, \quad (7.5)$$

where $\beta = 0.8$, $\gamma = 0.7$, $\tau = 0.1$, $S_i(t)$ is the external input, $\eta_i(t)$ is Gaussian white noise, t_j^k is the k-th firing time of the j-th neuron, the firing time is defined as the time when $u_i(t)$ exceeds an arbitrary threshold θ, $t_i^f(t)$ is the latest firing time of the i-th neuron at time t, d_p is the uniform time delay, and $\alpha(t)$ is the alpha function with height g_{peak}. The parameters are fixed at $d_p = 3$, $\theta = 0$, and $g_{peak} = 0.45$ in the following.

Let us make the above N neurons store p random patterns ξ_i^μ ($i = 1, 2, \cdots, N$, $\mu = 1, 2, \cdots, p$), generated according to the probability density function

$$P(\xi_i^\mu) = (1 - a)\delta(\xi_i^\mu) + a\delta(\xi_i^\mu - 1), \quad (7.6)$$

where $\delta(x)$ denotes the delta function and a ($0 \leq a \leq 1$) is the average of ξ_i^μ. Following Yoshioka and Shiino [117], the connection coefficients J_{ij} are defined as

$$J_{ij} = \frac{1}{Na(1 - a)} \sum_{\mu=1}^{p} \xi_i^\mu (\xi_j^\mu - a). \quad (7.7)$$

Note that the matrix $J_{ij} \propto \sum_\mu \xi_i^\mu(\xi_j^\mu - a)$ is used instead of the usual $J_{ij} \propto \sum_\mu(\xi_i^\mu - a)(\xi_j^\mu - a)$ so as not to give negative inputs to the neurons which store 0's, because the FN neuron can fire even with the negative input due to the rebound effect [125, 126, 127].

The external input $S_i(t)$ is defined as

$$S_i(t) = x_i U_0 U(t) \quad (x_i \in \{0,1\}), \tag{7.8}$$

$$\equiv \begin{cases} x_i U_0 & \text{if } t \geq 0 \\ 0 & \text{otherwise} \end{cases}, \tag{7.9}$$

where $U(t)$ is a step function, x_i is the binary factor which determines whether the input is injected to the i-th neuron or not, and U_0 is the intensity of the input. In the following, U_0 is fixed at $U_0 = 0.1$, which is so small that each neuron cannot fire without the fluctuation $\eta_i(t)$. Using the binary factor x_i, the input overlap m_{in}^μ, which measures the correlation between the pattern $\xi^\mu = (\xi_1^\mu, \xi_2^\mu, \cdots, \xi_N^\mu)$ and the external input $S(t) = (S_1(t), S_2(t), \cdots, S_N(t))$, is defined as

$$m_{in}^\mu = \frac{1}{Na(1-a)} \sum_{i=1}^{N} (\xi_i^\mu - a)(x_i - a). \tag{7.10}$$

7.3 Fluctuation-induced Memory Retrieval

Following the above configurations, numerical simulations are carried out for $N = 200$, $p = 3$, and $a = 0.5$. Without loss of generality, the pattern ξ^1 can be defined as

$$\xi_i^1 = \begin{cases} 1 & 1 \leq i \leq 100 \\ 0 & \text{otherwise} \end{cases}, \tag{7.11}$$

and the patterns ξ^2 and ξ^3 are determined randomly following the probability density function (7.6). The external input is derived by determining the binary factors x_i randomly so that the input overlap m_{in}^1 with the pattern ξ^1 takes 0.5. To measure the correlation between the pattern ξ^μ and the time series $u_i(t)$ $(i = 1, 2, \cdots, N)$, $u_i(t)$ is transformed into the binary series $y_i(t) \in \{0, 1\}$ written as

$$y_i(t) = \begin{cases} 1 & \text{if } t < t_i^f(t) + \Delta_d \\ 0 & \text{otherwise} \end{cases}, \tag{7.12}$$

where the parameter Δ_d is set close to the characteristic width of the output pulse, and $\Delta_d = 4$ is used in the following. Then the output overlap m_{out}^μ between the pattern ξ^μ and the binary series $y = (y_1(t), y_2(t), \cdots, y_N(t))$ is defined as

$$m_{out}^\mu = \frac{1}{Na(1-a)} \sum_{i=1}^{N} (\xi_i^\mu - a)(y_i - a). \tag{7.13}$$

At the time $t = 0$, the variables u_i and v_i are set around the equilibrium, namely, $u_i \simeq -1.2$ and $v_i \simeq -0.63$. The firing times of all the neurons for the fluctuation intensity $D = 0.001$ are shown in Fig. 7.1(a), and it is observed that all the neurons are firing

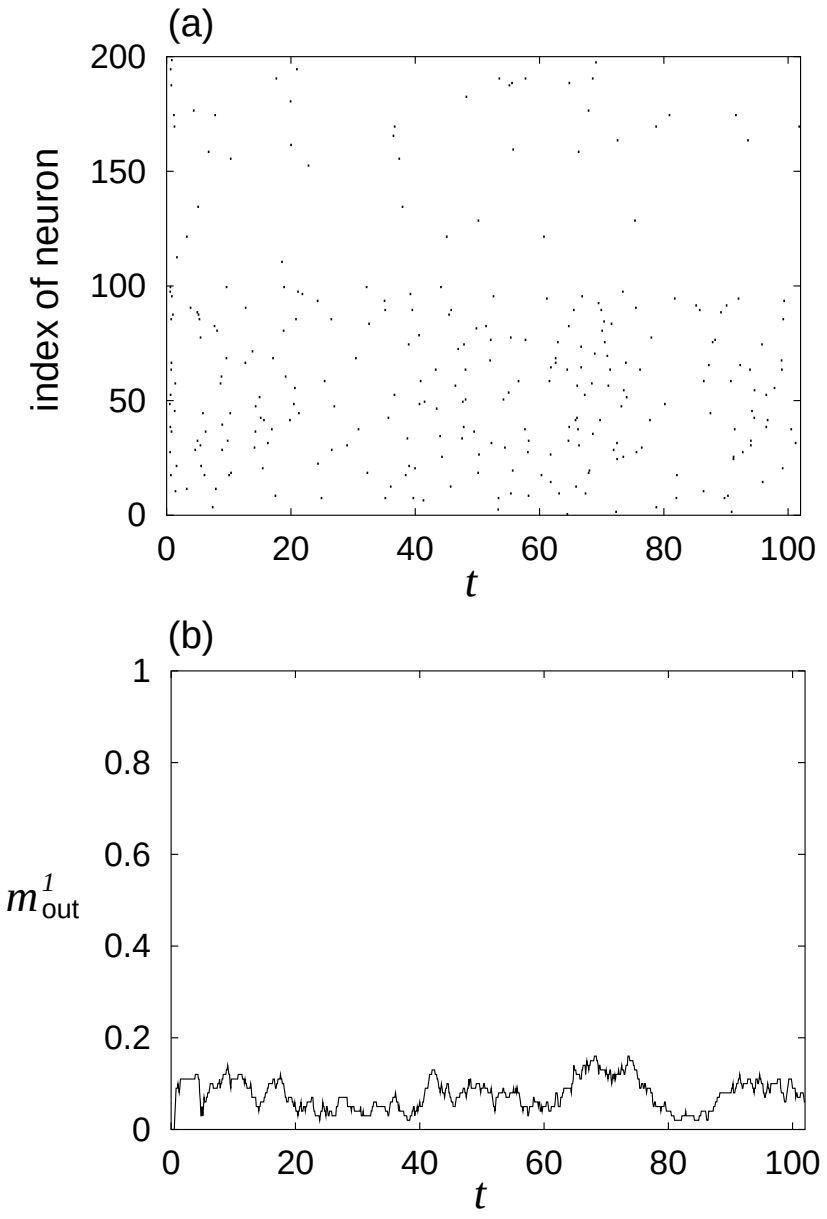

Figure 7.1 The result of a numerical simulation, (a) the firing times of all the neurons and (b) the output overlap m^1_{out} with the pattern ξ^1, for $N = 200$, $p = 3$, $a = 0.5$, and $D = 0.001$. All the neurons are firing randomly, thus the retrieval of the pattern ξ^1 fails.

randomly. The output overlap m^1_{out} with the pattern ξ^1 obtained from the time series in Fig. 7.1(a) is shown in Fig. 7.1(b). It is observed that m^1_{out} fluctuates around 0, thus it can be concluded that the retrieval of the pattern ξ^1 fails.

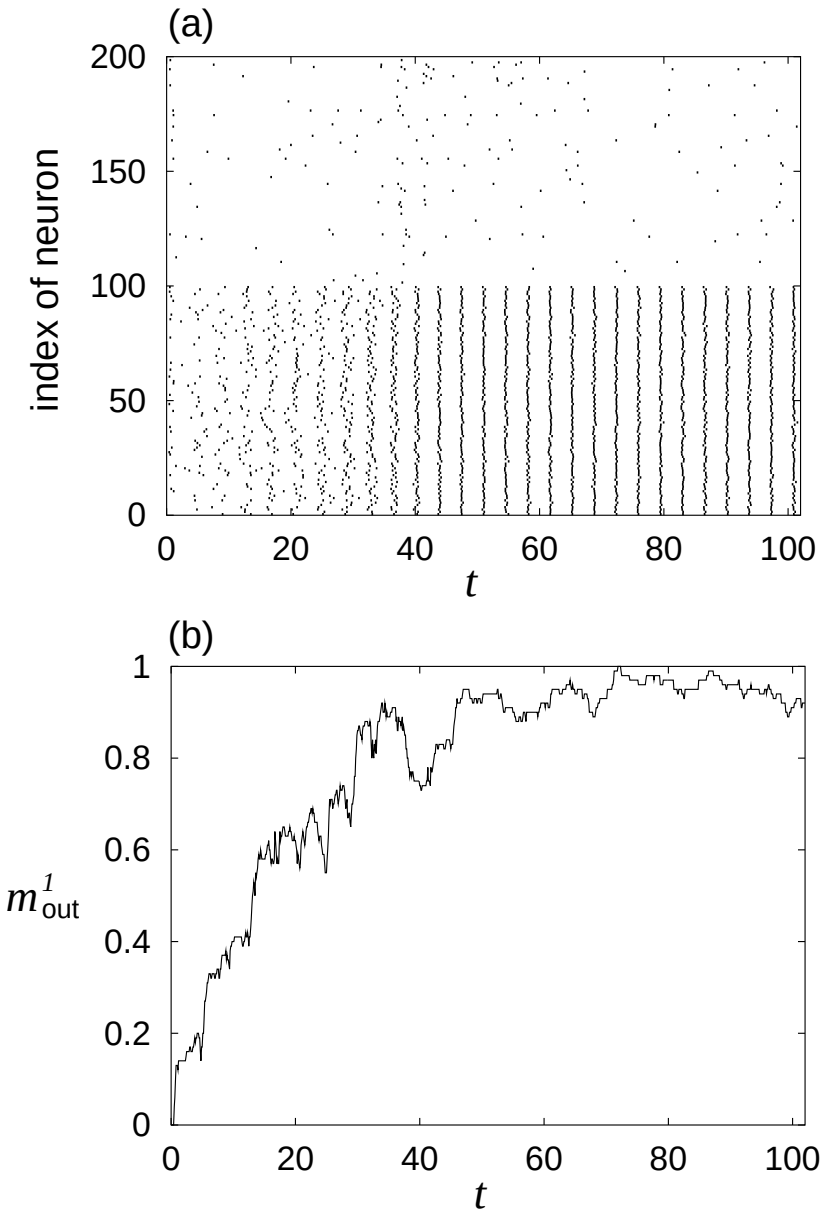

Figure 7.2 The result of a numerical simulation, (a) the firing times of all the neurons and (b) the output overlap m^1_{out} with the pattern ξ^1, for $N = 200$, $p = 3$, $a = 0.5$, and $D = 0.0015$. The retrieval of the pattern ξ^1 is successful.

The firing times of all the neurons for $D = 0.0015$ are shown in Fig. 7.2(a). It is observed that all the neurons seem to fire randomly at small t, but at $t \simeq 40$ the neurons which store 1's for the pattern ξ^1 start to fire periodically and synchronously. And in Fig. 7.2(b), the output overlap m^1_{out} increases to about 0.9 at $t \simeq 40$, so in this case the

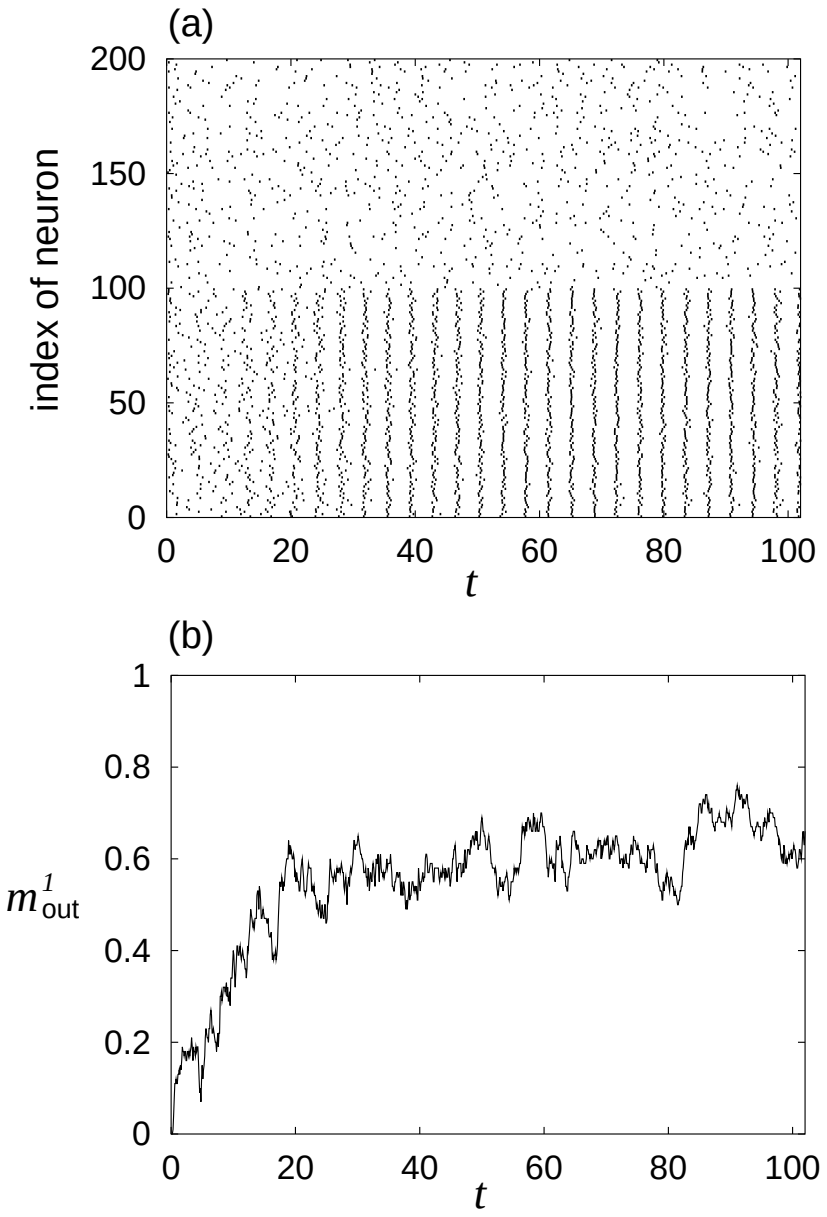

Figure 7.3 The result of a numerical simulation, (a) the firing times of all the neurons and (b) the output overlap m^1_{out} with the pattern ξ^1, for $N = 200$, $p = 3$, $a = 0.5$, and $D = 0.004$. The neurons which store 0's for the pattern ξ^1 fire with high firing rates due to the large fluctuation intensity, thus the output overlap is lower than the case of $D = 0.0015$.

retrieval of the pattern ξ^1 is successful.

The result of a simulation for $D = 0.004$ are shown in Fig. 7.3. The periodic and

synchronous firings are observed again, but the neurons which store 0's for the pattern ξ^1 fire with high firing rates due to the large fluctuation intensity, thus the output overlap is lower than the case of $D = 0.0015$.

In Fig. 7.4, the output overlap m^1_{out} at a sufficiently large t is plotted against the fluctuation intensity D for the input overlap $m^1_{in} = 0.8$, 0.6, and 0.05. The other param-

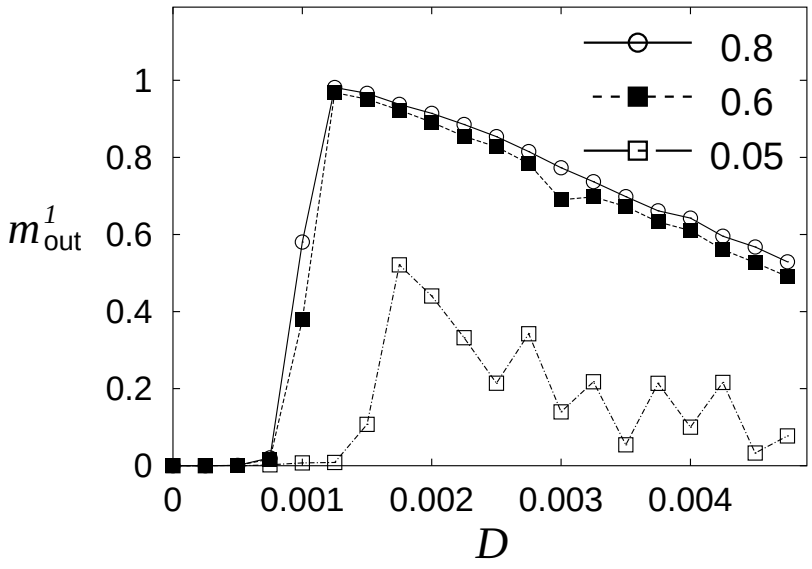

Figure 7.4 The output overlap m^1_{out} against the fluctuation intensity D for $m^1_{in} = 0.8, 0.6$, and 0.05 with $N = 200$, $p = 3$, and $a = 0.5$. Stochastic resonance-like phenomenon is observed for $m^1_{in} = 0.8$ and 0.6.

eters are identical with the previous cases. For $m^1_{in} = 0.8$ and 0.6, the output overlap m^1_{out} increases with the increase of the fluctuation intensity D, and it decreases with the increase of D over the optimal intensity $D_0 \simeq 0.0011$. This phenomenon is similar to so-called stochastic resonance, where a weak input signal is enhanced by its background fluctuation and observed in many nonlinear systems [67, 68, 69, 70]. For $m^1_{in} = 0.05$, the retrieval of the pattern ξ^1 fails for any value of D.

For the fixed fluctuation intensity $D = 0.0015$, the numerically obtained basin of attraction is shown as a function of the loading rate $\alpha = p/N$ in Fig. 7.5. For each loading rate α, two points are plotted, namely, the upper is the equilibrium value of the output overlap m^1_{out}, and the lower is the minimum input overlap m^1_{in} which gives the successful memory-retrieval. For $\alpha < 0.04$, the standard deviations shown by the error bars are relatively small, but for $\alpha \geq 0.04$, they take larger values, that is, the memory-retrieval states are destabilized. Thus it can be concluded that the storage capacity α_c is about 0.04. For further discussions, theoretical analyses of the associative memory [120, 121] are required.

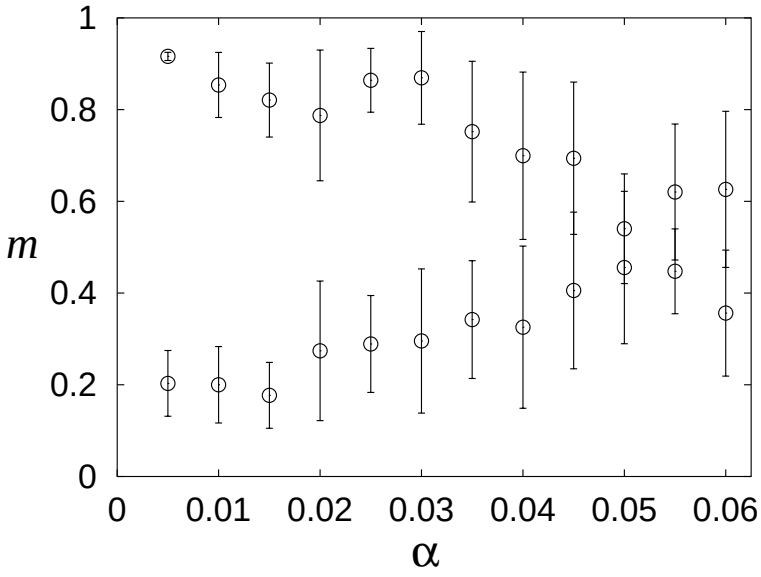

Figure 7.5 The basin of attraction for $N = 200$, $D = 0.0015$, and $a = 0.5$. The error bar denotes the standard deviation for ten samples. The storage capacity is estimated to be about 0.04.

7.4 Theoretical Analysis of Fluctuation-induced Memory Retrieval

In this section, we give a qualitative explanation for the fluctuation-induced memory retrieval. In the following, the system with $p = 1$ is considered for simplicity. Let us define the set of indices of neurons which store 0's in the pattern $\xi^\mu = (\xi_1^\mu, \xi_2^\mu, \cdots, \xi_N^\mu)$ as $G^\mu(0)$, and the set of indices of neurons which store 1's in the pattern ξ^μ as $G^\mu(1)$. The input K_i injected into the i-th neuron is written as

$$
\begin{aligned}
K_i &= \eta_i \quad \text{for } i \in G^1(0), && (7.14)\\
K_i &= \frac{1}{Na(1-a)} \sum_{j=1}^{N} (\xi_j^1 - a)\alpha_j(t) + U_0 + \eta_i, && (7.15)\\
&= \frac{1}{Na(1-a)} \left(\sum_{j \in G^1(0)} (\xi_j^1 - a)\alpha_j(t) + \sum_{j \in G^1(1)} (\xi_j^1 - a)\alpha_j(t) \right) \\
&\quad + U_0 + \eta_i, && (7.16)\\
&= -\frac{1}{N(1-a)} \sum_{j \in G^1(0)} \alpha_j(t) + \frac{1}{Na} \sum_{j \in G^1(1)} \alpha_j(t) + U_0 + \eta_i, && (7.17)\\
&= -\langle \alpha_j(t) \rangle_{j \in G^1(0)} + \langle \alpha_j(t) \rangle_{j \in G^1(1)} + U_0 + \eta_i \quad \text{for } i \in G^1(1), && (7.18)
\end{aligned}
$$

$$\alpha_j(t) \equiv \sum_{k\in\kappa(i,j)} \alpha(t - t_j^k - d_p), \tag{7.19}$$

$$\kappa(i,j) = \{k|t_i^f(t) - d_p < t_j^k < t - d_p\}, \tag{7.20}$$

where $\langle\cdot\rangle_{j\in A}$ denotes the ensemble average over the set A. Note that the external input $S(t)$ is injected only to the neurons in $G^1(1)$ for simplicity. Because fluctuations for different neurons are statistically independent, the neurons in $G^1(0)$ fire randomly and independently. On the other hand, the neurons in $G^1(1)$ have the common input $\langle\alpha_j(t)\rangle_{j\in G^1(1)}$, thus their firings may be correlative with each other. In the following, we treat this dynamics. To omit the dependence of K_i on the index i in the identical set $G(\cdot)$, the set $\kappa(i,j)$ is substituted with

$$\kappa(j) \equiv \{k|t_j^k < t - d_p\}, \tag{7.21}$$

for simplicity.

Let us consider an ensemble of N neurons with the uniform coupling term $\langle\alpha_j(t)\rangle_{1\le j\le N}$ and the external input $U_0+\eta_i$, namely, eqs. (7.1) and (7.2) with $J_{ij} = 1/N$ and $S_i(t) = U_0$. Note that this model approximates the dynamics of neurons in $G^1(1)$, and that the term $\langle\alpha_j(t)\rangle_{j\in G^1(0)}$ in eq. (7.18) is neglected for simplicity. Then let us consider the number of neurons which fire in the narrow time interval $[t, t+\Delta_w]$ and denote it by Nz_n. The perturbation with height $\simeq g_{peak}z_n$ caused by those firings is injected to all the neurons after the delay d_p. Let us denote the number of neurons which fire with this perturbation in the time interval $[t+d_p, t+d_p+\Delta_w]$ by Nz_{n+1}, and assume the relation $z_{n+1} = g(z_n)$. If the FN neuron acts like a threshold device with the threshold θ, $g(z_n)$ for the fluctuation intensity $D = 0$ is a step function which takes 1 for $g_{peak}z_n + U_0 \ge \theta$ and takes 0 otherwise. It is difficult to derive $g(z_n)$ for $D \neq 0$, but it is expected to be a monotonically increasing function of z_n.

The numerical derivation of $g(z_n)$ is performed as follows. First, sufficiently strong pulses are injected to some neurons. The number of neurons, which fire with the effect of the input pulses and fluctuations, gives the value of z_n. By preparing a variety of input pulses, we can generate a set of z_n's. The value of $z_{n+1} = g(z_n)$ is determined from the number of neurons which fire after the delay d_p. Numerically obtained $g(z_n)$ for $D = 0.0005$, 0.0011, and 0.0012 with $N = 200$ and $U_0 = 0.1$ is plotted in Fig. 7.6. The width Δ_w of the time interval is set at the same size as the width Δ_d of the output pulse. It is observed that the number of intersecting points of $y = g(z)$ with $y = z$ is three for $D < D_0 \simeq 0.0011$ and one for $D > D_0$, the intersecting point $z \simeq 1$ is always stable for any D, and the other intersecting points are generated by a saddle-node bifurcation at $D = D_0$. A schematic diagram is shown in Fig. 7.7.

Because all the neurons are set around the equilibrium at the time $t = 0$, the initial value of z_n is $z_0 \simeq 0$. Thus, for $D < D_0$, the system are stable at $z \simeq 0$ and almost all the neurons are quiescent. On the other hand, for $D > D_0$, any z_n converges to the stable fixed point $z \simeq 1$, which means that all the neurons fire synchronously and periodically with the period d_p. In other words, the target pattern is retrieved for $D > D_0$.

Next, let us consider the dependence of m_{out} on D is investigated for $D > D_0$. Assume that the neurons in $G^1(1)$ fire synchronously and periodically with the period

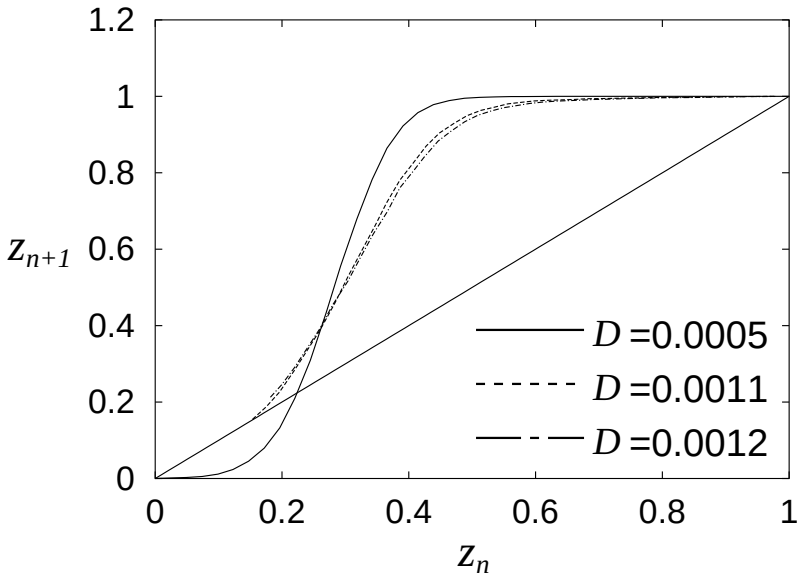

Figure 7.6 Numerically obtained $g(z_n)$ for D=0.0005, 0.0011, and 0.0012 with $N = 200$ and $U_0 = 0.1$. A saddle-node bifurcation at $D \simeq 0.0011$ is observed.

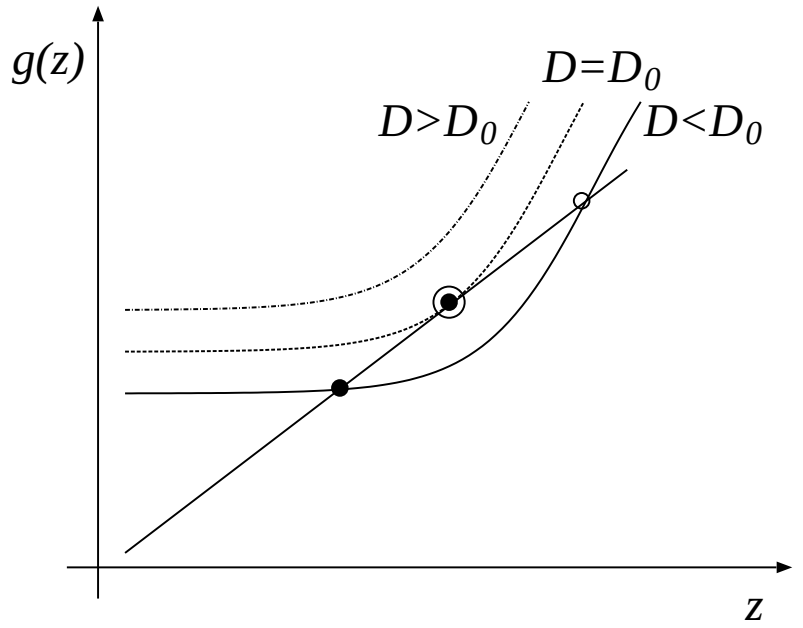

Figure 7.7 A schematic diagram of bifurcation of $g(z)$.

d_p and that the neurons in $G^1(0)$ are firing randomly with the firing rate depending on

D as $r_{G0} = r_0 \exp(-B/D)$, where r_0 and B are constants. Note that this firing rate is the inverse of the first passage time for a particle in a double-well potential to cross the potential barrier [34], and is introduced only for simplicity.

The distribution of the ratio k of the neurons in $G^0(0)$ which fire in a time interval of width Δ_w and its average $\langle k \rangle$ are written as

$$P(k) = {}_{N(1-a)}C_{N(1-a)k}(1-\exp(-r_{G0}\Delta_w))^{N(1-a)k}(\exp(-r_{G0}\Delta_w))^{N(1-a)(1-k)}, \quad (7.22)$$

$$\langle k \rangle = 1-\exp(-r_{G0}\Delta_w). \quad (7.23)$$

With $\langle k \rangle$, m_{out} is approximately given by

$$m^1_{out} = \frac{1}{Na(1-a)}\sum_i (\xi^1_i - a)(y_i - a), \quad (7.24)$$

$$= \frac{1}{Na(1-a)}[(1-a)(1-a)Na + (-a)(1-a)N(1-a)\langle k \rangle + (-a)(-a)N(1-a)(1-\langle k \rangle)], \quad (7.25)$$

$$= \exp\left[-r_0\Delta_w \exp\left(-\frac{B}{D}\right)\right]. \quad (7.26)$$

Note that eq. (7.26) decreases monotonically with the increase of D. This gives the quantitative description of the decrease of m_{out} for $D \geq D_0$.

7.5 Alternate Retrieval of Two Patterns

In our network, the memory is represented by the synchronized periodic firings of the neurons which store 1's, and this period is determined by the time delay d_p. Thus the system has a large degree of freedom along the time axis for the large d_p, that is, during the time between the firings by one pattern, the system can retrieve other patterns, in other words, this system can process some "tasks" simultaneously.

To see this ability, numerical simulations are performed for $N = 200$, $p = 3$, $a = 0.5$, and $d_p = 6.5$. Note that the time delay d_p is about twice as long as $d_p = 3$ used in the above sections. For simplicity, the patterns ξ^1 and ξ^2 are defined as

$$\xi^1_i = \begin{cases} 1 & 1 \leq i \leq 100 \\ 0 & \text{otherwise} \end{cases}, \quad (7.27)$$

$$\xi^2_i = \begin{cases} 1 & 51 \leq i \leq 150 \\ 0 & \text{otherwise} \end{cases}, \quad (7.28)$$

respectively, and the pattern ξ^3 is determined randomly following the probability density function (7.6). The external input $S(t)$ is defined thus that the binary factor x_i satisfies,

$$x_i = \begin{cases} 1 & 51 \leq i \leq 100 \\ 0 & \text{otherwise} \end{cases}. \quad (7.29)$$

Note that both input overlaps m^1_{out} and m^2_{out} take 0.5.

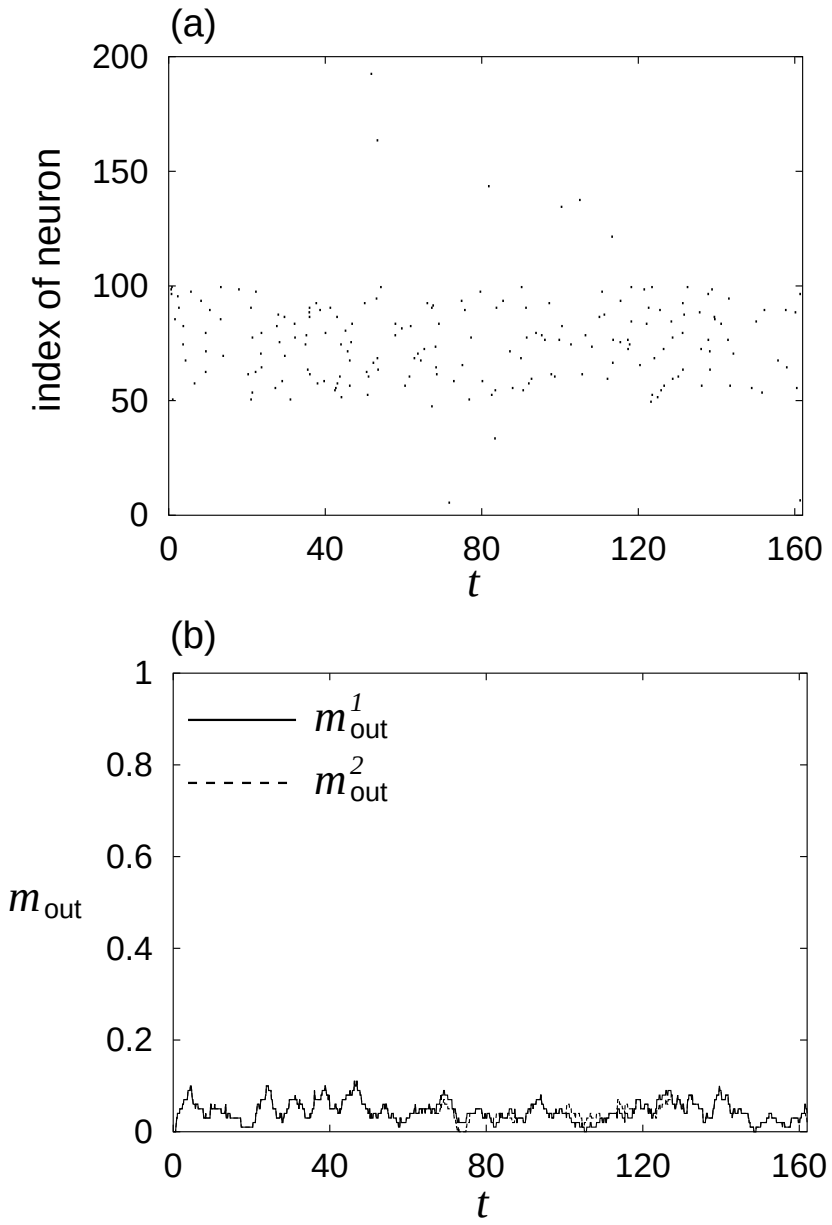

Figure 7.8 The result of a numerical simulation, (a) the firing times and (b) the output overlaps, for $N = 200$, $p = 3$, $a = 0.5$, $D = 0.0009$, and $d_p = 6.5$. The retrievals of both patterns ξ^1 and ξ^2 fail.

For the fluctuation intensity $D = 0.0009$, the firing times of all the neurons and the output overlaps m^1_{out} and m^2_{out} are plotted in Figs. 7.8(a) and 7.8(b), respectively. It is observed that the retrievals of both patterns ξ^1 and ξ^2 fail with this fluctuation intensity.

The firing times of all the neurons for the fluctuation intensity $D = 0.0015$ are plotted

in Fig. 7.9(a). It is shown that the two patterns ξ^1 and ξ^2 are retrieved alternatively,

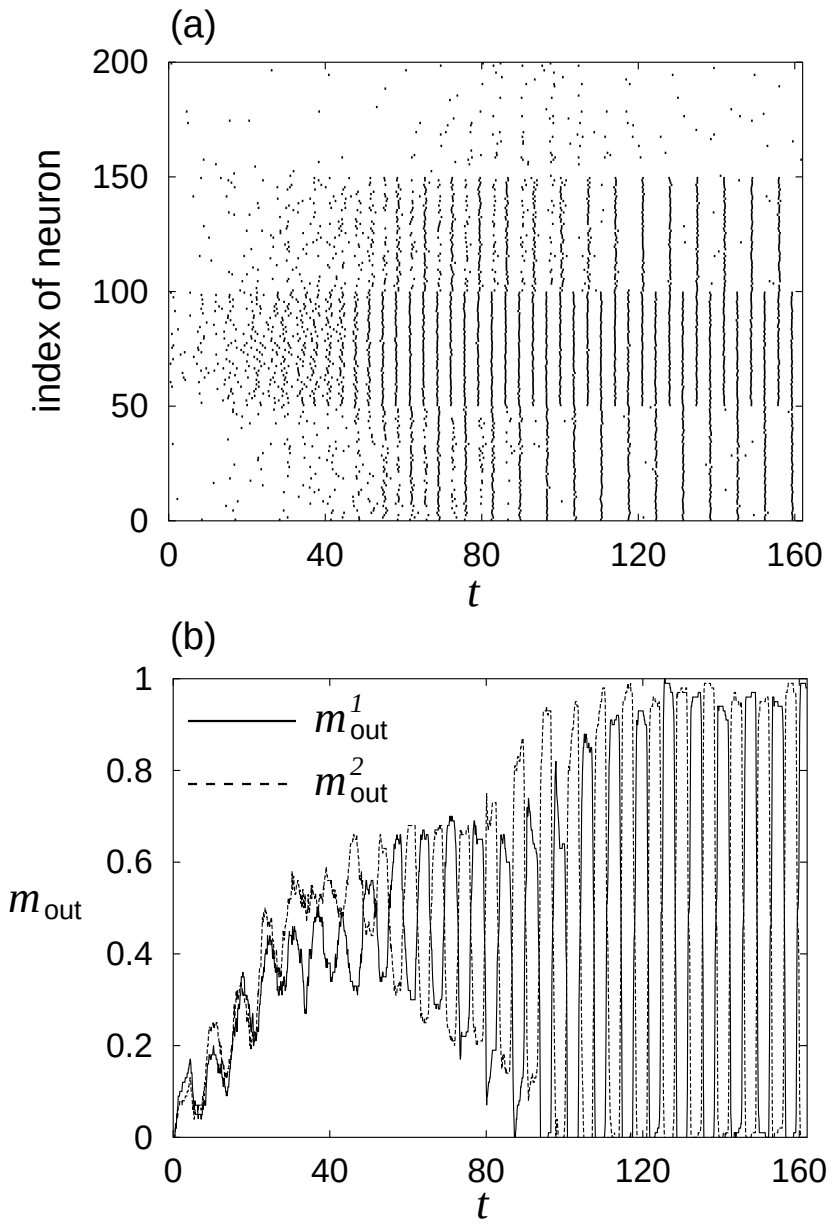

Figure 7.9 The result of a numerical simulation, (a) the firing times and (b) the output overlaps, for $N = 200$, $p = 3$, $a = 0.5$, $D = 0.0015$, and $d_p = 6.5$. The alternate retrieval of two patterns is observed as the anti-phase oscillations of two output overlaps.

accompanied by the time difference $d_p/2$. The output overlaps m^1_{out} and m^2_{out} derived from the data in Fig. 7.9(a) are shown in Fig. 7.9(b). The alternate retrieval of two patterns is observed as the antiphase oscillations of two output overlaps.

The result of a numerical simulation for $D = 0.004$ is shown in Fig. 7.10. In Fig.

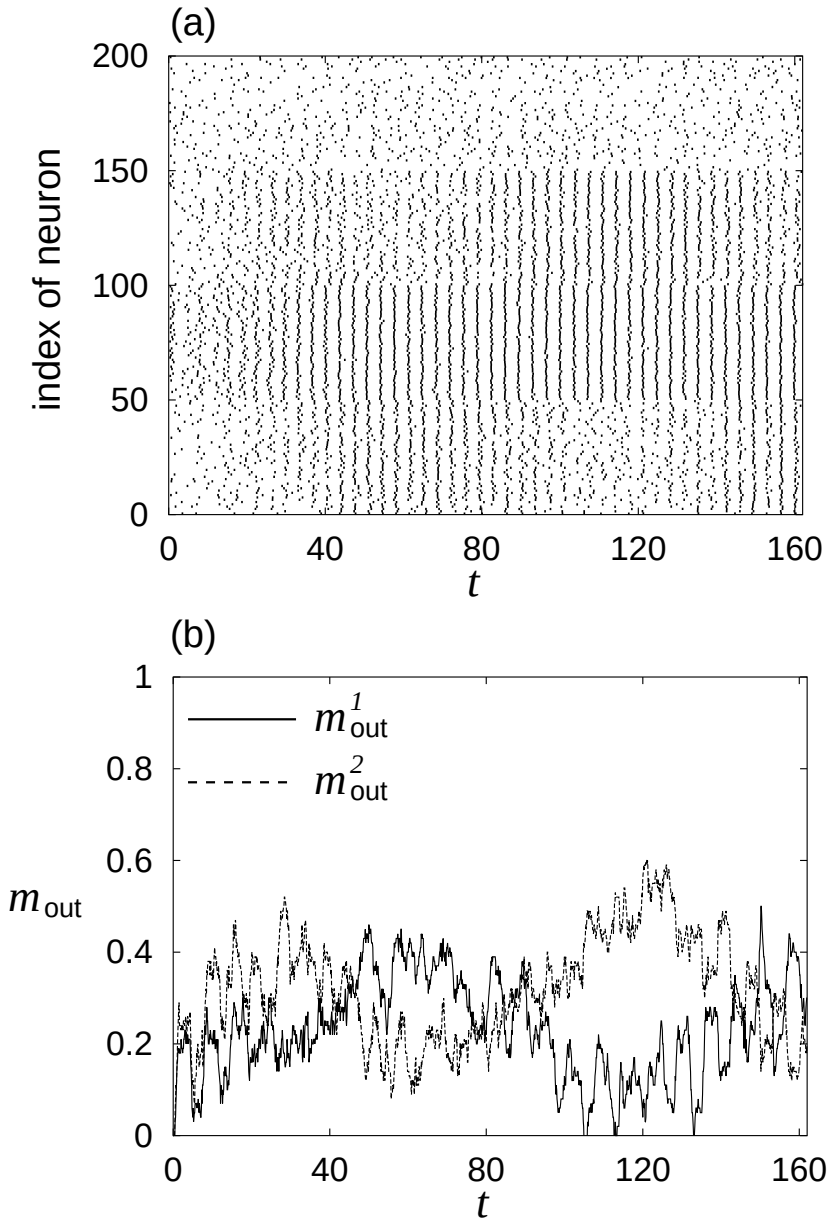

Figure 7.10 The result of a numerical simulation, (a) the firing times and (b) the output overlaps, for $N = 200$, $p = 3$, $a = 0.5$, $D = 0.004$, and $d_p = 6.5$. All the neurons are firing with high firing rates, thus the retrievals of both patterns ξ^1 and ξ^2 fail.

7.10(a), it is observed that all the neurons are firing with high firing rates, thus the retrievals of both patterns ξ^1 and ξ^2 fail as in Fig. 7.10(b).

From above results, it can be concluded that our system has an ability to retrieve two patterns simultaneously as the alternate firings of particular neurons, and the fluctuation intensity D plays a significant role to realize this dynamics.

7.6 Results and Discussions

The associative memory in a pulsed neural network composed of the chemically coupled FitzHugh-Nagumo models with a time delay is investigated. In this network, the memory is represented by the synchronous periodic firings of the particular neurons. It is found that the memory retrieval in this system is achieved by adding fluctuations, and there exists an optimal fluctuation intensity for memory retrieval. This phenomenon is similar to so-called stochastic resonance (SR), where the weak input signal is enhanced by its background fluctuations. Though there is no time-dependent input in our model, the mechanism of associative memory is driven and enhanced by its background fluctuation. The basin of attraction of this system is investigated numerically, and its storage capacity is found to be $\alpha_c \simeq 0.04$. This storage capacity is smaller than $\alpha_c = 0.138$ for the Hopfield model [123], and comparable to $\alpha_c = 0.038$ for the coupled phase oscillators [124]. It is found that our network has an ability that the previous models do not have, that is, an ability to retrieve two patterns as the alternate firings of the particular neurons. While such dynamics utilizing the degree of freedom along the time axis is proposed by Wang *et al.* for the network of bursting neurons [119], our model has the properties that the component of memory is the single pulse of each neuron, and that fluctuations in the system is indispensable.

As for the fluctuations in the neural system, SR in a single neuron is often investigated, and it is proposed that the sensory system may utilize SR in order to improve the sensitivity to the external input. Our results show that fluctuations can play a more functional role in higher order dynamics in the brain, such as the memory retrieval in the associative memory. Collins *et al.* propose that regulation of the fluctuation intensity is not required for a network of large numbers of neurons [89]. In our dynamics, however, regulation of the fluctuation intensity is required for optimal intensity (see Fig. 7.4).

It might be difficult to control the thermal fluctuations, but, if the sum of enormous presynaptic inputs act as fluctuations, it might be natural to control their intensities. It is known that stochastic resonance also takes place by fluctuation-like presynaptic inputs [83, 84, 85, 86]. In such a case, the dynamics of the system might be controlled by its background fluctuation [92, 93, 94].

Chapter 8

Networks Storing Sparse Patterns with Hierarchical Correlations

8.1 Introduction

Recently, the sparsely encoded associative memory is extensively investigated by enormous researchers. The coding of the memory is called "sparse" when the number of excited neurons is much smaller than that of quiescent ones, in other words, the firing rate of the network is small. It is known that the storage capacity for sparse patterns diverges as the firing rate of the pattern approaches 0. The existence of the sparsely encoded associative memory in the brain is discussed in physiological experiments (for a review, see Ref. [129]).

On the other hand, it is known that the mixed states of the stored patterns, which are nonlinear superpositions of stored patterns, also become equilibria of the network. The typical mixed states are the OR patterns, the AND patterns, and the majority decision mixed states [131]. In Ref. [130], the dynamics of the network storing memory patterns with hierarchical correlations are analyzed, and the mixed states of stored patterns are considered. Such mixed states may be interpreted as unnecessary patterns which accompany with stored patterns, but some researchers relate the stabilization of mixed states of stored patterns with a "concept formation" [128] and discuss the validity of this relation in the physiological experiments [131, 132].

In this chapter, we consider the sparsely encoded associative memory in the coupled FitzHugh-Nagumo models and the effect of fluctuations in the system. In Sec. 8.2, sparse patterns with hierarchical correlations are defined. In Sec. 8.3, the six patterns stored in the network are defined. In Sec. 8.4, the results of numerical simulations are presented. It is shown that the target pattern and the OR pattern which is one of the mixed patterns are retrieved individually by controlling the fluctuation intensity. In Secs. 8.5 and 8.6, theoretical analyses are presented. Results and discussions are given in the final section.

8.2 Patterns with Hierarchical Correlations

In the following, a network of the FN neurons which stores sparse patterns with firing rate $a \ll 0.5$, namely, the system governed by eqs. (7.1), (7.2), and (7.7) for $a \ll 0.5$ is treated. The sparsely encoded associative memory in a network of Hodgkin-Huxley models is investigated in Ref. [133] and the high storage capacity is observed. In our model, the memory patterns stored in the network are defined as follows. First, pattern vectors $\xi^\mu = (\xi_1^\mu, \xi_2^\mu, \cdots, \xi_N^\mu)$ $(\mu = 1, 2, \cdots, p)$ are randomly generated according to the probability density (7.6). By applying the bit transformation to ξ_i^μ, p_1 groups of patterns composed of p_2 patterns with overlap b are obtained. Note that the relationship $p = p_1 p_2$ holds and the overlap between the patterns ξ and ζ is defined as

$$m(\xi, \zeta) \equiv \frac{1}{Na(1-a)} \sum_{i=1}^{N} (\xi_i - a)(\zeta_i - a). \tag{8.1}$$

Let us denote the j-th pattern in the i-th group as $\zeta^{(i,j)}$. The overlap between two patterns which belong to different groups takes zero, namely, the patterns have hierarchical correlations [130] characterized by

$$\begin{aligned} &m(\zeta^{(i,j)}, \zeta^{(k,l)}) = (b + (1-b)\delta_{jl})\delta_{ik}, \\ &(1 \le i, k \le p_1, \ \ 1 \le j, l \le p_2). \end{aligned} \tag{8.2}$$

The connection coefficients J_{ij} are defined as

$$J_{ij} = \frac{1}{Na(1-a)} \sum_{k=1}^{p_1} \sum_{l=1}^{p_2} \zeta_i^{(k,l)} (\zeta_j^{(k,l)} - a). \tag{8.3}$$

The OR pattern vector $\zeta^{OR(k)} = (\zeta_1^{OR(k)}, \zeta_2^{OR(k)}, \cdots, \zeta_N^{OR(k)})$ of the k-th group is defined as

$$\zeta_i^{OR(k)} = U\left(\sum_{l=1}^{p_2} \zeta_i^{(k,l)} \right), \tag{8.4}$$

$$U(x) = \begin{cases} 1 & \text{if} \quad x > 0 \\ 0 & \text{otherwise} \end{cases}. \tag{8.5}$$

Generally, the mixed states of stored patterns in the k-th group is defined as

$$\zeta_i^{mix(k)} = U\left(\sum_{l=1}^{p_2} \zeta_i^{(k,l)} - \theta \right), \tag{8.6}$$

where θ is an arbitrary threshold [131]. Note that p_2 mixed states are defined by changing θ. It is known that the mixed states of the stored patterns are also memorized in the network. The storage capacity of the OR patterns diverges in the sparse limit $a \to 0$, and the storage capacities of other mixed states converge to 0 in the limit $a \to 0$. Thus the OR patterns are "typical" mixed states in the sparse limit. In the following we consider only the OR patterns as the mixes states of stored patterns.

The overlap between the state of the network and the pattern ζ is defined as

$$m_{out} = \frac{1}{Nf(1-f)} \sum_{i=1}^{N} (y_i - f)(\zeta_i - f), \tag{8.7}$$

$$f = \frac{1}{N} \sum_{i=1}^{N} \zeta_i, \tag{8.8}$$

where y_i is the binary series which depends on the state of the network defined by eq. (7.12).

In the following sections, we demonstrate that the target pattern $\zeta^{(1,1)}$ and the OR pattern $\zeta^{OR(1)}$ of the first group can be retrieved individually by controlling the fluctuation intensity D.

8.3 Definition of Six Pattern Vectors

In the following, only the case with $a = 0.1$, $p_1 = 2$, and $p_2 = 3$ is considered for simplicity. A schematic diagram of six patterns $\zeta^{(k,l)}$ $(k = 1, 2,\ l = 1, 2, 3)$ is shown in

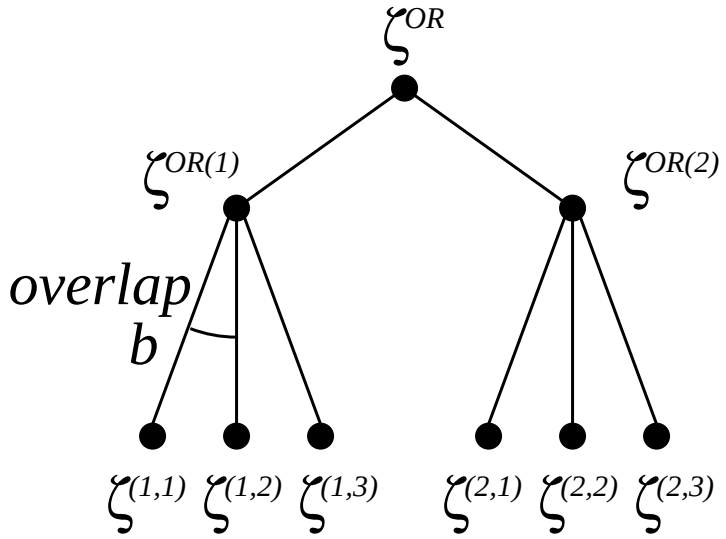

Figure 8.1 A schematic diagram of six pattern vectors.

Fig. 8.1. First, let us denote the set of indices of neurons which store 1's in the pattern $\zeta^{(k,l)}$ by

$$G(k,l) = \{i | \zeta_i^{(k,l)} = 1, 1 \le i \le N\}. \tag{8.9}$$

The sets $G(1,l)$ in the space of neuron indices are shown in Fig. 8.2. Note that the number of elements of the set $G(k,l)$ is

$$\#G(k,l) = \sum_{i=1}^{N} \zeta_i^{(k,l)} = Na. \tag{8.10}$$

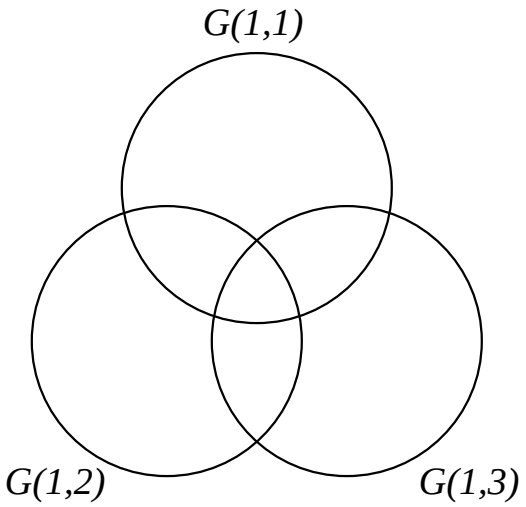

Figure 8.2 The sets $G(1,l)$ in the space of neuron indices.

Because the overlap between the patterns $\zeta^{(k,l_1)}$ and $\zeta^{(k,l_2)}$ $(l_1 \neq l_2)$ is b, the number of elements of the intersection of $G(k,l_1)$ and $G(k,l_2)$ is calculated to be

$$\begin{aligned} \#\left(G(k,l_1) \cap G(k,l_2)\right) &= \sum_{i=1}^{N} \zeta_i^{(k,l_1)} \zeta_i^{(k,l_2)}, & (8.11) \\ &= Na(a+b-ab) \quad (l_1 \neq l_2). & (8.12) \end{aligned}$$

Though the number of elements of the set $G(k,1) \cap G(k,2) \cap G(k,3)$ is not determined by the parameters a and b, we assume that the probability that the element of $G(k,1) \cap G(k,2)$ belongs to $G(k,1) \cap G(k,2) \cap G(k,3)$ is identical with the probability that the element of $G(k,1)$ belongs to $G(k,3)$. Under such an assumption, the number of elements of the set $G(k,1) \cap G(k,2) \cap G(k,3)$ is calculated to be

$$\#\left(G(k,1) \cap G(k,2) \cap G(k,3)\right) = Na(a+b-ab)^2. \tag{8.13}$$

Thus the number of elements of the joint set of $G(1,1)$, $G(1,2)$, and $G(1,3)$ is $Na[3 - 3(a+b-ab) + (a+b-ab)^2]$, and we denote it as N_{all} in the following.

Without loss of generality, the pattern $\zeta^{(1,1)}$ can be defined as

$$\zeta_i^{(1,1)} = \begin{cases} 1 & 1 \leq i \leq Na = 24 \\ 0 & \text{otherwise} \end{cases}, \tag{8.14}$$

and $\zeta^{(1,2)}$ and $\zeta^{(1,3)}$ are defined so that the OR pattern $\zeta^{OR(1)}$ of the first group satisfies

$$\zeta_i^{OR(1)} = \begin{cases} 1 & 1 \leq i \leq N_{all} = 62 \\ 0 & \text{otherwise} \end{cases}. \tag{8.15}$$

The patterns $\zeta^{(2,l)}$ $(l = 1,2,3)$ are determined randomly so that they satisfy eq. (8.2).

8.4 Fluctuation-induced Pattern Selection

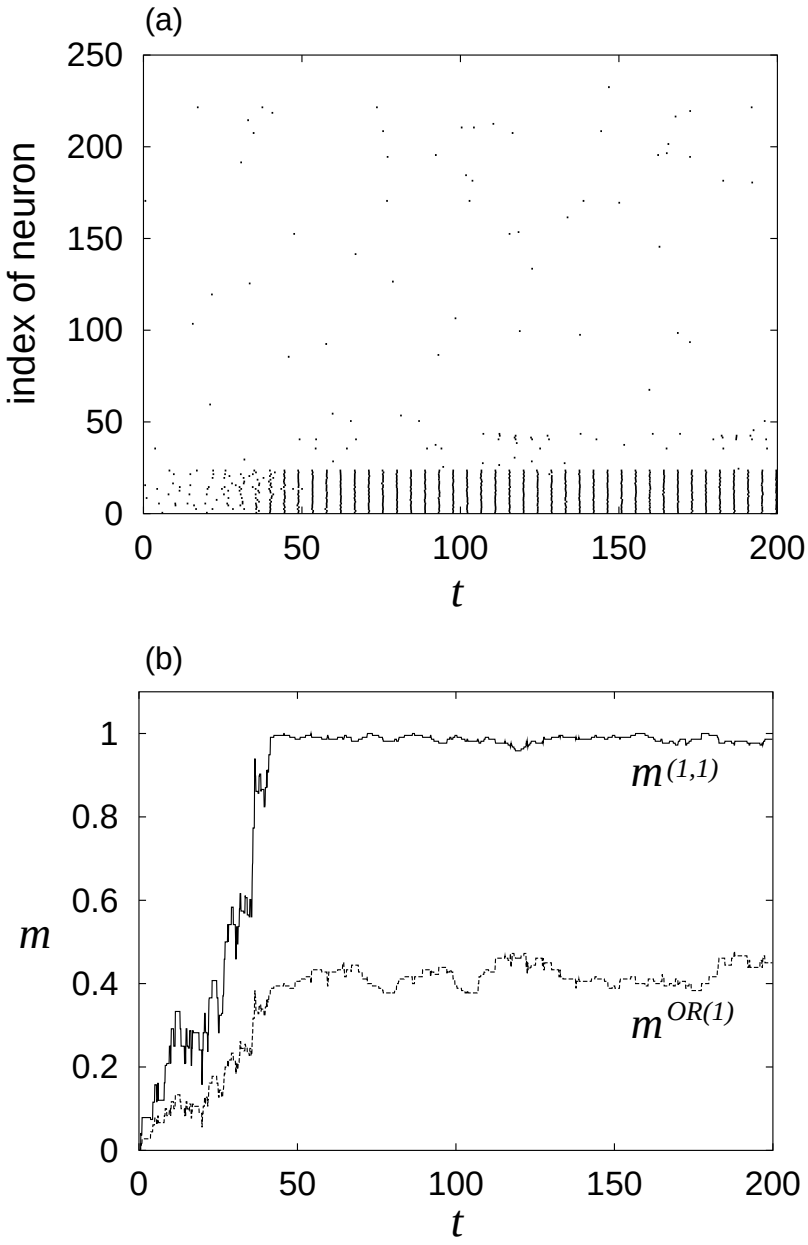

Figure 8.3 The result of a numerical simulation, (a) the firing times of all the neurons and (b) the overlaps $m^{(1,1)}$ and $m^{OR(1)}$ for $N = 240$, $b = 0.07$, and $D = 0.001$. The retrieval of the pattern $\zeta^{(1,1)}$ is successful.

Under the above configurations, numerical simulations are performed for $N = 240$, $a = 0.1$, $b = 0.07$, $m_{in}^{(1,1)} = 0.6$, and $g_{peak} = 0.5$. At the time $t = 0$, the variables u_i and

v_i are set around the equilibrium, namely, $u_i \simeq -1.2$ and $v_i \simeq -0.63$.

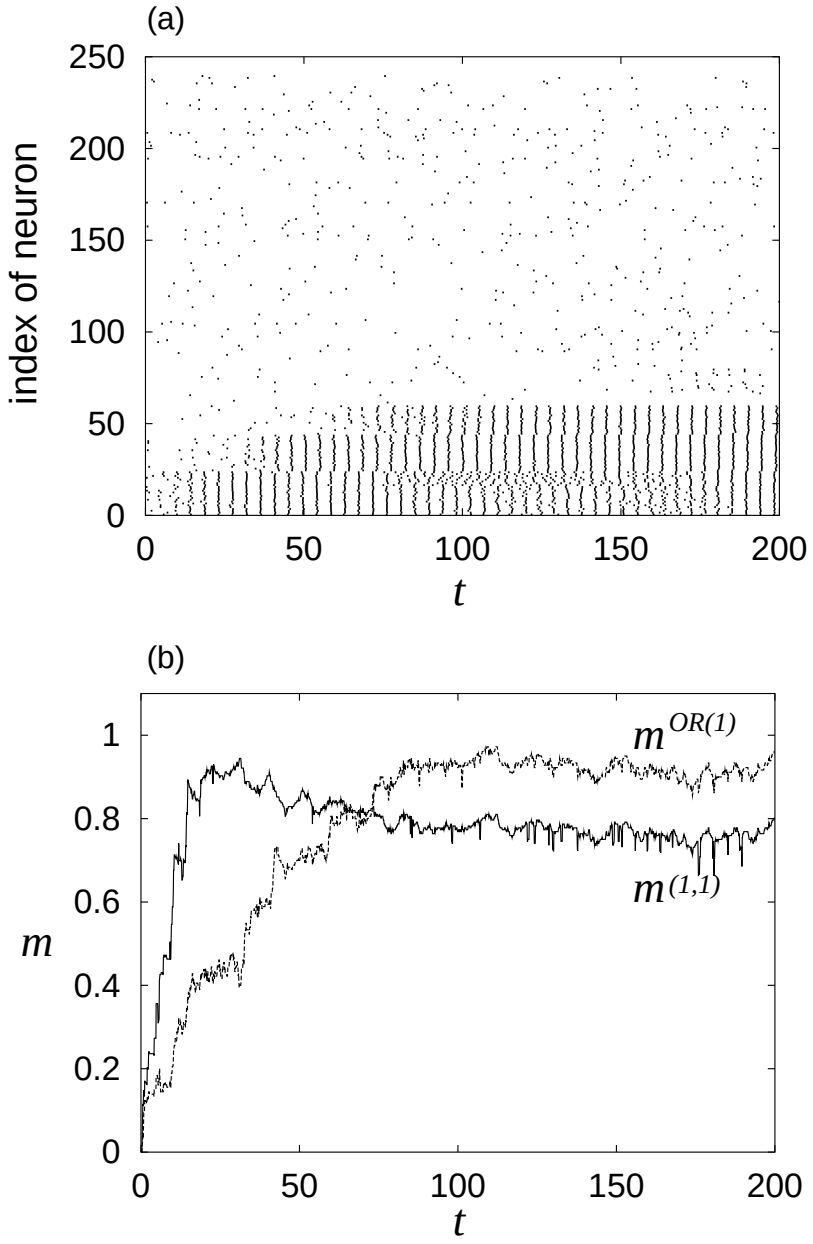

Figure 8.4 The result of a numerical simulation, (a) the firing times of all the neurons and (b) the overlaps $m^{(1,1)}$ and $m^{OR(1)}$ for $N = 240$, $b = 0.07$, and $D = 0.0017$. The retrieval of the OR pattern $\zeta^{OR(1)}$ is successful.

The firing times of all the neurons for the fluctuation intensity $D = 0.001$ are shown in Fig. 8.3(a). It is observed that the neurons which store 1's in the pattern $\zeta^{(1,1)}$ start

to fire periodically at $t \simeq 50$. Let us denote the overlap between the state of the network and the pattern $\zeta^{(1,1)}$ as $m^{(1,1)}$, and the overlap between the state of the network and the OR pattern $\zeta^{OR(1)}$ of the first group as $m^{OR(1)}$. The time series of overlaps $m^{(1,1)}$ and $m^{OR(1)}$ are shown in Fig. 8.3(b). The overlap $m^{(1,1)}$ reaches almost 1 at $t \simeq 50$, thus the retrieval of pattern $\zeta^{(1,1)}$ is successful.

The result of a numerical simulation for $D = 0.017$ is shown in Fig. 8.4. At small t, the pattern $\zeta^{(1,1)}$ is retrieved, but at $t \simeq 80$, it is observed that $m^{OR(1)}$ exceeds $m^{(1,1)}$, thus in this case the OR pattern $\zeta^{OR(1)}$ is successfully retrieved.

From the above results, it can be concluded that the target pattern is retrieved for the small fluctuation intensity, and the OR pattern is retrieved for the moderate fluctuation intensity.

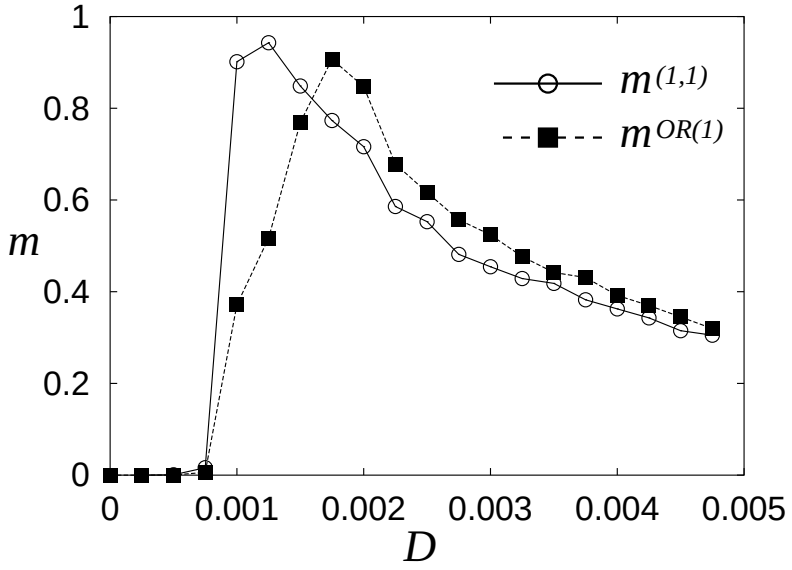

Figure 8.5 The asymptotic values of the overlaps $m^{(1,1)}$ and $m^{OR(1)}$ as a function of the fluctuation intensity D for $N = 240$ and $b = 0.07$. Each overlap is numerically obtained by averaging the value over $150 \leq t \leq 200$.

In Fig. 8.5, the asymptotic values of overlaps $m^{(1,1)}$ and $m^{OR(1)}$ are plotted against the fluctuation intensity D. It is observed that the overlap $m^{(1,1)}$ takes a maximum at $D \simeq 0.001$, and the overlap $m^{OR(1)}$ takes a maximum at $D \simeq 0.0017$. Thus it can be concluded that the target pattern and the OR pattern can be retrieved individually by controlling the fluctuation intensity. In other words, a pattern selection is induced by the fluctuations in the system.

The asymptotic values of the overlaps as a function of the fluctuation intensity D for $b = 0$ and 0.1 are shown in Figs. 8.6 (a) and (b), respectively. For $b = 0$, it is observed that only the target pattern $\zeta^{(1,1)}$ is successfully retrieved, and for $b = 0.1$, it is observed that only the OR pattern $\zeta^{OR(1)}$ is successfully retrieved. Thus it is concluded that the

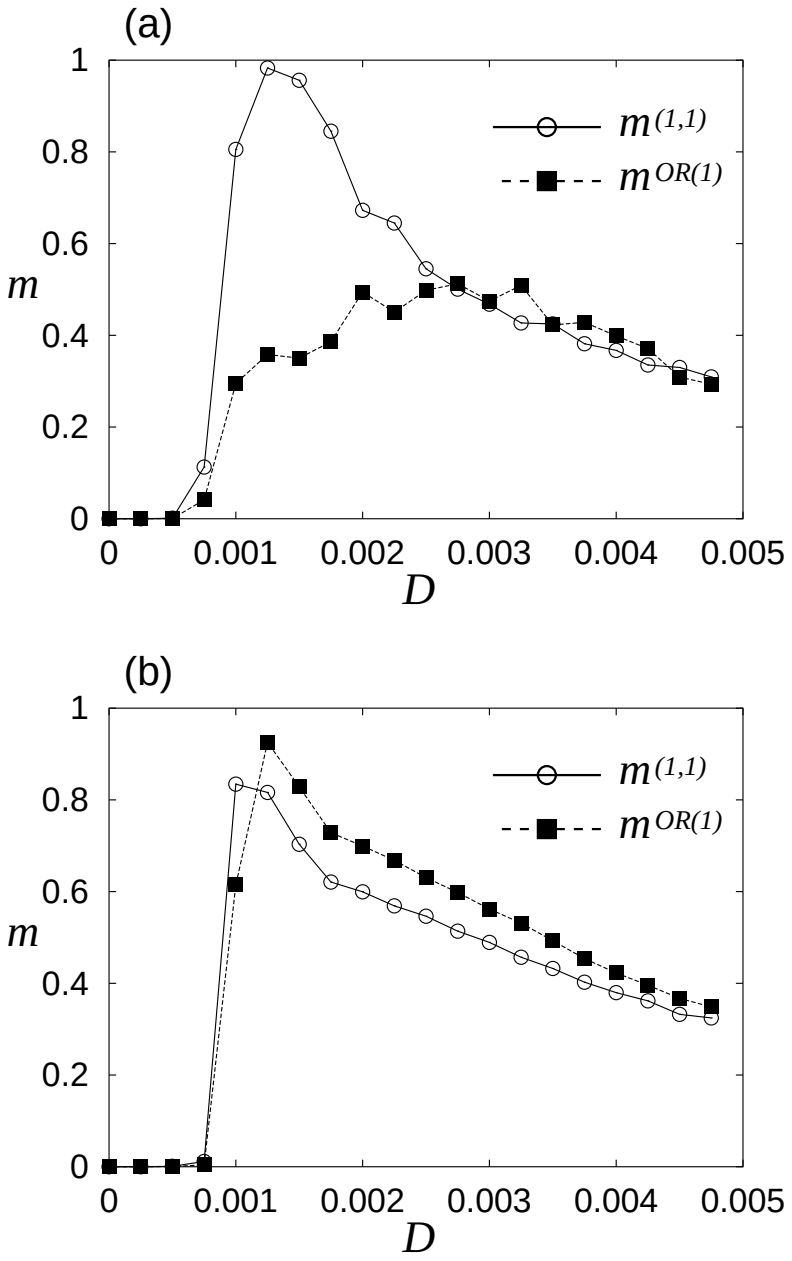

Figure 8.6 The asymptotic values of the overlaps $m^{(1,1)}$ and $m^{OR(1)}$ as a function of the fluctuation intensity D for (a) $b = 0$ and (b) $b = 0.1$ with $N = 240$. Each overlap is numerically obtained by averaging its value over $150 \leq t \leq 200$. (a) Only the target pattern is successfully retrieved. (b) Only the OR pattern is successfully retrieved.

overlap b between the patterns in the identical group is important to retrieve both the

target pattern and the OR pattern.

As shown in Figs. 8.3 and 8.4, there is a characteristic time required for the retrieval of patterns. Let us define the periods to retrieve the patterns $\zeta^{(1,1)}$ and $\zeta^{OR(1)}$ as $T^{(1,1)}$ and $T^{OR(1)}$, respectively. The dependences of $T^{(1,1)}$ and $T^{OR(1)}$ on the fluctuation intensity D for $b = 0.07$ are shown in Fig. 8.7. It is observed that $T^{(1,1)}$ and $T^{OR(1)}$ diverge at

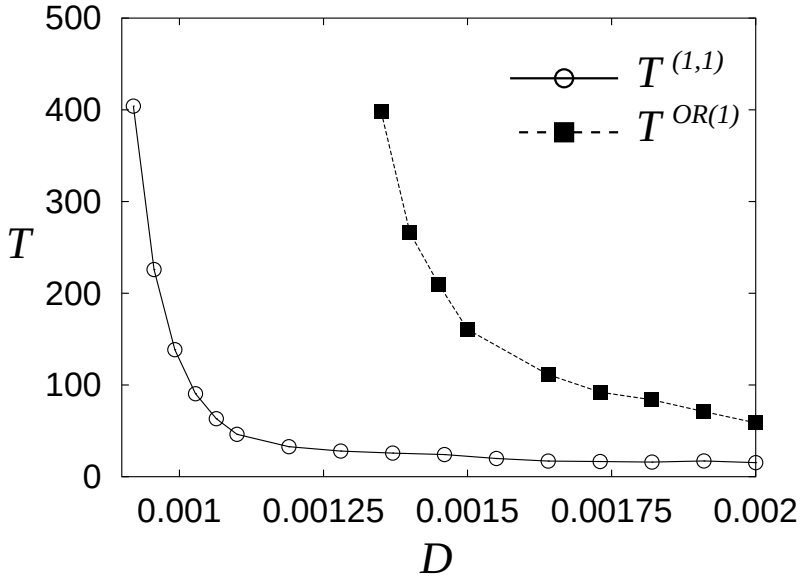

Figure 8.7 The dependences of $T^{(1,1)}$ and $T^{OR(1)}$ on the fluctuation intensity D for $b = 0.07$. The data are obtained by taking the mean values of $100 \sim 200$ samples. The number of samples depends on the fluctuation intensity D.

$D = 0.0009$ and 0.0013, respectively. It is because the retrieval of patterns is realized by saddle-node bifurcations with the parameter D. This dynamics is treated in the following sections.

8.5 Theoretical Analysis of Fluctuation-induced Pattern Selection (1)

In this section, we give a qualitative explanation for the fluctuation-induced pattern selection. In the following, the system with $p_1 = 1$ and $p_2 = 3$, namely, a network which stores three patterns $\zeta^{(1,l)}$ $(l = 1, 2, 3)$ with overlap b is considered for simplicity. The external input is injected only to the neurons in the set $G(1, 1)$. In the following, we treat only the dynamics of the neurons in the set $G(1, 1) \cup G(1, 2) \cup G(1, 3)$ for simplicity.

Let us consider the number of neurons which fire in the narrow time interval $[t, t+\Delta_w]$ and denote it by Naz_n. The perturbation caused by those firings is injected to the

particular neurons after the delay d_p. Let us denote the number of neurons which fire with this perturbation in the time interval $[t + d_p, t + d_p + \Delta_w]$ by Naz_{n+1}, and assume the relation $z_{n+1} = g(z_n)$.

Numerical derivation of $g(z_n)$ is performed as follows. Note that the simplified dynamics introduced in Appendix B is used to obtain $g(z_n)$. First, sufficiently strong pulses are injected to some neurons. The number of neurons, which fire with the effect of the input pulses and fluctuations, gives the value of z_n. By preparing a variety of input pulses, we can generate a set of z_n's. The value of $z_{n+1} = g(z_n)$ is determined from the number of neurons which fire after the delay d_p. Numerically obtained $g(z_n)$ for $D = 0.0005$, 0.001, and 0.0017 with $Na = 100$ and $U_0 = 0.1$ is shown in Fig. 8.8. The

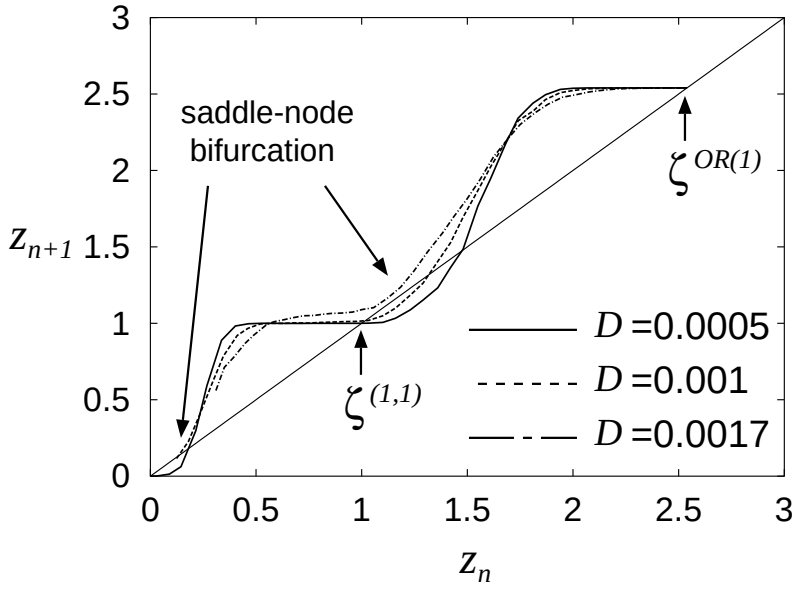

Figure 8.8 The relationship between z_n and z_{n+1} for $b = 0.07$. The data are obtained by taking the mean value of 50 samples.

intersecting points of $g(z_n)$ with a line $z_{n+1} = z_n$ are the fixed points, and they are stable if the differential coefficient of $g(z_n)$ at the fixed point is smaller than 1, and otherwise they are unstable. It is shown that there are three stable fixed points at $z \simeq 0, 1$, and 2.6 for $D = 0.0005$. Because all the neurons are set around the equilibrium at the time $t = 0$, the initial value of z_n is $z_0 \simeq 0$. Thus the system are stable at $z \simeq 0$ and almost all the neurons are quiescent.

At $D = 0.001$, a pair of stable and unstable fixed points at $z \simeq 0$ disappears by a saddle-node bifurcation, and the system reaches the stable fixed point at $z \simeq 1$, namely, the pattern $\zeta^{(1,1)}$ is retrieved.

At a point between $D = 0.001$ and 0.0017, a pair of stable and unstable fixed points at $z \simeq 1$ also disappears, and the system reaches the stable fixed point at $z = N_{all}/Na \simeq 2.6$, namely, the pattern $\zeta^{OR(1)}$ is retrieved.

The retrievals of the pattern $\zeta^{(1,1)}$ and the OR pattern $\zeta^{OR(1)}$ are realized by such dynamics. This analysis is similar to the theoretical analysis of the propagation of synchronized spikes in the feedforward synfire chain [134].

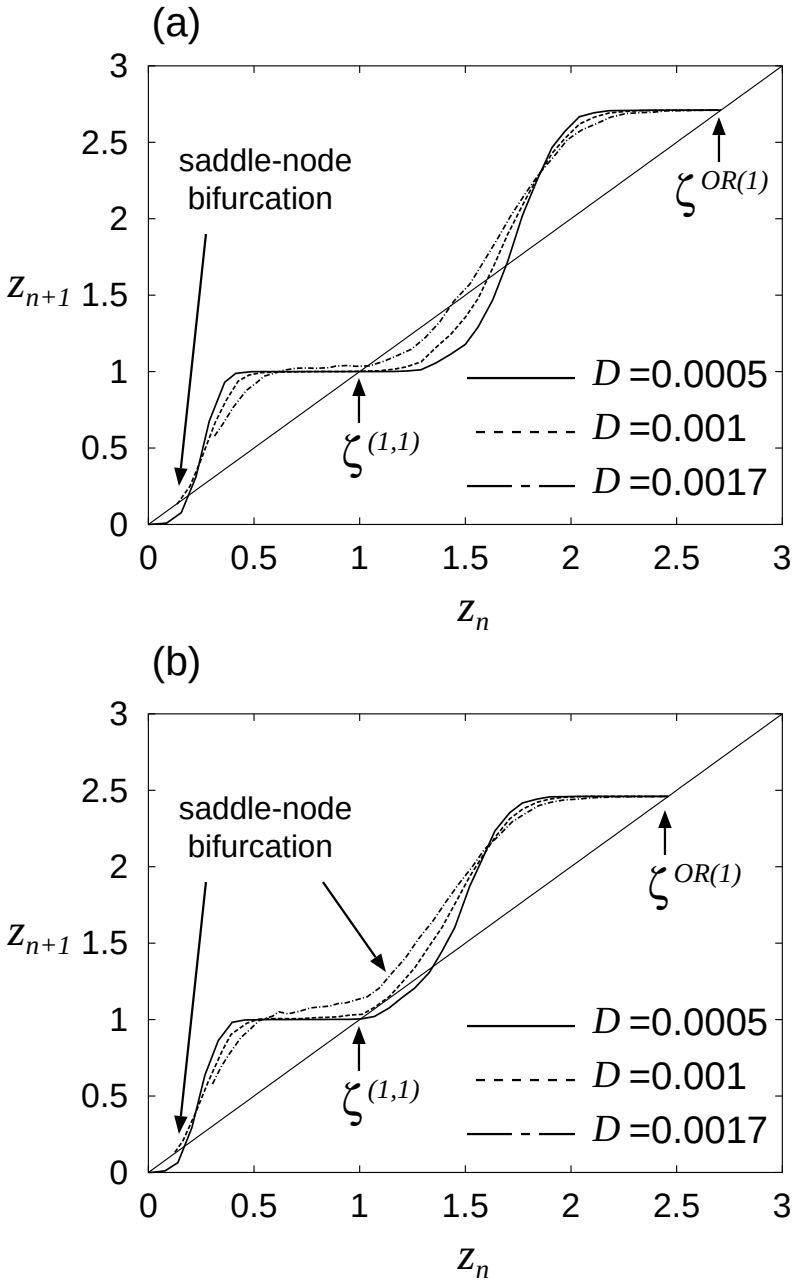

Figure 8.9 The relationship between z_n and z_{n+1} for (a) $b = 0$ and (b) $b = 0.1$. The data are obtained by taking the mean value of 50 samples.

The numerically obtained $g(z_n)$ for $b = 0$ and 0.1 are shown in Figs. 8.9 (a) and (b), respectively. For $b = 0$, the stable fixed point at $z \simeq 1$ exists even for large D, thus the OR pattern $\zeta^{OR(1)}$ is not retrieved. For $b = 0.1$, the stable fixed points at $z \simeq 0$ and 1 disappear at almost the identical fluctuation intensity $D \simeq 0.001$, thus only the OR pattern $\zeta^{OR(1)}$ is retrieved.

8.6 Theoretical Analysis of Fluctuation-induced Pattern Selection (2)

In the previous section, the fluctuation-induced pattern selection is analyzed with a one dimensional map of the number z_n of the neurons which fire in the narrow time interval. In this section, an analysis based on a two dimensional map is presented.

As shown in Fig. 8.10, two variables z_n and σ_n are defined as the number of the firing neurons and the standard deviation of the firing times in the narrow time interval, respectively. The width of the time interval is set at a value around the time delay of

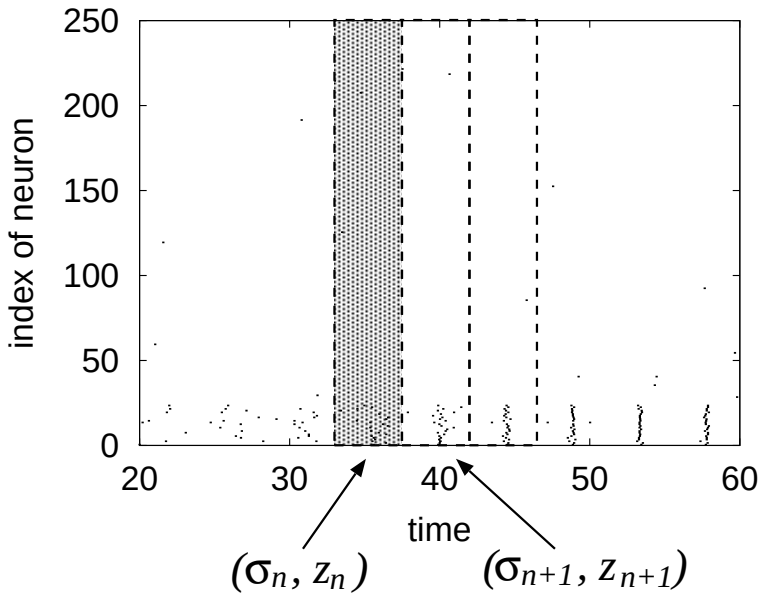

Figure 8.10 The definition of the two variables z_n and σ_n. The width of the time interval is set at a value around the time delay of the network, namely, the period of the periodic firing.

the network, namely, the period of the periodic firing. In the following, the discrete-time dynamics of (σ_n, z_n) $(n = 0, 1, 2 \cdots)$ is considered. The numerical simulations are performed for $Na = 100$, $p_1 = 1$, and $p_2 = 3$ for the simplified dynamics introduced in Appendix B.

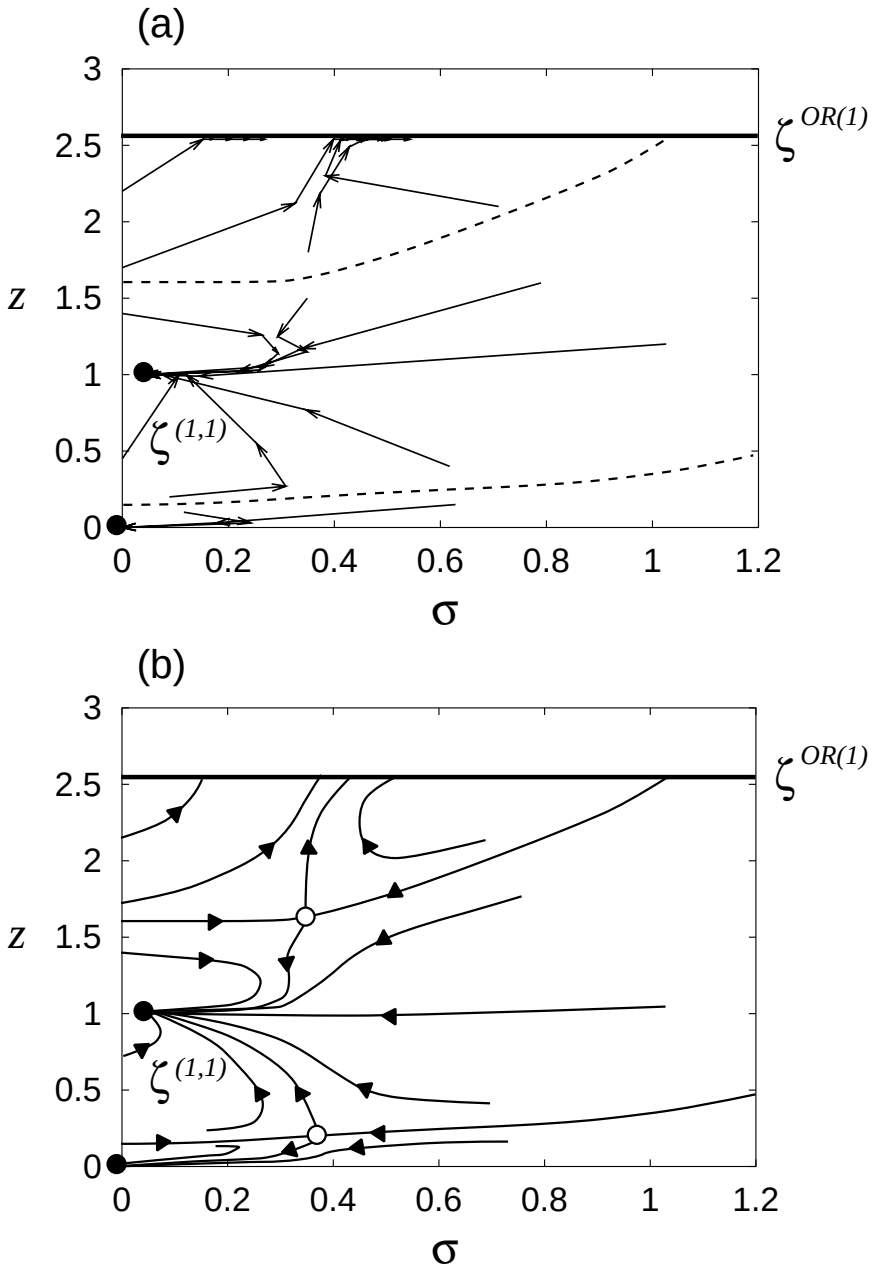

Figure 8.11 The flows in the (σ, z) plane for $D = 0.0005$. (a) The numerically obtained flows and (b) the schematic flows deduced from (a).

The numerically obtained flows in the (σ, z) plane for $D = 0.0005$ are shown in Fig. 8.11 (a). Note that the number z_n of the firing neurons is normalized by the number of the neurons which store 1's in the pattern $\zeta^{(1,1)}$, namely, Na. Three attractors in the

(σ, z) plane are observed. One is (0,0), and the rests are the attractors corresponding to $\zeta^{(1,1)}$ and $\zeta^{OR(1)}$. The reason why the attractor denoting $\zeta^{OR(1)}$ is not a single node but a line $z \simeq 2.6$ is given later. When the number of the initially firing neurons is sufficiently

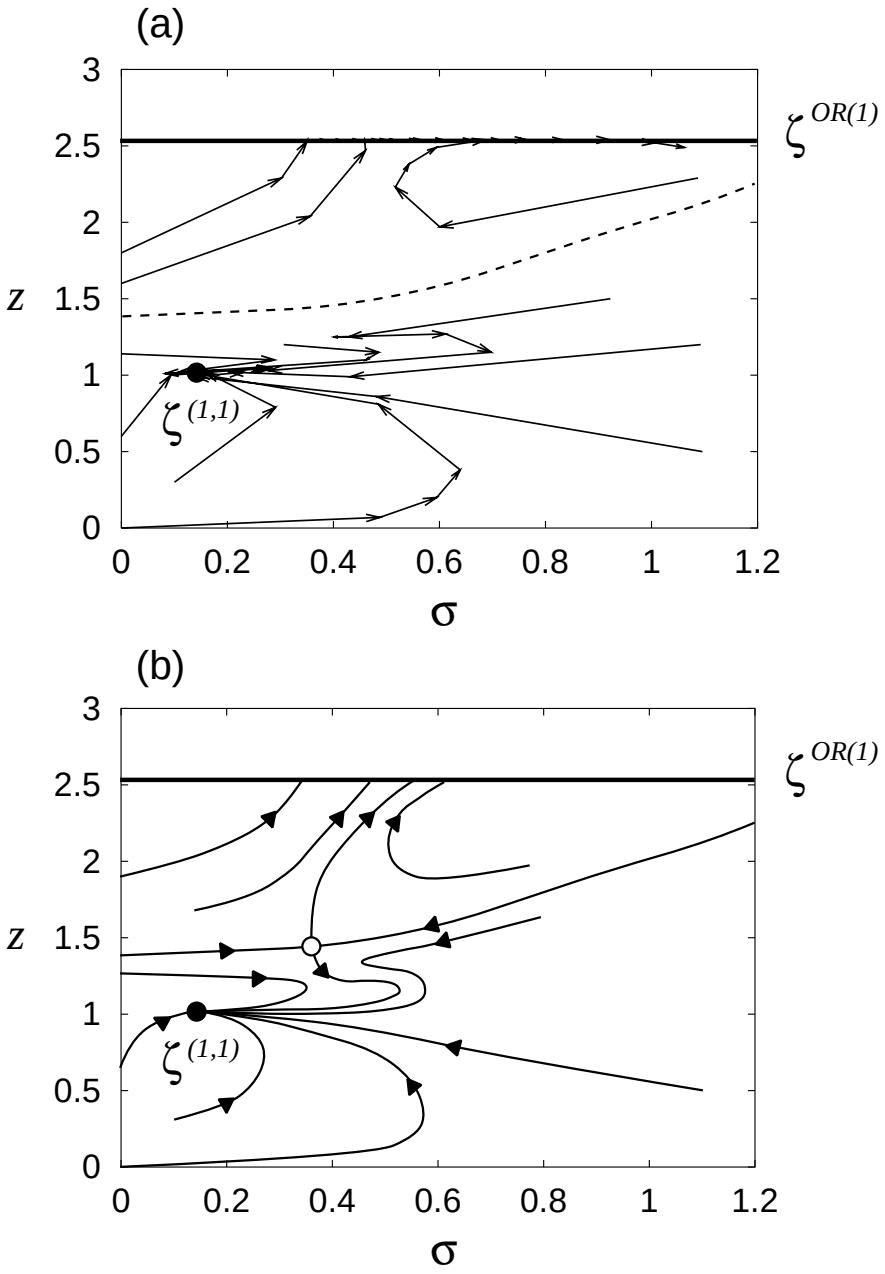

Figure 8.12 The flows in the (σ, z) plane for $D = 0.0012$. (a) The numerically obtained flows and (b) the schematic flows deduced from (a).

small, namely, $z_0 \simeq 0$, it is observed that (σ_n, z_n) converges to (0,0). In other words, the memory retrieval fails for $z_0 \simeq 0$ with $D = 0.0005$ because almost all the neurons cannot fire with this fluctuation intensity. Note that the system cannot cross the dotted curve about $z_n \simeq 0.2$ shown in Fig. 8.11 (a), which shows the boundary of the basins for the attractors (0,0) and $\zeta^{(1,1)}$. This boundary seems to be the stable manifold of a saddle at about $(\sigma, z) = (0.4, 0.2)$ shown in Fig. 8.11 (b).

The numerically obtained flows in the (σ, z) plane for $D = 0.0012$ are shown in Fig. 8.12 (a). The attractor at about (0,0) disappears because of a saddle-node bifurcation, thus the system initially put at (0,0) converges to the attractor at about (0.15,1), which denotes the pattern $\zeta^{(1,1)}$.

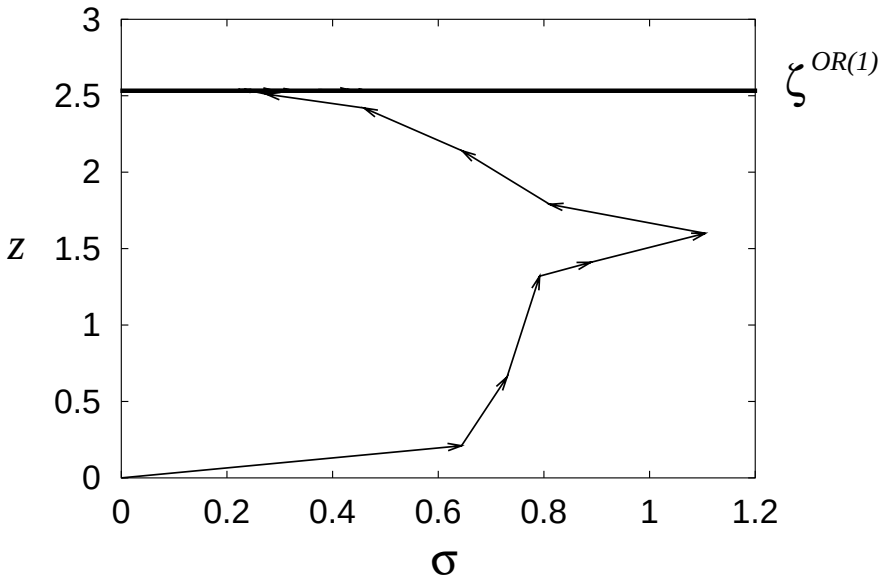

Figure 8.13 The numerically obtained flows in the (σ, z) plane for $D = 0.002$.

The numerically obtained flows in the (σ, z) plane for $D = 0.002$ are shown in Fig. 8.13. The attractor which denotes the pattern $\zeta^{(1,1)}$ disappears because of a saddle-node bifurcation again, thus the system initially put at (0,0) converges to the line at $z \simeq 2.6$ which denotes the pattern $\zeta^{OR(1)}$.

As previously noted, the pattern $\zeta^{OR(1)}$ cannot denoted by a single node in the (σ, z) plane, because all the neurons which store 1's in $\zeta^{OR(1)}$ cannot synchronize each other as shown in Fig. 8.14. The step inputs are injected to the neurons which store 1's in the pattern $\zeta^{(1,1)}$, thus they fire slightly earlier than the other neurons.

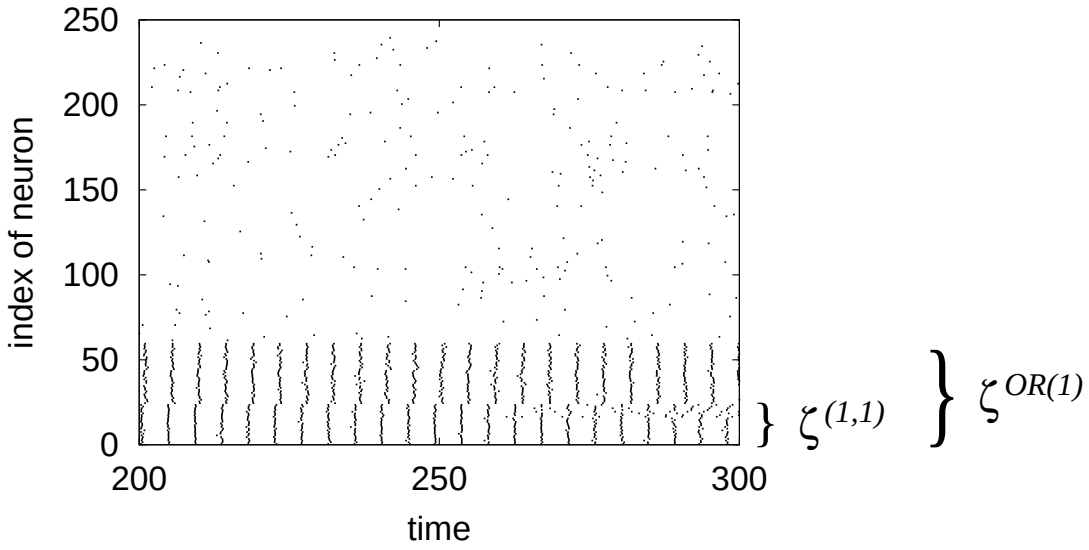

Figure 8.14 The firing times of all the neurons in the system for $N = 240$, $b = 0.07$, and $D = 0.0017$. It is observed that the neurons in the range from 1 to 24 fire slightly earlier than the other neurons.

8.7 Results and Discussions

The associative memory in a pulsed neural network storing sparse patterns with hierarchical correlations is investigated. The stored memory patterns composed of 0/1 digits are represented by the synchronous periodic firings in the network. It is found that the retrieval of the target pattern is achieved by adding fluctuations to the system. This phenomenon is similar to so-called stochastic resonance, where a weak input signal is enhanced by its background fluctuations. Besides the target pattern, the OR pattern which is the nonlinear superposition of the three patterns which belong to the identical group is also retrieved with the help of fluctuations and its optimal fluctuation intensity is larger than that of the target pattern. Thus the target pattern and the OR pattern are retrieved individually by controlling the fluctuation intensity, in other words, a fluctuation-induced pattern selection takes place. Theoretical analyses of the above results are also presented, and it is found that the fluctuation-induced pattern selection is realized by successive saddle-node bifurcations parameterized by the fluctuation intensity.

The OR pattern may be interpreted as unnecessary patterns which accompany with stored patterns, but some researchers relate the stabilization of mixed states of stored patterns with a "concept formation" [128], and discuss the validity of this relation in the physiological experiments [131, 132]. If the OR pattern is meaningful in the information processing, the above results suggest that the fluctuations in the system might play significant roles in the brain.

Part IV

Conclusions

Chapter 9

Conclusions and Discussions

9.1 Conclusions

Concerning the fluctuation which is observed in biological sensory systems and cortical neuronal networks, the roles of fluctuations in pulsed neural networks are investigated. As a model of a single neuron, the FitzHugh-Nagumo model is used, and two kinds of couplings of neurons are considered, namely, the electrical coupling which is often observed in sensory systems, and the chemical coupling which is widely seen in cortical neuronal networks.

In Part II, the effects of fluctuations in the network of electrically coupled FitzHugh-Nagumo models are investigated.

In Chap. 4, the network of electrically coupled FitzHugh-Nagumo models without time delays is treated. The periodic pulse trains and Gaussian white noise are appended to the network, and the dependence of the network on the fluctuation intensity is investigated. In the single neuron model, it is observed that so-called stochastic resonance (SR) takes place, that is, the correlation between the input and the output is maximized at an optimal fluctuation intensity. In the coupled system, it is found that the optimal fluctuation intensity increases with the increase of the coupling strength in the network, and the asymptotic value of the optimal fluctuation intensity is proportional to the number of neurons. We analyzed this dependence of the fluctuation intensity on the number of neurons theoretically. Using this property, a network composed of thirty neurons, which can separate a superimposed periodic pulse train by controlling the fluctuation intensity, is constructed.

In Chap. 5, the system treated in Chap. 4 is treated again. It is observed that the correlation between the input and the output takes a maximum as a function of not only the fluctuation intensity but also the coupling strength. This phenomenon called array-enhanced stochastic resonance (AESR) is analyzed theoretically. By transforming the dynamics of N neurons into that of the mean dynamics $\boldsymbol{X}$ and the deviation $\delta\boldsymbol{x}^{(i)}$, it is found that AESR is caused by the term $\propto -X_1(\delta x_1)^2$, particularly by the correlation between $(\delta x_1)^2$ and X_1. The character of the fluctuations of $(\delta x_1)^2$ are also investigated, and it is found that the deviation of the peak value C_{peak} of the approximation from that of the network of N neurons is caused by the asymmetry of the distribution of the

fluctuations of $(\delta x_1)^2$, and the correlation between the fluctuations of $(\delta x_1)^2$ and the mean dynamics X_1.

In Chap. 6, the network of electrically coupled FitzHugh-Nagumo models with a time delay is treated. Similarly to the previous chapters, the periodic inputs and Gaussian white noise are appended to the network. When the time delay d_p and the frequency f of the periodic input pulse train satisfy the relationship $d_p = 1/f$, it is observed that an optimal fluctuation intensity which maximizes the correlation coefficient increases with the increase of the coupling strength, and the peak value of the correlation coefficient decreases with the increase of the coupling strength. For the time delay $d_p = 1/f - d_f$ dependent on the firing delay d_f, a deterministic firing is induced at the optimal fluctuation intensity, which increases with the increase of the number of neurons. Using these properties, a network composed of two assemblies is constructed. It separates a superimposed periodic pulse train, and its dynamics can be controlled by fluctuations. In this network, a rearrangement of the synchronously oscillating assembly by controlling the fluctuation intensity is observed.

In Part III, the effects of fluctuations in the network of chemically coupled FitzHugh-Nagumo models are investigated.

In Chap. 7, the associative memory in the network of chemically coupled FitzHugh-Nagumo models with a time delay is treated. The stored patterns are composed of 0/1 digits, and represented by the synchronous periodic firings of the particular neurons in the network. In this chapter, the case where the mean value of the stored patterns is 0.5 is considered. It is found that the memory retrieval in this system is achieved by adding fluctuations, and there exists an optimal fluctuation intensity for memory retrieval. Though there is no time-dependent input in our model, the mechanism of associative memory is driven and enhanced by its background fluctuation. The basin of attraction of this system is investigated numerically, and its storage capacity is found to be $\alpha_c \simeq 0.04$. By the analysis with a one dimensional map, it is found that the fluctuation-induced memory retrieval is realized by a saddle-node bifurcation in this map. It is also found that our network has an ability that the previous models do not have, that is, an ability to retrieve two patterns as the alternate firings of the particular neurons.

In Chap. 8, the network treated in Chap. 7 is treated again. The stored patterns are sparse, namely, the mean value of the patterns is small, and they have hierarchical correlations. As shown in Chap. 7, the retrieval of the target pattern is achieved by adding fluctuations to the system. It is also found that the OR pattern which is the nonlinear superposition of the three patterns which belong to the identical group is also retrieved with the help of fluctuations and its optimal fluctuation intensity is larger than that of the target pattern. Thus the target pattern and the OR pattern are retrieved individually by controlling the fluctuation intensity, in other words, a fluctuation-induced pattern selection takes place. Theoretical analyses of the above results are also presented, and it is found that the fluctuation-induced pattern selection is realized by successive saddle-node bifurcations parameterized by the fluctuation intensity.

9.2 Discussions

In this thesis, a network with electrical couplings and a network with chemical couplings are considered, and the effect of fluctuations is investigated. For both cases, it is found that the fluctuations in the system can bring beneficial effects to the network. Moreover, they can play functional roles like parameters which control the dynamical state of the network. For example, the superimposed periodic pulse train is separated into the periodic components by controlling the fluctuation intensity in the network with electrical couplings (Chaps. 4 and 6), and the target pattern and the OR pattern are retrieved individually by controlling the fluctuation intensity in the network of chemical couplings (Chap. 8). These results suggest that the fluctuations might be important in the information processing in neural systems.

As shown in Chap. 1, there are several sources of fluctuations in the neural system, such as, the fluctuations in the outer world, the stochasticity of the ion channels, the synaptic unreliability, the fluctuations of the sum of presynaptic inputs, and chaos caused by the nonlinearity of the neuron.

In the sensory system, which is modeled by the network with electrically couplings, the fluctuations in the system might be caused mainly by the fluctuations in the outer world and the stochasticity of the ion channels, thus it shall be difficult to control the fluctuations in the system. However, with the mechanism of AESR, the correlation between the input and the output can be maximized by controlling the coupling strength of the network for the fixed fluctuation intensity. Thus it is concluded that the maximization of the correlation can be realized in the sensory system by controlling the coupling strength.

In the cortical neural network, which is modeled by the network with chemical couplings, the fluctuations in the system might be caused mainly by the synaptic unreliability and the fluctuations of the sum of presynaptic inputs. As shown in Chap. 1, they can be controlled by the release probabilities of chemical transmitters and the activities of presynaptic neurons. Thus the fluctuation-induced memory retrieval and the pattern selection might be realizable in the cortical neuronal networks.

Appendix A

Analytical Derivation of $\langle(\delta x_1)^2\rangle_{app2}$

In this appendix, we analytically derive the term $\langle(\delta x_1)^2\rangle_{app2}$ given by eq. (5.33), namely,

$$\langle(\delta x_1)^2\rangle_{app2} = \frac{(1-N^{-1})D}{2\tau(w-1+X_1^2)}, \tag{A.1}$$

from the stochastic differential equation

$$\begin{aligned}
\frac{d}{dt}\delta x_1 &= -\frac{1}{\tau}(w-1+X_1^2)\delta x_1 - \frac{1}{\tau}\delta x_2 + \frac{1}{\tau}\tilde{\eta}, &\text{(A.2)}\\
\frac{d}{dt}\delta x_2 &= \delta x_1 - \beta\delta x_2, &\text{(A.3)}\\
\langle\tilde{\eta}(t)\tilde{\eta}(t')\rangle &= (1-N^{-1})D\delta(t-t'), &\text{(A.4)}
\end{aligned}$$

where the suffix (i) which denotes the index of the neuron is omitted for simplicity.

With the vector $\boldsymbol{x} = (\delta x_1, \delta x_2)^t$, eqs. (A.2) and (A.3) are written as

$$\frac{d}{dt}\boldsymbol{x} = A(t)\boldsymbol{x} + \boldsymbol{f}(t). \tag{A.5}$$

Let us denote the solution of $\dot{\boldsymbol{x}} = A(t)\boldsymbol{x}$ as $\boldsymbol{x}(t) = B(t)\boldsymbol{x}(0)$ by the solution matrix $B(t)$. Then the solution of eq. (A.5) is written as

$$\boldsymbol{x}(t) = B(t)\boldsymbol{x}(0) + B(t)\int_0^t dsB^{-1}(s)\boldsymbol{f}(s). \tag{A.6}$$

Note that the solution matrix $B(t)$ rapidly converges to 0 as $t \to \infty$ for sufficiently large w.

With $\tilde{\eta} = 0$, eq. (A.2) is solved to be

$$\delta x_1(t) = \phi(t,0)\delta x_1(0) - \frac{1}{\tau}\int_0^t ds\phi(t,s)\delta x_2(s), \tag{A.7}$$

where

$$\phi(t,s) \equiv \exp\left[-\frac{1}{\tau}(w-1)(t-s) - \frac{1}{\tau}\int_s^t dt' X_1^2(t')\right]. \tag{A.8}$$

With the assumption that $B(t) \to 0$ as $t \to \infty$, the condition that $\phi(t,0) \to 0$ as $t \to \infty$ is required.

If the convergence of $\phi(t,s) \sim \phi(t-s,0)$ to 0 as $t-s \to \infty$ is sufficiently rapid, $\delta x_2(s)$ in eq. (A.7) can be replaced by $\delta x_2(t)$. With this assumption, eq. (A.7) becomes

$$\begin{aligned} \delta x_1(t) &\simeq \phi(t)\delta x_1(0) - \psi(t)\delta x_2(t), && \text{(A.9)} \\ \phi(t) &\equiv \phi(t,0), && \text{(A.10)} \\ \psi(t) &\equiv \frac{1}{\tau}\int_0^t ds\phi(t,s). && \text{(A.11)} \end{aligned}$$

Substituting eq. (A.9) in eq. (A.3), we obtain

$$\frac{d}{dt}\delta x_2 = \phi(t)\delta x_1(0) - (\psi(t)+\beta)\delta x_2, \tag{A.12}$$

and it is solved as

$$\delta x_2(t) = \exp\left[-\int_0^t ds(\psi(s)+\beta)\right]\delta x_2(0) + \int_0^t ds \exp\left[-\int_s^t dt'(\psi(t')+\beta)\right]\phi(s)\delta x_1(0). \tag{A.13}$$

From eqs. (A.9) and (A.13), we obtain

$$\begin{aligned} B_{21}(t) &= \int_0^t ds \exp\left[-\int_s^t dt'(\psi(t')+\beta)\right]\phi(s), && \text{(A.14)} \\ B_{22}(t) &= \exp\left[-\int_0^t ds(\psi(s)+\beta)\right], && \text{(A.15)} \\ B_{11}(t) &= \phi(t) - \psi(t)B_{21}(t), && \text{(A.16)} \\ B_{12}(t) &= -\psi(t)B_{22}(t). && \text{(A.17)} \end{aligned}$$

With $\delta x_1(0) = 0$, $\delta x_2(0) = 0$, $\boldsymbol{f}(t) = (\tilde{\eta}(t)/\tau, 0)^t$, and eq. (A.6), we obtain

$$\delta x_1(t) = \frac{1}{\tau}\int_0^t ds\tilde{\eta}(s)\left[B_{11}(t){B^{-1}}_{11}(s) + B_{12}(t){B^{-1}}_{21}(s)\right]. \tag{A.18}$$

The term in the brackets in eq. (A.18) is calculated to be

$$\begin{aligned} [\cdots] &= [B_{11}(t)B_{22}(s) - B_{12}(t)B_{21}(s)]/[B_{11}(s)B_{22}(s) - B_{12}(s)B_{21}(s)], && \text{(A.19)} \\ &= \frac{\phi(t)B_{22}(s) - \psi(t)[B_{22}(s)B_{21}(t) - B_{22}(t)B_{21}(s)]}{\phi(s)B_{22}(s)}, && \text{(A.20)} \\ &= \phi(t,s) - \psi(t)\frac{B_{21}(t)B_{22}(s) - B_{21}(s)B_{22}(t)}{\phi(s)B_{22}(s)}. && \text{(A.21)} \end{aligned}$$

With the assumption that the convergence of $\phi(s)$ to 0 as $s \to \infty$ is sufficiently rapid, the lower bound s of the integration in eq. (A.14) can be replaced by 0, and we obtain

$$B_{21}(t) \simeq B_{22}(t)\int_0^t ds\phi(s). \tag{A.22}$$

With eq. (A.22), the second term in eq. (A.21) is transformed into

$$\psi(t)B_{22}(t)\left[\int_0^t dt'\phi(t') - \int_0^s dt'\phi(t')\right]/\phi(s) = \psi(t)B_{22}(t)\int_s^t dt'\phi(t',s), \tag{A.23}$$

thus we obtain

$$\delta x_1(t) = \frac{1}{\tau}\int_0^t ds\tilde{\eta}(s)\phi(t,s) - \frac{1}{\tau}\psi(t)B_{22}(t)\int_0^t ds\tilde{\eta}(s)\int_s^t dt'\phi(t',s). \tag{A.24}$$

Let us consider the order of the magnitude of the second term in eq. (A.24). With the assumption that the convergence of $\phi(t,s)$ to 0 as $t-s\to\infty$ is sufficiently rapid, $\int_s^t dt'\phi(t',s)$ $(s<t)$ and $\psi(t)$ have constant magnitudes independently of t, $\int_0^t ds\tilde{\eta}(s)\sim\sqrt{t}$, and $B_{22}(t)$ decreases exponentially with t, thus we obtain

$$\delta x_1(t) \simeq \frac{1}{\tau}\int_0^t ds\tilde{\eta}(s)\phi(t,s). \tag{A.25}$$

From eq. (A.25), the variance of $\delta x_1(t)$ is written as

$$\langle\delta x_1(t)^2\rangle \simeq \frac{\tilde{D}}{\tau^2}\int_0^t ds\phi(t,s)^2, \tag{A.26}$$

$$= \frac{\tilde{D}}{\tau^2}\int_0^t ds\exp\left[-\frac{2}{\tau}(w-1)(t-s) - \frac{2}{\tau}\int_s^t dt'X_1^2(t')\right], \tag{A.27}$$

where $\tilde{D}\equiv(1-N^{-1})D$.

If $(w-1)/\tau$ is sufficiently large, by replacing $X(t')$ by $X(t)$, we obtain

$$\langle\delta x_1(t)^2\rangle \simeq \frac{\tilde{D}}{\tau^2}\int_0^t ds\exp\left[-\frac{2}{\tau}(w-1+X_1^2(t))(t-s)\right], \tag{A.28}$$

$$= \frac{\tilde{D}}{\tau}\frac{1-\exp\left[-\frac{2}{\tau}(w-1+X_1^2(t))t\right]}{2(w-1+X_1^2(t))}, \tag{A.29}$$

$$= \frac{(1-N^{-1})D}{2\tau(w-1+X_1^2)}, \tag{A.30}$$

where $t\to\infty$ is considered in order to obtain the final stationary form.

Appendix B

Dynamics of the Network Storing Three Patterns

In Chaps. 7 and 8, the networks of the FitzHugh-Nagumo neurons storing p random patterns composed of 0/1 digits are treated. In such systems, for the network storing a single pattern, the neurons are classified into two groups, namely, the neurons which store 0's in that pattern, and the neurons which store 1's. Thus the neurons are classified into 2^p groups for the network storing p patterns. For example, in Sec. 7.4, the network storing a single pattern is classified into two groups, namely, the sets $G^1(0)$ and $G^1(1)$.

Similarly, the network storing three patterns treated in Sec. 8.5 is classified into $2^3 = 8$ groups of neurons. In this appendix, we introduce this classification and consider the dynamics of each group.

Consider the network storing three patterns $\zeta^{(1,l)}$ $(l = 1, 2, 3)$ and denote the set of indices of neurons which store 1's in the pattern $\zeta^{(1,l)}$ as $G(1, l)$. As shown in Fig. B.1,

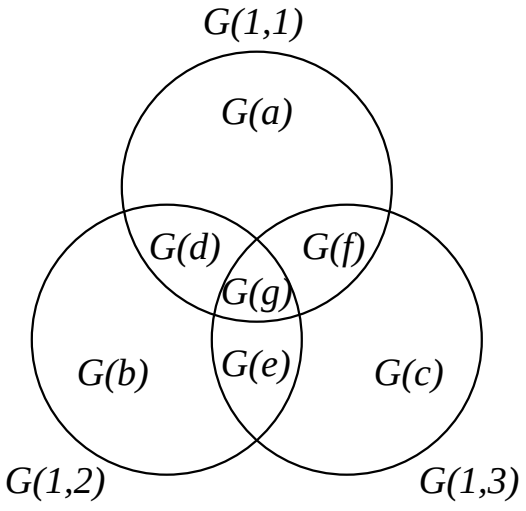

Figure B.1 The sets $G(1, l)$ in the space of neuron indices.

the sets $G(1,l)$ $(l=1,2,3)$ are decomposed as

$$G(1,1) = G(a) \cup G(d) \cup G(f) \cup G(g), \tag{B.1}$$
$$G(1,2) = G(b) \cup G(d) \cup G(e) \cup G(g), \tag{B.2}$$
$$G(1,3) = G(c) \cup G(e) \cup G(f) \cup G(g), \tag{B.3}$$

where

$$G(a) = G(1,1) \cap \overline{G(1,2)} \cap \overline{G(1,3)}, \tag{B.4}$$
$$G(b) = \overline{G(1,1)} \cap G(1,2) \cap \overline{G(1,3)}, \tag{B.5}$$
$$G(c) = \overline{G(1,1)} \cap \overline{G(1,2)} \cap G(1,3), \tag{B.6}$$
$$G(d) = G(1,1) \cap G(1,2) \cap \overline{G(1,3)}, \tag{B.7}$$
$$G(e) = \overline{G(1,1)} \cap G(1,2) \cap G(1,3), \tag{B.8}$$
$$G(f) = G(1,1) \cap \overline{G(1,2)} \cap G(1,3), \tag{B.9}$$
$$G(g) = G(1,1) \cap G(1,2) \cap G(1,3). \tag{B.10}$$

We also define the set of indices of neurons which store 0's for all the patterns as $G(0)$, namely, $G(0) = \overline{G(1,1) \cup G(1,2) \cup G(1,3)}$. From the definitions (7.1) and (8.3), the input K_i injected into the i-th neuron is written as

$$K_i = \eta_i \quad \text{for} \ \ i \in G(0), \tag{B.11}$$
$$K_i = \langle \alpha_j(t) \rangle_{j \in G(1,1)} - \langle \alpha_j(t) \rangle_{j \in \overline{G(1,1)}} + U_0 + \eta_i \quad \text{for} \ \ i \in G(a), \tag{B.12}$$
$$K_i = \sum_{l \in \{1,2\}} \left(\langle \alpha_j(t) \rangle_{j \in G(1,l)} - \langle \alpha_j(t) \rangle_{j \in \overline{G(1,l)}} \right) + U_0 + \eta_i \quad \text{for} \ \ i \in G(d), \tag{B.13}$$
$$K_i = \sum_{l \in \{1,3\}} \left(\langle \alpha_j(t) \rangle_{j \in G(1,l)} - \langle \alpha_j(t) \rangle_{j \in \overline{G(1,l)}} \right) + U_0 + \eta_i \quad \text{for} \ \ i \in G(f), \tag{B.14}$$
$$K_i = \sum_{l=1}^{3} \left(\langle \alpha_j(t) \rangle_{j \in G(1,l)} - \langle \alpha_j(t) \rangle_{j \in \overline{G(1,l)}} \right) + U_0 + \eta_i \quad \text{for} \ \ i \in G(g), \tag{B.15}$$
$$K_i = \langle \alpha_j(t) \rangle_{j \in G(1,2)} - \langle \alpha_j(t) \rangle_{j \in \overline{G(1,2)}} + \eta_i \quad \text{for} \ \ i \in G(b), \tag{B.16}$$
$$K_i = \langle \alpha_j(t) \rangle_{j \in G(1,3)} - \langle \alpha_j(t) \rangle_{j \in \overline{G(1,3)}} + \eta_i \quad \text{for} \ \ i \in G(c), \tag{B.17}$$
$$K_i = \sum_{l \in \{2,3\}} \left(\langle \alpha_j(t) \rangle_{j \in G(1,l)} - \langle \alpha_j(t) \rangle_{j \in \overline{G(1,l)}} \right) + \eta_i \quad \text{for} \ \ i \in G(e), \tag{B.18}$$
$$\alpha_j(t) = \sum_{k \in \kappa(i,j)} \alpha(t - t_j^k - d_p), \tag{B.19}$$
$$\kappa(i,j) = \{k | t_i^f(t) - d_p < t_j^k < t - d_p\}, \tag{B.20}$$

where $\langle \cdot \rangle_{j \in A}$ denotes the ensemble average over the set A. To omit the dependence of K_i on the index i in the identical set $G(\cdot)$, the set $\kappa(i,j)$ is substituted with

$$\kappa(j) = \{k | t_j^k < t - d_p\}, \tag{B.21}$$

for simplicity.

In the numerical derivation of the one dimensional map $g(z_n)$ in Sec. 8.5, the network with the input K_i is treated, and the dynamics of the neurons in $G(0)$ are neglected for simplicity.

Acknowledgement

I am grateful to the supervising Professor Yoichi Okabe for his stimulating discussions and encouragement. I am also grateful to the referees of this Ph.D. thesis, Professor Kazuyuki Aihara, Professor Akira Hirose, Professor Kiyoharu Aizawa, and Professor Takehiko Horita for their careful readings of this thesis and valuable discussions.

And I thank all the members of Okabe and Hirose laboratory for their sincere friendships.

Lastly, I would like to express my gratitude to my parents for their mental and economic supports for my research activity.

Bibliography

[1] C. U. M. Smith, *Biology of Sensory Systems* (John Wiley & Sons Ltd, West Sussex, England, 2000).

[2] D. Mellon, "Electrical Responses from Dually Innervated Tactile Receptors on the Thorax of the Crayfish," *Journal of Experimental Biology* **40**, 137-148 (1963).

[3] K. Wiese, "Mechanoreceptors for Near-field Water Displacements in Crayfish," *Journal of Neurophysiology* **39**, 816-833 (1976).

[4] W. Gnatzy and R. Heusslein, "Digger Wasp Against Crickets," *Naturwissenschaften* **73**, 212-215 (1986).

[5] J. M. Camhi, W. Tom, and S. Volman, "The Escape Behavior of the Cockroach Periplaneta americana," *Journal of Comparative Physiology A* **128**, 203-212 (1978).

[6] C. Koch and I. Segev, *Methods in Neuronal Modeling* (The MIT Press, Cambridge, MA, U.S.A, 1989).

[7] E. Neher and B. Sakmann, "Single-channel Currents Recorded from Membrane of Denervated Frog Muscle Fibres," *Nature* **260**, 799-802 (1976).

[8] F. Conti, L. J. de Felice, and E. Wanke, "Potassium and Sodium Ion Current Noise in the Membrane of the Squid Giant Axon," *Journal of Physiology* **248**, 45-82 (1975).

[9] F. Conti and E. Neher, "Single Channel Recordings of K^+ Currents in Squid Axons," *Nature* **285**, 140-143 (1980).

[10] L. J. DeFelice and A. Isaac, "Chaotic States in a Random World: Relationship Between the Nonlinear Differential Equations of Excitability and the Stochastic Properties of Ion Channels," *Journal of Statistical Physics* **70**, 339-354 (1992).

[11] S. W. Kuffler, J. G. Nicholls, and A. R. Martin, *From Neuron to Brain* (Sinauer Associates Inc. Publishers, Sunderland, Massachusetts, 1984).

[12] P. Fatt and B. Katz, "Spontaneous Subthreshold Activity at Motor Nerve Endings," *Journal of Physiology* **117**, 109-128 (1952).

[13] J. del Castillo and B. Katz, "Quantal Components of the End-plate Potential," *Journal of Physiology* **124**, 560-573 (1954).

[14] I. A. Boyd and A. R. Martin, "The End-plate potential in Mammalian Muscle," *Journal of Physiology* **132**, 74-91 (1956).

[15] E. W. Johnson and A. Wernig, "The Binomial Nature of Transmitter Release at the Crayfish Neuromuscular Junction," *Journal of Physiology* **218**, 757-767 (1971).

[16] C. Rosenmund, J. D. Clements, and G. L. Westbrook, "Nonuniform Probability of Glutamate Release at a Hippocampal Synapse," *Science* **262**, 754-757 (1993).

[17] N. A. Hessler, A. M. Shirke, and R. Malinow, "The Probability of Transmitter Release at a Mammalian Central Synapse," *Nature* **366**, 569-572 (1993).

[18] A. M. Thomson, J. Deuchars, and D. C. West, "Single Axon Excitatory Postsynaptic Potentials in Neocortical Interneurons Exhibit Pronounced Paired Pulse Facilitation," *Neuroscience* **54**, 347-360 (1993).

[19] A. M. Thomson, J. Deuchars, and D. C. West, "Large, Deep Layer Pyramid-Pyramid Single Axon EPSPs in Slices of Rat Motor Cortex Display Paired Pulse and Frequency-Dependent Depression, Mediated Presynaptically and Self-Facilitation, Mediated Postsynaptically," *Journal of Neurophysiology* **70**, 2354-2369 (1993).

[20] H. Markram and M. Tsodyks, "Redistribution of Synaptic Efficacy Between Neocortical Pyramidal Neurons," *Nature* **382**, 807-810 (1996).

[21] A. Zador, "Impact of Synaptic Unreliability on the Information Transmitted by Spiking Neurons," *Journal of Neurophysiology* **79**, 1219-1229 (1998).

[22] M. V. Tsodyks and H. Markram, "The Neural Code Between Neocortical Pyramidal Neurons Depends on Neurotransmitter Release Probability," *Proceedings of the National Academy of Sciences of the USA* **94**, 719-723 (1997).

[23] W. H. Calvin and C. F. Stevens, "Synaptic Noise and Other Sources of Randomness in Motoneuron Interspike Intervals," *Journal of Neurophysiology* **31**, 574-587 (1968).

[24] L. J. Croner, K. Purpura, and E. Kaplan, "Response Variability in Retinal Ganglion Cells of Primates," *Proceedings of the National Academy of Sciences USA* **90**, 8128-8130 (1993).

[25] M. J. Korenberg, H. M. Sakai, and K. Naka, "Dissection of the Neuron Network in the Catfish Inner Retina. III. Interpretation of Spike Kernels," *Journal of Neurophysiology* **61**, 1110-1120 (1989).

[26] H. Noda and W. R. Adey, "Firing Variability in Cat Association Cortex During Sleep and Wakefulness," *Brain Research* **18**, 513-526 (1970).

[27] W. R. Softky and C. Koch, "The Highly Irregular Firing of Cortical Cells is Inconsistent with Temporal Integration of Random EPSPs," *The Journal of Neuroscience* **13**, 334-350 (1993).

[28] M. N. Shadlen and W. T. Newsome, "Noise, Neural Codes and Cortical Organization," *Current Opinion in Neurobiology* **4**, 569-579 (1994).

[29] W. R. Softky, "Simple Codes versus Efficient Codes," *Current Opinion in Neurobiology* **5**, 239-247 (1995).

[30] M. N. Shadlen and W. T. Newsome, "Is There a Signal in the Noise?," *Current Opinion in Neurobiology* **5**, 248-250 (1995).

[31] M. Abeles, "Role of the Cortical Neuron: Integrator or Coincidence Detector?," *Israel Journal of Medical Sciences* **18**, 83-92 (1982).

[32] P. König, A. K. Engel, and W. Singer, "Integrator or Coincidence Detector? The Role of the Cortical Neuron Revisited," *Trends in Neuroscience* **19**, 130-137 (1996).

[33] S. O. Rice, "Mathematical Analysis of Random Noise," in *Selected Papers on Noise and Stochastic Processes*, edited by N. Wax (Dover, New York, 1954), pp. 133-294.

[34] C. W. Gardiner, *Handbook of Stochastic Methods* (Springer-Verlag, Berlin, 1985).

[35] Ö. Bernander, R. J. Douglas, K. A. C. Martin, and C. Koch, "Synaptic Background Activity Influences Spatiotemporal Integration in Single Pyramidal Cells," *Proceedings of the National Academy of Sciences USA* **88**, 11569-11573 (1991).

[36] C. Koch, "Computation and the Single Neuron," *Nature* **385**, 207-210 (1997).

[37] T. J. Sejnowski, "The Year of Dendrite," *Science* **275**, 178-179 (1997).

[38] W. Softky, "Sub-millisecond Coincidence Detection in Active Dendrite Trees," *Neuroscience* **58**, 13-41 (1994).

[39] S. Shinomoto, Y. Sakai, and S. Funahashi, "The Ornstein-Uhlenbeck Process does not Reproduce Spiking Statistics of Neurons in Prefrontal Cortex," *Neural Computation* **11**, 935-951 (1999).

[40] Y. Sakai, S. Funahashi, and S. Shinomoto, "Temporally Correlated Inputs to Leaky Integrate-and-firing Models can Reproduce Spiking Statistics of Cortical Neurons," *Neural Networks* **12**, 1181-1190 (1999).

[41] C. F. Stevens and A. M. Zador, "Input Synchrony and the Irregular Firing of Cortical Neurons," *Nature Neuroscience* **1**, 210-217 (1998).

[42] M. V. Tsodyks and T. Sejnowski, "Rapid State Switching in Balanced Cortical Network Models," *Network: Computation in Neural Systems* **6**, 111-124 (1995).

[43] C. van Vreeswijk and H. Sompolinsky, "Chaos in Neuronal Networks with Balanced Excitatory and Inhibitory Activity," *Science* **274**, 1724-1726 (1996).

[44] M. Gur, A. Beylin, and D. M. Snodderly, "Response Variability of Neurons in Primary Visual Cortex (V1) of Alert Monkeys," *The Journal of Neuroscience* **17**, 2914-2920 (1997).

[45] R. R. de Ruyter van Steveninck, G. D. Lewen, S. P. Strong, R. Koberle, and W. Bialek, "Reproducibility and Variability in Neural Spike Trains," *Science* **275**, 1805-1808 (1997).

[46] M. J. Berry, D. K. Warland, and M. Meister, "The Structure and Precision of Retinal Spike Trains," *Proceedings of the National Academy of Sciences USA* **94**, 5411-5416 (1997).

[47] Z. F. Mainen and T. J. Sejnowski, "Reliability of Spike Timing in Neocortical Neurons," *Science* **268**, 1503-1506 (1995).

[48] A. C. Tang, A. M. Bartels, and T. J. Sejnowski, "Cholinergic Modulation Preserves Spike Timing under Physiologically Realistic Fluctuating Input," *Advances in Neural Information Processing Systems* **9**, 111-117 (1997).

[49] L. G. Nowak, M. V. Sanchez-Vives, and D. A. McCormick, "Influence of Low and High Frequency Inputs on Spike Timing in Visual Cortical Neurons," *Cerebral Cortex* **7**, 487-501 (1997).

[50] E. Schneidman, B. Freedman, and I. Segev, "Ion Channel Stochasticity may be Critical in Determining the Reliability and Precision of Spike Timing," *Neural Computation* **10**, 1679-1703 (1998).

[51] H. Hayashi, S. Ishizuka, M. Ohta, and K. Hirakawa, "Chaotic Behavior in the Onchidium Giant Neuron Under Sinusoidal Stimulation," *Physics Letters A* **88**, 435-438 (1982).

[52] G. Matsumoto, K. Aihara, M. Ichikawa, and A. Tasaki, "Periodic and Nonperiodic Responses of Membrane Potentials in Squid Giant Axons Duaring Sinusoidal Current Stimulation," *Journal of Theoretical Neurobiology* **3**, 1-14 (1984).

[53] K. Aihara, G. Matsumoto, and Y. Ikegaya, "Periodic and Nonperiodic Responses of a Periodically Forced Hodgkin-Huxley Oscillator," *Journal of Theoretical Biology* **109**, 249-269 (1984).

[54] H. Hayashi and S. Ishizuka, "Chaotic Nature of Bursting Discharges in the Onchidium Pacemaker Neuron," *Journal of Theoretical Biology* **156**, 269-291 (1992).

[55] M. Falcke, R. Huerta, M. I. Rabinovich, H. D. I. Abarbanel, R. C. Elson, and A. I. Selverston, "Modeling Observed Chaotic Oscillations in Bursting Neurons: The Role of Calcium Dynamics and IP_3," *Biological Cybernetics* **82**, 517-527 (2000).

[56] W. J. Freeman, "Simulation of Chaotic EEG Patterns with a Dynamic Model of the Olfactory System," *Biological Cybernetics* **56**, 139-150 (1987).

[57] Y. Yao and W. J. Freeman, "Model of Biological Pattern Recognition with Spatially Chaotic Dynamics," *Neural Networks* **3**, 153-170 (1990).

[58] W. J. Freeman, "Neural Mechanism Underlying Destabilization of Cortex by Sensory Input," *Physica D* **75**, 151-164 (1994).

[59] K. Aihara, T. Takabe, and M. Toyoda, "Chaotic Neural Networks," *Physics Letters A* **144**, 333-340 (1990).

[60] I. Tsuda, "Dynamic Link of Memory - Chaotic Memory Map in Nonequilibrium Neural Networks," *Neural Networks* **5**, 313-326 (1992).

[61] M. Adachi and K. Aihara, "Associative Dynamics in a Chaotic Neural Network," *Neural Networks* **10**, 83-98 (1997).

[62] L. Goldman and J. S. Albus, "Computation of Impulse Conduction in Myelinated Fibers; Theoretical Basis of the Velocity-diameter Relation," *Biophysical Journal* **8**, 596-607 (1968).

[63] G. Matsumoto and I. Tasaki, "A Study of Conduction Velocity in Nonmyelinated Nerve Fibers," *Biophysical Journal* **20**, 1-13 (1977).

[64] C. E. Carr and M. Konishi, "A Circuit for Detection of Interaural Time Differences in the Brain Stem of the Barn Owl," *The Journal of Neuroscience* **10**, 3227-3246 (1990).

[65] K. Matsumoto and I. Tsuda, "Noise-induced Order," *Journal of Statistical Physics* **31**, 87-106 (1983).

[66] H. Daido, "Correlation Resonance in Noise-driven Coupled Nonlinear Oscillators," *Physica D* **116**, 325-341 (1998).

[67] F. Moss, D. Pierson, and D. O'Gorman, "Stochastic Resonance: Tutorial and Update," *International Journal of Bifurcation and Chaos* **4**, 1383-1397 (1994).

[68] M. I. Dykman, D. G. Luchinsky, R. Mannella, P. V. E. McClintock, N. D. Stein, and N. G. Stocks, "Stochastic Resonance in Perspective," *Nuovo Cimento D* **17**, 661-683 (1995).

[69] L. Gammaitoni, P. Hänggi, P. Jung, and F. Marchesoni, "Stochastic Resonance," *Reviews of Modern Physics* **70**, 223-287 (1998).

[70] K. Wiesenfeld and F. Jaramillo, "Minireview of Stochastic Resonance," *CHAOS* **8**, 539-548 (1998).

[71] A. R. Bulsara, S. B. Lowen, and C. D. Rees, "Cooperative Behavior in the Periodically Modulated Wiener Process: Noise-induced Complexity in a Model Neuron," *Physical Review E* **49**, 4989-5000 (1994).

[72] A. R. Bulsara, T. C. Elston, C. R. Doering, S. B. Lowen, and K. Lindenberg, "Cooperative Behavior in Periodically Driven Noisy Integrate-fire Models of Neuronal Dynamics," *Physical Review E* **53**, 3958-3969 (1996).

[73] T. Shimokawa, K. Pakdaman, and S. Sato, "Time-scale Matching in the Response of a Leaky Integrate-and-fire Neuron Model to Periodic Stimulus with Additive Noise," *Physical Review E* **59**, 3427-3443 (1999).

[74] A. Longtin, "Stochastic Resonance in Neuron Models," *Journal of Statistical Physics* **70**, 309-327 (1993).

[75] K. Wiesenfeld, D. Pierson, E. Pantazelou, C. Dames, and F. Moss, "Stochastic Resonance on a Circle," *Physical Review Letters* **72**, 2125-2129 (1994).

[76] A. Longtin and D. R. Chialvo, "Stochastic and Deterministic Resonances for Excitable Systems," *Physical Review Letters* **81**, 4012-4015 (1998).

[77] S. Lee and S. Kim, "Parameter Dependence of Stochastic Resonance in the Stochastic Hodgkin-Huxley Neuron," *Physical Review E* **60**, 826-830 (1999).

[78] J. K. Douglass, L. Wilkens, E. Pantazelou, and F. Moss, "Noise Enhancement of Information Transfer in Crayfish Mechanoreceptors by Stochastic Resonance," *Nature* **365**, 337-340 (1993).

[79] X. Pei, L. A. Wilkens, and F. Moss, "Light Enhances Hydrodynamic Signaling in the Multimodal Caudal Photoreceptor Interneurons of the Crayfish," *Journal of Neurophysiology* **76**, 3002-3011 (1996).

[80] B. J. Gluckman, T. I. Netoff, E. J. Neel, W. L. Ditto, M. L. Spano, and S. J. Schiff, "Stochastic Resonance in a Neuronal Network from Mammalian Brain," *Physical Review Letters* **77**, 4098-4101 (1996).

[81] B. J. Gluckman, P. So, T. I. Netoff, M. L. Spano, and S. J. Schiff, "Stochastic Resonance in Mammalian Neuronal Networks," *CHAOS* **8**, 588-598 (1998).

[82] D. Nozaki, D. J. Mar, P. Grigg, and J. J. Collins, "Effects of Colored Noise on Stochastic Resonance in Sensory Neurons," *Physical Review Letters* **82**, 2402-2405 (1999).

[83] G. Mato, "Stochastic Resonance in Neural Systems: Effect of Temporal Correlation in the Spike Trains," *Physical Review E* **58**, 876-880 (1998).

[84] G. Mato, "Stochastic Resonance using Noise Generated by a Neural Network," *Physical Review E* **59**, 3339-3343 (1999).

[85] Y. Sakumura and K. Aihara, "Stochastic Resonance by Modulation Detecting Neuron," in *Proceedings of the fifth International Conference on Neural Information Processing*, edited by S. Usui and T. Omori (Ohmsha, Tokyo, 1998), pp. 951-954.

[86] J. Feng and B. Tirozzi, "Stochastic Resonance Tuned by Correlations in Neural Models," *Physical Review E* **61**, 4207-4211 (2000).

[87] D. Nozaki, J. J. Collins, and Y. Yamamoto, "Mechanism of Stochastic Resonance Enhancement in Neuronal Models Driven by $1/f$ Noise," *Physical Review E* **60**, 4637-4644 (1999).

[88] F. Moss and X. Pei, "Neurons in Parallel," *Nature* **376**, 211-212 (1995).

[89] J. J. Collins, C. C. Chow, and T. T. Imhoff, "Stochastic Resonance without Tuning," *Nature* **376**, 236-238 (1995).

[90] T. Shimokawa, A. Rogel, K. Pakdaman, and S. Sato, "Stochastic Resonance and Spike-timing Precision in an Ensemble of Leaky Integrate and Fire Neuron Models," *Physical Review E* **59**, 3461-3470 (1999).

[91] S. Tanabe, S. Sato, and K. Pakdaman, "Response of an Ensemble of Noisy Neuron Models to a Single Input," *Physical Review E* **60**, 7235-7238 (1999).

[92] T. Kanamaru, T. Horita, and Y. Okabe, "Stochastic Resonance in the Hodgkin-Huxley Network," *Journal of Physical Society of Japan* **67**, 4058-4063 (1998).

[93] T. Kanamaru, T. Horita, and Y. Okabe, "Stochastic Resonance for the Superimposed Periodic Pulse Train," *Physics Letters A* **255**, 23-30 (1999).

[94] T. Kanamaru and Y. Okabe, "Stochastic Resonance in a Pulse Neural Network with a Propagational Time Delay," *BioSystems* **58**, 101-107 (2000).

[95] M. Löcher, D. Cigna, E. R. Hunt, G. A. Johnson, F. Marchesoni, L. Gammaitoni, M. E. Inchiosa, and A. R. Bulsara, "Stochastic Resonance in Coupled Nonlinear Dynamic Elements," *CHAOS* **8**, 604-615 (1998).

[96] J. F. Lindner, B. K. Meadows, W. L. Ditto, M. E. Inchiosa, and A. R. Bulsara, "Array Enhanced Stochastic Resonance and Spatiotemporal Synchronization," *Physical Review Letters* **75**, 3-6 (1995).

[97] M. Löcher, G. A. Johnson, and E. R. Hunt, "Spatiotemporal Stochastic Resonance in a System of Coupled Diode Resonators," *Physical Review Letters* **77**, 4698-4701 (1996).

[98] B. Hu and C. Zhou, "Phase Synchronization in Coupled Nonidentical Excitable Systems and Array-enhanced Coherence Resonance," *Physical Review E* **61**, R1001-R1004 (2000).

[99] H. Fujii, H. Ito, K. Aihara, N. Ichinose, and M. Tsukada, "Dynamical Cell Assembly Hypothesis – Theoretical Possibility of Spatio-temporal Coding in the Cortex," *Neural Networks* **9**, 1303-1350 (1996).

[100] G. Palm, A. M. H. J. Aertsen, and G. L. Gerstein, "On the Significance of Correlations Among Neuronal Spike Trains," *Biological Cybernetics* **59**, 1-11 (1988).

[101] A. R. Bulsara and A. Zador, "Threshold Detection of Wideband Signals: A Noise-induced Maximum in the Mutual Information," *Physical Review E* **54**, R2185-R2188 (1996).

[102] F. Chapeau-Blondeau, "Noise-enhanced Capacity via Stochastic Resonance in an Asymmetric Binary Channel," *Physical Review E* **55**, 2016-2019 (1997).

[103] W. H. Press, S. A. Teukolsky, W. T. Vetterling, and B. P. Flannery, *Numerical Recipes in C* (Cambridge University Press, Cambridge, 1988).

[104] I. Tsuda, "Dynamic Link of Memory – Chaotic Memory Map in Nonequilibrium Neural Networks," *Neural Networks* **5**, 313-326 (1992).

[105] M. Adachi and K. Aihara, "Associative Dynamics in a Chaotic Neural Network," *Neural Networks* **10**, 83-98 (1997).

[106] T. Aoyagi, "Network of Neural Oscillators for Retrieving Phase Information," *Physical Review Letters* **74**, 4075-4078 (1995).

[107] T. Aoyagi and K. Kitano, "Effect of Random Synaptic Dilution in Oscillator Neural Networks," *Physical Review E* **55**, 7424-7428 (1997).

[108] K. Kitano and T. Aoyagi, "Effect of Random Synaptic Dilution on Recalling Dynamics in an Oscillator Neural Network," *Physical Review E* **57**, 5914-5919 (1998).

[109] T. Aonishi, K. Kurata, and M. Okada, "Statistical Mechanics of an Oscillator Associative Memory with Scattered Natural Frequencies," *Physical Review Letters* **82**, 2800-2803 (1999).

[110] F. C. Hoppensteadt and E. M. Izhikevich, "Oscillatory Neurocomputers with Dynamic Connectivity," *Physical Review Letters* **82**, 2983-2986 (1999).

[111] T. Aoyagi and M. Nomura, "Oscillator Neural Network Retrieving Sparsely Coded Phase Patterns," *Physical Review Letters* **83**, 1062-1065 (1999).

[112] M. Yamana, M. Shiino, and M. Yoshioka, "Oscillator Neural Network Model with Distributed Native Frequencies," *Journal of Physics A* **32**, 3525-3533 (1999).

[113] S. Uchiyama and H. Fujisaka, "Analysis of Oscillator Neural Network without Lyapunov Function," *Journal Physics A* **32**, 4623-4640 (1999).

[114] M. Yoshioka and M. Shiino, "Associative Memory Storing an Extensive Number of Patterns Based on a Network of Oscillators with Distributed Natural Frequencies in the Presence of External White Noise," *Physical Review E* **61**, 4732-4744 (2000).

[115] W. Gerstner, R. Ritz, and J. L. van Hemmen, "Why Spikes? Hebbian Learning and Retrieval of Time-resolved Excitation Patterns," *Biological Cybernetics* **69**, 503-515 (1993).

[116] W. Maass and T. Natschläger, "Network of Spiking Neurons can Emulate Arbitrary Hopfield Nets in Temporal Coding," *Network* **8**, 355-371 (1997).

[117] M. Yoshioka and M. Shiino, "Associative Memory based on Synchronized Firing of Spiking Neurons with Time-delayed Interactions," *Physical Review E* **58**, 3628-3639 (1998).

[118] T. Kanamaru and Y. Okabe, "Associative Memory Retrieval Induced by Fluctuations in a Pulsed Neural Network," *Physical Review E* **62**, 2629-2635 (2000).

[119] D. Wang, J. Buhmann, and C. von der Malsburg, "Pattern Segmentation in Associative Memory," *Neural Computation* **2**, 94-106 (1990).

[120] S. Amari and K. Maginu, "Statistical Neurodynamics of Associative Memory," *Neural Networks* **1**, 63-73 (1988).

[121] M. Shiino and T. Fukai, "Self-consistent Signal-to-noise Analysis and its Application to Analogue Neural Networks with Asymmetric Connections," *Journal of Physics A* **25**, L375-L381 (1992).

[122] M. Okada, "A Hierarchy of Macrodynamical Equations for Associative Memory," *Neural Networks* **8**, 833-838 (1995).

[123] D. J. Amit, H. Gutfreund, and H. Sompolinsky, "Storing Infinite Numbers of Patterns in a Spin-glass Model of Neural Networks," *Physical Review Letters* **55**, 1530-1533 (1985).

[124] J. Cook, "The Mean-field Theory of a Q-state Neural Network Model," *Journal of Physics A* **22**, 2057 (1989).

[125] D. H. Perkel and B. Mulloney, "Motor Pattern Production in Reciprocally Inhibitory Neurons Exhibiting Postinhibitory Rebound," *Science* **185**, 181-183 (1974).

[126] J. D. Enderle and E. J. Engelken, "Simulation of Oculomotor Post-inhibitory Rebound Burst Firing Using a Hodgkin-Huxley Model of a Neuron," *Biomedical Sciences Instrumentation* **31**, 53-58 (1995).

[127] W. K. Luk and K. Aihara, "Synchronization and Sensitivity Enhancement of the Hodgkin-Huxley Neurons due to Inhibitory Inputs," *Biological Cybernetics* **82**, 455-467 (2000).

[128] S. Amari, "Neural Theory of Association and Concept-formation," *Biological Cybernetics* **26**, 175-185 (1977).

[129] M. Okada, "Notions of Associative Memory and Sparse Coding," *Neural Networks* **9**, 1429-1458 (1996).

[130] K. Toya, K. Fukushima, Y. Kabashima, and M. Okada, "Bi-stability of Mixed States in Neural Network Storing Hierarchical Patterns," *preprint*, cond-mat/9909276.

[131] T. Kimoto and M. Okada, "Mixed State on a Sparsely Encoded Associative Memory Model," *preprint*, cond-mat/9911187.

[132] Y. Sugase, S. Yamane, S. Ueno, and K. Kawano, "Global and Fine Information Coded by Single Neurons in the Temporal Visual Cortex," *Nature* **400**, 869-873 (1999).

[133] H. Hasegawa, "A Sparse-code Associative Memory of Hodgkin-Huxley Neuron Networks with Willshaw-type Synaptic Couplings," *preprint*, cond-mat/0007198.

[134] M. Diesmann, M. Gewaltig, and A. Aertsen, "Stable Propagation of Synchronous Spiking in Cortical Neural Networks," *Nature* **402**, 529-533 (1999).